ISSN 1331-1611
9 771331 161005

KoG

SCIENTIFIC - PROFESSIONAL JOURNAL
OF CROATIAN SOCIETY FOR GEOMETRY AND GRAPHICS

No. 28. (2024)
ISSN 1331-1611

KoG

Official publication of the Croatian Society for Geometry and Graphics publishes scientific and professional papers from the fields of geometry, applied geometry and computer graphics.

Founder and Publisher

Croatian Society for Geometry and Graphics

Editors

SONJA GORJANC, Faculty of Civil Engineering, University of Zagreb, Croatia
EMA JURKIN, Faculty of Mining, Geology and Petroleum Engineering, University of Zagreb (Editor-in-Chief)
MARIJA ŠIMIĆ HORVATH, Faculty of Architecture, University of Zagreb, Croatia

Design

Miroslav Ambruš-Kiš

Layout

Sonja Gorjanc, Ema Jurkin

Cover Illustration

Georg Glaeser, photography

Print

SAND d.o.o., Zagreb

URL address

http://www.hdgg.hr/kog
http://hrcak.srce.hr

Edition

150

Published annually

Guide for authors
Please, see the page 68.

KoG is reviewed by zbMATH and Scopus.

This issue has been financially supported by the Ministry of Science, Education and Youth.

ISSN 1331–1611

No. 28
Zagreb, 2024

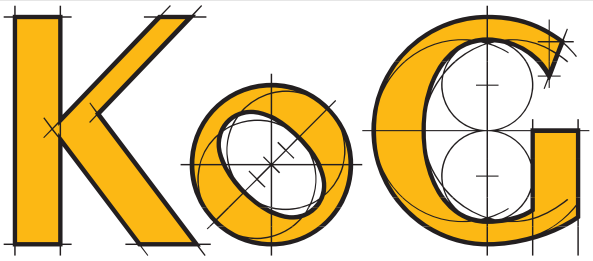

SCIENTIFIC AND PROFESSIONAL JOURNAL OF
CROATIAN SOCIETY FOR GEOMETRY AND GRAPHICS

CONTENTS

ISSN 1331–1611

BROJ 28
Zagreb, 2024

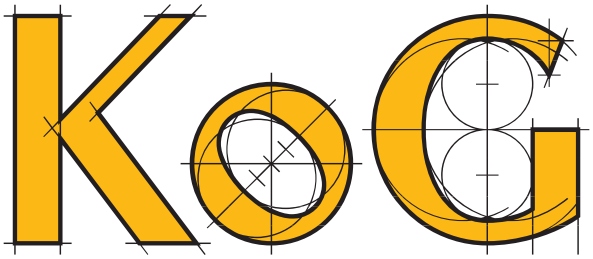

ZNANSTVENO-STRUČNI ČASOPIS
HRVATSKOG DRUŠTVA ZA GEOMETRIJU I GRAFIKU

SADRŽAJ

ORIGINALNI ZNANSTVENI RADOVI

PREGLEDNI RADOVI

STRUČNI RADOVI

https://doi.org/10.31896/k.28.1
Original scientific paper
Accepted 1. 8. 2024.

KONSTANTINOS MYRIANTHIS
HELLMUTH STACHEL

On Permutations of Desarguesian Sextuples

On Permutations of Desarguesian Sextuples

ABSTRACT

Desargues's theorem plays an essential role at the axiomatic foundations of Projective Geometry. The configuration behind this theorem contains ten lines, the sides of two triangles, three lines through the center and the axis. We focus on the ordered sextuple of intersection points with the axis and call it Desarguesian. A permutation of this sextuple is called admissible if it preserves the property of being Desarguesian. Some permutations are admissible only if Pappus's theorem holds in the plane. Under this assumption we can prove that for each permutation there exist particular Desarguesian sextuples which remain Desarguesian under the permutation.

Key words: Desargues's theorem, Pappus's theorem, Desarguesian sextuple, involution

MSC2020: 51A30

O permutacijama Desarguesovih šestorki

SAŽETAK

Desarguesov teorem ima bitnu ulogu u aksiomatskim temeljima projektivne geometrije. Konfiguracija iz ovog teorema sastoji se od deset pravaca: šest stranica dvaju trokuta, triju pravaca kroz središte i od osi. Usredotočujemo se na uređenu šestorku sjecišta s osi koju nazivamo Desarguesovom. Permutacija ove šestorke se naziva dopustivom ako čuva svojstvo "biti Desarguesov". Neke su permutacije dopustive samo ako u ravnini vrijedi Pappusov teorem. Pod ovom pretpostavkom dokazujemo da za svaku permutaciju postoje određene Desarguesove šestorke koje ostaju Desarguesove nakon djelovanja te permutacije.

Ključne riječi: Desarguesov teorem, Pappusov teorem, Desarguesova šestorka, involucija

1 Introduction

At the beginning of the twentieth century, Gerhard Hessenberg proved in a synthetic way that Pappus's theorem implies Desargues's theorem [11]. A number of relevant papers has been created since then, all in the context of using Pappus's Theorem for proving Desargues's Theorem (note [6], [15, p. 35], and in particular [18] and [13] with comments on Hessenberg's proofs). The converse is not true. The main result in this direction dates already back to David Hilbert's 'Grundlagen der Geometrie' [12] in 1899 (see [20, p. 78–168]). Hilbert defined an addition and a multiplication of points on a line and proved that each Desarguesian projective plane is isomorphic to a projective coordinate plane over a (not necessarily commutative) field. Moreover, the Desarguesian plane is Pappian if and only if this field is commutative. More about the algebraization of Desarguesian projective planes can be found, e.g., in [16, 10, 2, 4, 13], the latter even with many details on Pappus's theorem. An extensive survey on results obtained during the last about hundred years around the theorems of Desargues and Pappus together with a wealth of references has been provided in [14].

Our work focusses on the Desargues configuration and the ordered sextuple of points on the axis (Fig. 1). We call this sextuple 'Desarguesian' and study permutations that preserve the property of being Desarguesian. We confirm that a Desarguesian projective plane is Pappian if and only if Desarguesian sextuples remain Desarguesian under a certain transposition (Theorem 1) thus rephrasing a result from [9]. Our main result (Theorem 3) states that in Pappian planes for each permutation there exist Desarguesian sextuples which remain Desarguesian under the permutation. However, in the majority of cases the sextuple has to satisfy one particular condition in terms of cross ratios. Our paper concludes with analytic characterizations of Desarguesian sextuples in Desarguesian and in Pappian planes.

The included figures shall illustrate the underlying ideas. In general they cannot not serve as proofs since the real projective plane is Pappian.

2 Desarguesian sextuples

Definition 1 *In a Desarguesian projective plane, a sextuple* $(S_1,S_2,S_3,T_1,T_2,T_3)$ *of mutually different collinear points is called Desarguesian if there exists a Desargues configuration with center Z, axis a and two Z-perspective triangles* $P_1P_2P_3$ *and* $Q_1Q_2Q_3$ *such that for* $i=1,2,3$ *the point* T_i *is the intersection between a and the line passing through Z,* P_i *and* Q_i*, while for each permutation* (i,j,k) *of* $(1,2,3)$ *the point* $S_i \in a$ *is common to the sides* $[P_j,P_k]$ *and* $[Q_j,Q_k]$.[1]

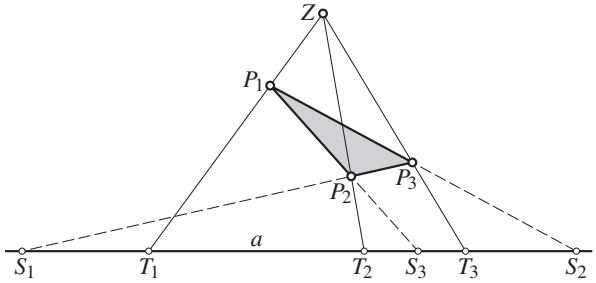

Figure 1: *Desarguesian sextuple* $(S_1,\dots,T_3)$ *on the line a together with the center Z and one triangle* $P_1P_2P_3$ *of a Desargues configuration. Any Z-perspective triangle* $Q_1Q_2Q_3$ *is not shown.*

Below we only pay attention to one of the two Z-perspective triangles, namely to $P_1P_2P_3$ (see Fig. 1). The existence of six mutually different points of a Desarguesian sextuple implies that $ZP_1P_2P_3$ is a quadrangle and for each i the points S_i and T_i belong to opposite sides of this quadrangle. Moreover, the axis a does not contain any vertex of this quadrangle. In finite projective planes Desarguesian sextuples exist only if the order is at least five. It is wellknown that the axiom of Desargues guarantees the existence of perspective collineations for any given center, axis and pair of corresponding points.

Lemma 1 *In Desarguesian projective planes, a Desarguesian sextuple* $(S_1,\dots,T_3)$ *on the axis a of a Desargues configuration does not depend on the choice of the center* $Z \notin a$ *and of the vertex* $P_1 \in [Z,T_1]\setminus\{Z,T_1\}$.

Proof. Beside a configuration with Z,P_1,P_2,P_3 let another center $Z' \notin a$ and a first vertex $P_1' \in [Z',T_1]\setminus\{Z',T_1\}$ of another triangle $P_1'P_2'P_3'$ be given. Then we obtain the remaining vertices as $P_2' = [Z',T_2]\cap[P_1'S_3]$ and $P_3' = [Z',T_3]\cap[P_1'S_2]$. If Z,Z',P_1,P_1' is a quadrangle, then exists in the Desarguesian plane a unique perspective collineation κ with the axis a and the center $C := [Z,Z']\cap[P_1,P_1']$ which sends P_1 to P_1' (Fig. 2). Since κ maps also P_2 to P_2' and P_3 to P_3', the side $[P_2',P_3']$ must pass through S_1.

If three of the four points Z,Z',P_1,P_1' are collinear, then we choose other points $Z'' \notin a$ and $P_1'' \in [Z'',T_1]\setminus\{Z'',T_1\}$ such that Z,Z'',P_1,P_1'' as well as Z',Z'',P_1',P_1'' form quadrangles. Now we can conclude as before using two collineations, one with $Z \mapsto Z''$ and the other with $Z'' \mapsto Z'$. This confirms the claim. □

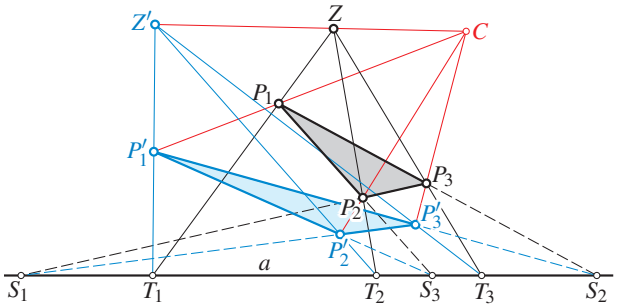

Figure 2: *There is a perspective collineation* κ *with center C and axis a that sends* Z,P_1,P_2,P_3 *respectively to* Z',P_1',P_2',P_3'.

Lemma 2 *If the sextuple* $(S_1,S_2,S_3,T_1,T_2,T_3)$ *is Desarguesian, then for each permutation* (i,j,k) *of the indices* $(1,2,3)$ *the sextuple* $(S_i,S_j,S_k,T_i,T_j,T_k)$ *is Desarguesian, too.*

Proof. This is trivial since we only need to renumber the vertices in the triangle $P_1P_2P_3$. □

Lemma 3 *If the sextuple* $(S_1,S_2,S_3,T_1,T_2,T_3)$ *is Desarguesian, then the sextuple* $(S_1,T_2,T_3,T_1,S_2,S_3)$ *is Desarguesian, too.*

Proof. Exchange in a corresponding configuration the points Z and P_1, while P_2 and P_3 and the axis a remain unchanged. This implies $S_2 \mapsto T_3$, $S_3 \mapsto T_2$, $T_2 \mapsto S_3$, and $T_3 \mapsto S_2$ and means that $(S_1,T_3,T_2,T_1,S_3,S_2)$ is Desarguesian. Finally we exchange the indices 2 and 3 in the sense of Lemma 2. Similarly, we can replace Z with P_2 or P_3 and obtain two other Desarguesian sextuples. □

Remark 1 *The statements of the Lemmas 2 and 3 can already be found in [16, p. 128]. The triples* (S_1,S_2,S_3) *and* (T_1,T_2,T_3) *are respectively called triangle triple and point triple (German: Dreieckstripel and Sterntripel), and the sextuple* $(S_1,\dots,T_3)$ *has the name quadrangular set of points (German: Viereckschnitt). The English notation dates back to [19, p. 49], where the symbol* $Q(T_1T_2T_3;S_1,S_2,S_3)$ *is used for Desarguesian sextuples. In [5, p. vii], this symbol is replaced by* $(S_1T_1)(S_2T_2)(S_3T_3)$. *In [17, p. 129], the name quadrilateral set stands for a Desarguesian sextuple. In [8], a 'quadrangular section' is axiomatically introduced as a ternary relation on the pairs*

[1] Throughout the paper we use the symbol $[X,Y]$ for the line connecting the two points X and Y.

of a set called 'line', and the line is called Desarguian if the statements of Lemma 2 and Lemma 3 hold. The Lemmas 2 and 3 are also subject of [9, Lemma 5.6], where the symbol $(S_1,T_1;S_2,T_2;S_3,T_3)$ *stands for the Desarguesian sextuple* $(S_1,\dots,T_3)$.

Definition 2 *A permutation of the six points of a Desarguesian sextuple is called admissible if the permuted sextupel is still Desarguesian.*

In view of Desarguesian sextuples, we call the pair consisting of the first and the fourth point of a sextuple the *first pair*. Similarly, the *second pair* consist of the second and the fifth point, and the *third pair* of the third and sixth point of the sextuple.

2.1 Characterizations of Pappian planes

In order to illustrate the role of admissible permutations, we present and prove two pertinent results that can already be found in the literature. The first is hidden in the statement of [9, Theorem 5.12].

Theorem 1 *A Desarguesian projective plane is Pappian if and only if for each Desarguesian sextuple* $(S_1,S_2,S_3,T_1,T_2,T_3)$ *the exchange of* (S_1,T_1) *in the first pair is admissible.*

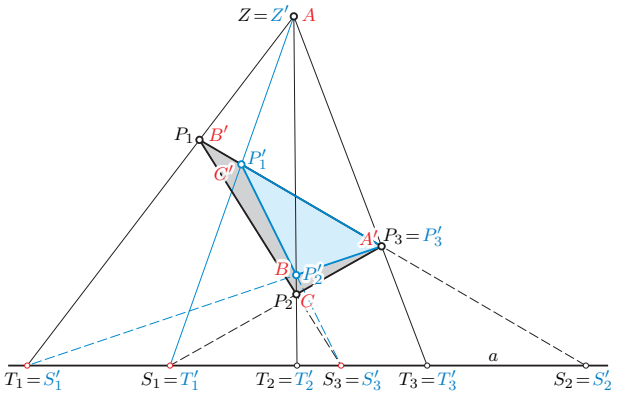

Figure 3: *Illustrating the statement of Theorem 1.*

Proof. Let $Z,\dots,P_3$ and $Z',\dots,P_3'$ be two Desargues configurations which share the axis a and on a the points $S_i=S_i'$ and $T_i=T_i'$ for $i=2,3$. In both cases, the six points $S_1,\dots,T_3$ and $S_1',\dots,T_3'$ are supposed to be mutually different. Then, without loss of generality, we can apply Lemma 1 and replace Z' by Z and P_3' by P_3 while the Desarguesian sextuples on a remain unchanged.
Suppose that for the second configuration holds $S_1'=T_1$ and $T_1'=S_1$ (see Fig. 3). Then a Pappus configuration is included: there are two triples of collinear points $(A,B,C):=(Z,P_2',P_2)$ and $(A',B',C'):=(P_3,P_1,P_1')$, and the intersection points $T_1=[A,B']\cap[A',B]$, $S_1=[A,C']\cap[A',C]$ and $S_3=[B,C']\cap[B',C]$ are collinear, too. This is the basis for confirming the stated characterization of Pappian projective planes.

(i) If the projective plane is Pappian, then $T_1'=S_1$ implies that $a=[S_1,S_3]$ is the Pappus axis. Consequently, the line $[A',B]=[P_3',P_2']$ must intersect the axis a at the point $S_1'=T_1$ on $[A,B']$. This means that both sextuples $(S_1,S_2,S_3,T_1,T_2,T_3)$ and $(S_1',\dots,T_3')=(T_1,S_2,S_3,S_1,T_2,T_3)$ are Desarguesian, i.e., the switch $S_1\leftrightarrow T_1$ preserves Desarguesian sextuples.

If in the Pappian plane the Fano axiom holds, then this is an immediate consequence of Desargues's involution theorem: pairs of opposite sides of the quadrangle $ZP_1P_2P_3$ intersect the line a in pairs (S_i,T_i) of an involution (note, e.g., [1, 5] or [7, Sect. 7.4]).

(ii) Conversely, let two collinear triples of points (A,B,C) and (A',B',C') on different lines be given such that no point coincides with the intersection of the two lines. Then we recognize two triangles $(P_1,P_2,P_3):=(B',C,A')$ and $(P_1',P_2',P_3'):=(C',B,A')$ in the figure as well as the center $Z=Z':=A$ of two Desargues configurations. We define the axis a as the connection of the two points $[A,C']\cap[A',C]$ and $[B,C']\cap[B',C]$. Thus, these points coincide respectively with $S_1=T_1'$ and $S_3=S_3'$. Moreover holds $S_2=S_2'$, $T_2=T_2'$ and $T_3=T_3'$ per definition. Now we can state: If the switch $S_1\leftrightarrow T_1$ preserves a sextuple of being Desarguesian, then follows $S_1'=T_1$, which means that also the point $[A,B']\cap[A',B]$ lies on the axis a. This confirms the validity of Pappus's theorem for the given points $A,\dots,C'$. □

According to Theorem 1, only in Pappian planes all Desarguesian sextuples $(S_1,\dots,T_3)$ remain Desarguesian if we commute the points in one pair (S_i,T_i). Note that by Lemma 2 a simultaneous switch in two pairs is already possible in Desarguesian planes. The corollary below addresses the simultaneous switch in all three pairs. The respective statement can already be found in [16, p. 140, no. 5].

Corollary 1 *A Desarguesian projective plane is Pappian if and only if each Desarguesian sextuple* $(S_1,S_2,S_3,T_1,T_2,T_3)$ *remains Desarguesian after exchanging* S_i *with* T_i *for all* $i=1,2,3$.

Proof. We apply at first Lemma 3 and replace $(S_1,\dots,T_3)$ by $(S_1,T_2,T_3,T_1,S_2,S_3)$. Then the claim (note Fig. 4) follows directly from Theorem 1. □

Another characterization of Pappian planes among the Desarguesian projective planes can, e.g., be found in [3].

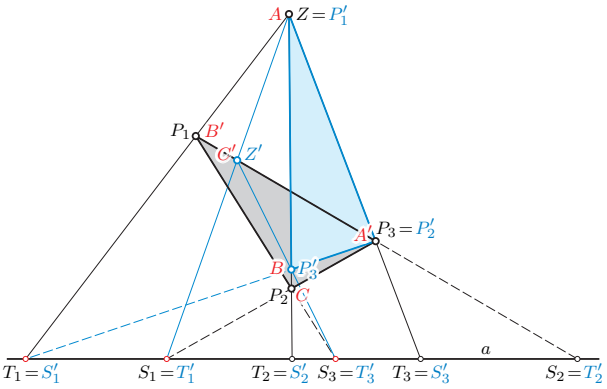

Figure 4: *Illustrating the statement of Corollary 1.*

3 Permutations in Desarguesian and in Pappian projective planes

The goal of this section is to determine for a given Desarguesian sextuple all permutations which are admissible, i.e., which preserve the property of being Desarguesian.

3.1 Non-Pappian case

Theorem 2 *If in a Desarguesian projective plane the sextuple* $(S_1,\dots,T_3)$ *is Desarguesian, then there exist at least* 24 *admissible permutations. In Pappian projective planes there exist at least* 48 *admissible permutations.*

Proof. In Desarguesian planes we can combine each permutation of the indices $1,2,3$ according to Lemm 2 with each of the permutations mentioned in Lemma 3 or with the identity.
In Pappian planes we proceed in the following way: The first three points in the sextuple define the last three since the sequence of subscripts is the same but the symbols S and T are exchanged. There are six possibilities for the sequence of indices. By virtue of Theorem 1 follows that for each symbol in the first triple we have the choice between S and T. This results in $6\cdot 2^3 = 48$ admissible permutations. In non-Pappian planes only those permutations are admissible where the first triple contains either no or exactly two T-points. □

3.2 Three instructive examples

As demonstrated in the following examples, under special conditions the number of admissible permutations can be higher than those mentioned in Theorem 2. These examples will be of fundamental importance for the proof of Theorem 3.

Example 1 Let $(S_1,\dots,T_3)$ be a Desarguesian sextuple in a Pappian Fano-plane where S_3 and T_2 are harmonic with respect to (w.r.t., for short) S_1 and T_1. What are the consequences?

The Desarguesian involution $\iota_1 : S_i \mapsto T_i$ for $i = 1,2,3$ transforms the harmonic quadruple (S_1T_1, S_3T_2) into (T_1S_1, T_3S_2). This means that the pairs (S_2,T_3) and (S_3,T_2) are corresponding under the involution ι_2 with the fixed points S_1 and T_1. The product $\iota_2\circ\iota_1$ commutes the points in the pairs (S_1,T_1), (S_2,S_3), and (T_2,T_3). Therefore, $\iota_3 := \iota_2\circ\iota_1 = \iota_1\circ\iota_2$ is again an involution and shows that the sextuple $(S_1,S_2,T_2,T_1,S_3,T_3)$ is again Desarguesian as well as $(S'_1,\dots,T'_3) = (S_1,T_2,S_3,T_1,T_3,S_2)$ (Fig. 5). These permutations are different from the 48 as mentioned in Theorem 2, since the resulting sextuples contain a pair with two S-points.
By exchanging the elements in the first pair or in the second pair, as well as by exchanging the subscripts 2 and 3, we obtain eight additional admissible permutations. On the other hand, the given harmonic position allows a simultaneous change $S_2 \leftrightarrow T_3$ and $S_3 \leftrightarrow T_2$. Thus, we end up with 16 additional admissible permutations, where (S_1,T_1) or (T_1,S_1) remains as the first pair:

$(S_1,S_2,T_2,T_1,S_3,T_3)$, $(S_1,S_3,T_3,T_1,S_2,T_2)$, $(T_1,S_2,T_2,S_1,S_3,T_3)$,
$(T_1,S_3,T_3,S_1,S_2,T_2)$, $(S_1,S_3,T_2,T_1,S_2,T_3)$, $(S_1,S_2,T_3,T_1,S_3,T_2)$,
$(T_1,S_3,T_2,S_1,S_2,T_3)$, $(T_1,S_2,T_3,S_1,S_3,T_2)$, $(S_1,T_3,S_3,T_1,T_2,S_2)$,
$(S_1,T_2,S_2,T_1,T_3,S_3)$, $(T_1,T_3,S_3,S_1,T_2,S_2)$, $(T_1,T_2,S_2,S_1,T_3,S_3)$,
$(S_1,T_2,S_3,T_1,T_3,S_2)$, $(S_1,T_3,S_2,T_1,T_2,S_3)$, $(T_1,T_2,S_3,S_1,T_3,S_2)$,
$(T_1,T_3,S_2,S_1,T_2,S_3)$.

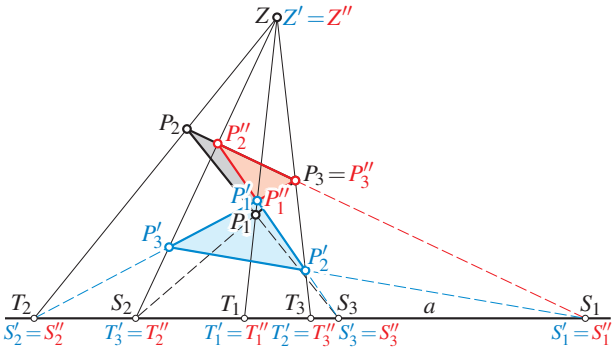

Figure 5: *A Desarguesian sextuple according to Example 1 with* $(S'_1,\dots,T'_3) = (S_1,T_2,S_3,T_1,T_3,S_2)$ *and the harmonic quadruples* (S_1T_1,S_2T_3) *and* (S_1T_1,S_3T_2) *(Type Ib in Theorem 3). After exchanging* T'_2 *and* T'_3*, we obtain a Desarguesian sextuple according to Example 2 with* $(S''_1,\dots,T''_3) = (S'_1,S'_2,S'_3,T'_1,T'_3,T'_2)$ *(Type Ia).*

Example 2 Suppose that with the Desarguesian sextuple $(S_1,\dots,T_3)$ also $(S_1,S_2,S_3,T_1,T_3,T_2)$ is Desarguesian.

Then in a Pappian Fano-plane there are two involutions, the involution ι_1 with $S_i \leftrightarrow T_i$ and ι_2 with $S_1 \leftrightarrow T_1$, $S_2 \leftrightarrow T_3$, and $S_3 \leftrightarrow T_2$. The product of these involutions sends, independent of the order, $S_1 \mapsto S_1$, $S_2 \leftrightarrow S_3$, $T_1 \mapsto T_1$, and $T_2 \leftrightarrow T_3$. Therefore this product is the involution ι_3 which keeps the points S_1 and T_1 fixed. Consequently, the pairs

(S_2,S_3) and (T_2,T_3) are in harmonic position w.r.t. (S_1,T_1) (note $(S_1',\dots,T_3')$ and $(S_1'',\dots,T_3'')$ in Fig. 5). This is sufficient, because ι_2 is the product of ι_1 and ι_3.

We have again three mutually commuting involutions like in Example 1. Indeed, we obtain the harmonic quadruples here from those in the Example 1 by exchanging the points S_2 and T_2. This can also be used to transfer the 16 additional admissible permutations from Example 1 to those of Example 2.

Example 3 Can it happen that with $(S_1,\dots,T_3)$ also $(S_1,S_2,S_3,T_3,T_1,T_2)$[2] is Desarguesian?

If both sextuples are Desarguesian, then there are two involutions involved, $\iota_1: S_i \leftrightarrow T_i$ and $\iota_2: S_1 \leftrightarrow T_3$, $S_2 \leftrightarrow T_1$, $S_3 \leftrightarrow T_2$. The product $\iota_1\circ\iota_2$ with $S_i \mapsto S_{i-1}$ and $T_j \mapsto T_{j+1}$ (subscripts modulo 3) is a cyclic projectivity with $(\iota_1\circ\iota_2)^3 = \mathrm{id}$ and $\iota_2\circ\iota_1 = (\iota_1\circ\iota_2)^{-1}$. On the other hand, there is a third involution involved: $\iota_3 := \iota_1\circ\iota_2\circ\iota_1 = \iota_2\circ\iota_1\circ\iota_2$ with $S_1 \leftrightarrow T_2$, $S_2 \leftrightarrow T_3$, $S_3 \leftrightarrow T_1$ satisfies $\iota_3^2 = (\iota_1\circ\iota_2)^3 = \mathrm{id}$. These three involutions are symmetric in the sense that for each permutation (i,j,k) of $(1,2,3)$ the transformation of ι_i by ι_j equals ι_k, i.e., $\iota_k = \iota_j\circ\iota_i\circ\iota_j$.

Necessary and sufficient for such Desarguesian sextuples in a Pappian Fano-plane is, for example, that the cross ratios $\mathrm{cr}(S_1S_2S_3T_1)$ and $\mathrm{cr}(S_3S_1S_2T_2)$ are equal[3] (see Fig. 7). The necessity follows from the projectivity $\iota_1\circ\iota_2$. Conversely, in the case of equal cross ratios there exists the projectivity $\pi: S_i \mapsto S_{i-1}$, $T_1 \mapsto T_2$. If $\iota_1: S_i \leftrightarrow T_i$ is an involution, then $\iota_1\circ\pi$ maps $S_1 \mapsto T_3$, $S_2 \mapsto T_1$, $S_3 \mapsto T_2$, and $T_1 \mapsto S_2$. Therefore $\iota_1\circ\pi$ is an involution and equal to ι_2 which guarantees the requested Desarguesian sextuple.

Due to $\iota_3 = \iota_1\circ\iota_2\circ\iota_1$, also $(S_1,S_2,S_3,T_2,T_3,T_1)$ is Desarguesian (Fig. 7). By virtue of Lemma 2 and Theorem 1, there exist at least 96 additional admissible permutations.

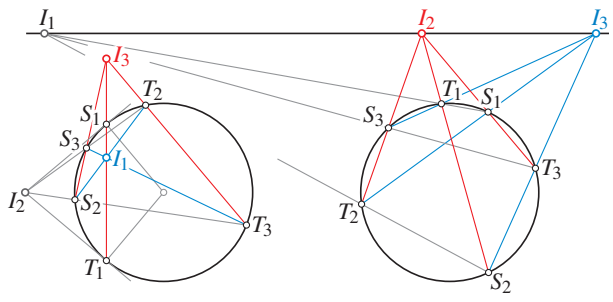

Figure 6: *Suppose that the axis a as carrier of the Desarguesian sextuple $(S_1,\dots,T_3)$ is stereographically projected on a conic. Then the points I_1,I_2,I_3 are the respective centers of the involutions ι_1,ι_2,ι_3 as used in Example 1 (left, Type Ib) and in Example 3 (right, Type IIa).*

At the examples above, the involutions ι_1, ι_2 and ι_3 act on the points $S_1,\dots,T_3$ of the axis a. If the involutions are shown in an isomorphic model on a conic, then each involution ι_j is represented by a center of involution I_j, the common point of the chords connecting corresponding points (see, e.g., [7, p. 251]). Figure 6 shows the involved centers I_1,I_2,I_3 in the Examples 1 and 2 on the left and that of Example 3 on the right.

3.3 Conditional cases in Pappian planes

Theorem 3 *Given a Pappian Fano-plane, then for each permutation of six elements there exist Desarguesian sextuples which remain Desarguesian under the permutation. Beside the 48 admissible permutations of the Desarguesian sextuple $(S_1,\dots,T_3)$ according to Theorem 2 we distinguish two types of permutations which are admissible under special conditions.*

Type I, *the permutation fixes one unordered pair of the given Desarguesian sextuple $(S_1,\dots,T_3)$: Then, in the permuted sextuple the remaining pairs are either (a) of the form (S_i,T_j) in any order, or (b) they contain a pair (S_i,S_j). After appropriate relabeling this yields either*

Type Ia: $(S_1,S_2,S_3,T_1,T_3,T_2)$ *(note Example 2) or*

Type Ib: $(S_1,T_2,S_3,T_1,T_3,S_2)$ *(Example 1, Fig. 6).*

Referring to the first case Ia, $(S_1,S_2,S_3,T_1,T_3,T_2)$ is Desarguesian if and only if (S_1,T_1) separates the pairs (S_2,S_3) and (T_2,T_3) harmonically. On the other hand, the sextuple Ib $(S_1,T_2,S_3,T_1,T_3,S_2)$ is Desarguesian if and only if (S_1,T_1) separates (S_2,T_3) and (S_3,T_2) harmonically. The latter sextuple can be converted into the first one by exchanging S_2 with T_2.

Type II, *no unordered pair of the given Desarguesian sextuple $(S_1,\dots,T_3)$ remains fixed under the permutation: Then, in the permuted sextuple the pairs are either (a) of the form (S_i,T_j), or (b) they contain a pair (S_i,S_j). There is a numbering such that we obtain either*

Type IIa: $(S_1,S_2,S_3,T_3,T_1,T_2)$ *(Example 3) or*

Type IIb: $(S_1,T_2,S_3,T_3,T_1,S_2)$.

Necessary and sufficient for the first sextuple IIa being Desarguesian is that there are equal cross ratios $\mathrm{cr}(S_1S_2S_3T_1) = \mathrm{cr}(S_3S_1S_2T_2)$. In the second case IIb the permutation is admissible if and only if $\mathrm{cr}(S_1T_2S_3T_1) = \mathrm{cr}(S_3S_1T_2S_2)$. Again, the second sextuple arises from the first one by exchanging S_2 with T_2.

Proof. Due to Lemma 1 and Theorem 1, in Pappian planes the Desarguesian sextuples remain Desarguesian if the order of the included pairs or the order in the pairs changes. For each permutation of the six points $(S_1,\dots,T_3)$ which keeps one pair fixed we can assume that this pair is (S_1,T_1).

[2] Note that here the permutation $(3,1,2)$ of the subscripts at the T-points is even. In comparison, the permutation $(1,3,2)$ in Example 2 is odd.

[3] This condition is not unique. It is easy to find other point quadruples with the property that the equality of their cross ratios guarantees that the requested permutation is admissible.

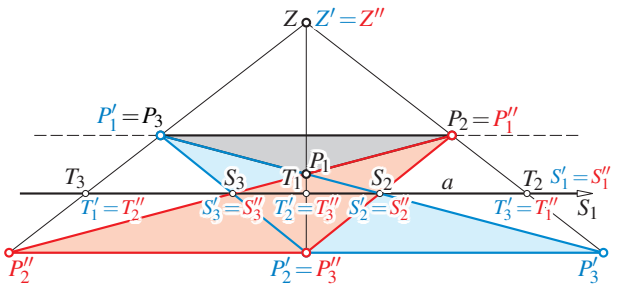

Figure 7: *Particular case according to Example 3 with* $(S_1',\dots,T_3') = (S_1,S_2,S_3,T_3,T_1,T_2)$ *(Type IIa) and* $(S_1'',\dots,T_3'') = (S_1,S_2,S_3,T_2,T_3,T_1)$ *where* S_1 *is a point at infinity. The depicted sextuple* $(S_1,\dots,T_3)$ *satisfies also the conditions for Type Ia from Theorem 3, for example with the triangle* $P_2'P_1'P_2$.

If the other pairs in the permuted sextuple are of the form (S_i,T_j) with $i \neq j$ (Type Ia), then they can be assumed as (S_2,T_3) and (S_3,T_2). The sextuple $(S_1,S_2,S_3,T_1,T_3,T_2)$ was analyzed in Example 2 under the condition that the Fano axiom holds. If one pair in the permuted sextuple is of the form (S_i,S_j) (Type Ib), then there is a particular numbering which yields $(S_1,T_2,S_3,T_1,T_3,S_2)$ as treated in Example 1.
The permutations of Type II are characterized by the condition that no unordered pair (S_i,T_i) is preserved. In the case (a) all pairs are supposed to be of the form (S_i,T_j) with $i \neq j$. Then there is a particular numbering such that the permuted sextuple is $(S_1,S_2,S_3,T_3,T_1,T_2)$ as analyzed in Example 3. If the permuted sextuple contains a pair of two S-points, then it contains also a pair of two T-points and a mixed pair (Type IIb). Hence, we can assume a numbering such that the permuted sextuple is $(S_1,T_2,S_3,T_3,T_1,S_2)$, which arises from Type IIa by exchanging S_2 and T_2. □

Remark 2 *A count in Pappian Fano-planes reveals: For sextuples of Type I there exist at least 64 additional admissible permutations. Sextuples of Type II have at least 144 additional admissible permutations.*
Beside the 48 admissible permutations for generic Desarguesian sextuples, there exist 144 admissible permutations for Desarguesian sextuples which satisfy the harmonic positions of the Type Ia and as many for the Type Ib. There are 96 permutations corresponding to Desarguesian sextuples of Type IIa and 288 of Type IIb.

The sextuple depicted in Fig. 7 satisfies simultaneously the conditions for Type IIa (Example 3) and Ia (Example 2). This means that $\mathrm{cr}(S_1S_2S_3T_1) = \mathrm{cr}(S_3S_1S_2T_2)$ and (S_1T_1,S_2S_3) as well as (S_1T_1,T_2T_3) are harmonic quadruples.
For sextuples which are simultaneously of the Types IIa and Ib, the cross ratio $\delta := \mathrm{cr}(S_1S_2S_3T_1) = \mathrm{cr}(S_3S_1S_2T_2)$ has to satisfy $\mathrm{cr}(S_1T_1S_3T_2) = -1$, hence $\mathrm{cr}(S_1S_3T_1T_2) = 2$ and $\mathrm{cr}(S_1S_3S_2T_1) = 1-\delta$, and as the product $\mathrm{cr}(S_1S_3S_2T_2) = 2(1-\delta) = \frac{1}{\delta}$. This results in the quadratic condition $2\delta^2 - 2\delta + 1 = 0$ which has no solution in the real projective plane.
Since exchanging S_2 and T_2 means a switch between the Types Ia and Ib as well as between IIa and IIb, Fig. 7 can easily be converted into an example which satisfies the conditions of the Types Ib and IIb. On the other hand, no real sextuple can simultaneously satisfy the conditions of the Types Ia and IIb.

4 Analytic characterizations of Desarguesian sextuples

4.1 Non-Pappian plane

In Desarguesian projective coordinate planes the points X are one-dimensional subspaces $\mathbf{x}\mathbb{F}$ of a three-dimensional right vector space over a (not necessarily commutative) field $\mathbb{F}$. The question arises what replaces the Desarguesian involution in non-Pappian planes?

Theorem 4 *The sextuple* $(\mathbf{s}_1\mathbb{F},\dots,\mathbf{t}_3\mathbb{F})$ *of mutually different points in a Desarguesian projective plane is Desarguesian if and only if there is a representation which satisfies* $\mathbf{s}_1+\mathbf{s}_2+\mathbf{s}_3 = \mathbf{0}$ *and*

$$\mathbf{t}_1 = \mathbf{s}_2\lambda_3 - \mathbf{s}_3\lambda_2,\ \mathbf{t}_2 = \mathbf{s}_3\lambda_1 - \mathbf{s}_1\lambda_3,\ \mathbf{t}_3 = \mathbf{s}_1\lambda_2 - \mathbf{s}_2\lambda_1 \quad (1)$$

for some $\lambda_1,\lambda_2,\lambda_2 \in \mathbb{F}\setminus\{0\}$.

Proof. (i) We begin with an analytic standard proof of Desargues's theorem: If the triangles $\mathbf{p}_1\mathbb{F}\,\mathbf{p}_2\mathbb{F}\,\mathbf{p}_3\mathbb{F}$ and $\mathbf{q}_1\mathbb{F}\,\mathbf{q}_2\mathbb{F}\,\mathbf{q}_3\mathbb{F}$ are perspective w.r.t. the point $\mathbf{z}\mathbb{F}$, then we can assume

$$\mathbf{p}_1+\mathbf{q}_1 = \mathbf{p}_2+\mathbf{q}_2 = \mathbf{p}_3+\mathbf{q}_3 = \mathbf{z}.$$

Hence, the intersection points between corresponding sides have coordinate vectors

$$\mathbf{s}_1 = \mathbf{p}_2-\mathbf{p}_3 = \mathbf{q}_3-\mathbf{q}_2,\ \mathbf{s}_2 = \mathbf{p}_3-\mathbf{p}_1 = \mathbf{q}_1-\mathbf{q}_3,$$
$$\mathbf{s}_3 = \mathbf{p}_1-\mathbf{p}_2 = \mathbf{q}_2-\mathbf{q}_1.$$

They satisfy $\mathbf{s}_1+\mathbf{s}_2+\mathbf{s}_3 = \mathbf{0}$, which expresses their collinearity.
The three vectors $(\mathbf{p}_1,\mathbf{p}_2,\mathbf{p}_3)$ form a basis of our vector space. Hence, there are scalars $\lambda_1,\lambda_2,\lambda_3 \in \mathbb{F}$ such that

$$\mathbf{z} = \mathbf{p}_1\lambda_1 + \mathbf{p}_2\lambda_2 + \mathbf{p}_3\lambda_3.$$

Since $\mathbf{z}\mathbb{F}\,\mathbf{p}_1\mathbb{F}\mathbf{p}_2\mathbb{F}\mathbf{p}_3\mathbb{F}$ is supposed to form a quadrangle, we have $\lambda_1\lambda_2\lambda_3 \neq 0$. This representation of $\mathbf{z}$ implies for the intersection point $\mathbf{t}_1\mathbb{F}$ between the lines $[Z,P_1]$ and $[S_2,S_3]$ a solution

$$\mathbf{t}_1 = \mathbf{s}_2\lambda_3 - \mathbf{s}_3\lambda_2,$$

since $\mathbf{t}_1$ is a linear combination of $\mathbf{s}_2$ and $\mathbf{s}_3$, and on the other hand

$$\begin{aligned}\mathbf{t}_1 &= \mathbf{z} - \mathbf{p}_1(\lambda_1+\lambda_2+\lambda_3)\\ &= (\mathbf{p}_2-\mathbf{p}_1)\lambda_2 + (\mathbf{p}_3-\mathbf{p}_1)\lambda_3 = \mathbf{s}_2\lambda_3 - \mathbf{s}_3\lambda_2.\end{aligned}$$

(ii) For proving the converse, we follow the computation in the reverse order: Let the vectors $\mathbf{s}_1,\dots,\mathbf{t}_3$ with $\mathbf{s}_1+\mathbf{s}_2+\mathbf{s}_3=\mathbf{0}$ be given according to (1). We specify any point $\mathbf{p}_1\mathbb{F}$ outside the line $[S_2,S_3]$ and define $\mathbf{p}_2 := \mathbf{p}_1 - \mathbf{s}_3$ and $\mathbf{p}_3 := \mathbf{s}_2+\mathbf{p}_1$. This implies $\mathbf{p}_2-\mathbf{p}_3 = -\mathbf{s}_3-\mathbf{s}_2 = \mathbf{s}_1$ and defines a triangle $\mathbf{p}_1\mathbb{F}\ \mathbf{p}_2\mathbb{F}\ \mathbf{p}_3\mathbb{F}$ with sides passing through the respective points $\mathbf{s}_i\mathbb{F}$ for $i=1,2,3$. We can verify that the point $\mathbf{z}\mathbb{F}$ with $\mathbf{z} := \mathbf{p}_1\lambda_1+\mathbf{p}_2\lambda_2+\mathbf{p}_3\lambda_3$ lies aligned with $\mathbf{t}_i\mathbb{F}$ and $\mathbf{p}_i\mathbb{F}$ for each i, thus confirming that the sextuple $(\mathbf{s}_1\mathbb{F},\dots,\mathbf{t}_3\mathbb{F})$ is Desarguesian. □

4.2 Pappian plane

In Pappian planes the underlying field $\mathbb{F}$ is commutative. Then, in the representations (1) of the three vectors $\mathbf{t}_1$, $\mathbf{t}_2$ and $\mathbf{t}_3$ as linear combinations of respectively two $\mathbf{s}$-vectors, the product $\lambda_3\lambda_1\lambda_2$ of the coefficients of the first terms equals the negative product of those of the second terms. This can be generalized.

Lemma 4 *In a Pappian projective plane, let* $(\mathbf{s}_1\mathbb{F},\dots,\mathbf{t}_3\mathbb{F})$ *be a sextuple of mutually different collinear points. Then this sextuple is Desarguesian if and only if for the representation*

$$\begin{aligned}\mathbf{t}_1 = \mathbf{s}_2\mu_{12}+\mathbf{s}_3\mu_{13},\quad \mathbf{t}_2 = \mathbf{s}_3\mu_{23}+\mathbf{s}_1\mu_{21},\\ \mathbf{t}_3 = \mathbf{s}_1\mu_{31}+\mathbf{s}_2\mu_{32}\end{aligned} \tag{2}$$

holds

$$\mu_{12}\mu_{23}\mu_{31} = -\mu_{13}\mu_{21}\mu_{32}. \tag{3}$$

Proof. The equality (3) of the products of coefficients remains valid when the vectors $\mathbf{s}_i$ or $\mathbf{t}_j$ are replaced by multiples $\mathbf{s}_i^* := \mathbf{s}_i\alpha_i$ or $\mathbf{t}_j^* := \mathbf{t}_j\beta_j$ with $\alpha_i,\beta_j \in \mathbb{F}\setminus\{0\}$. Hence, it means no restriction to assume a representation with $\mathbf{s}_1+\mathbf{s}_2+\mathbf{s}_3=\mathbf{0}$. Then, the representation (1) in Theorem 4 implies the equation (3) for Desarguesian sextuples. Since the six points are supposed to be mutually different, the products in (3) cannot vanish.
Conversely, we replace in (2) $\mathbf{t}_2$ by $\mathbf{t}_2^* := -\mathbf{t}_2\mu_{21}^{-1}\mu_{12}$ and $\mathbf{t}_3$ by $\mathbf{t}_3^* := -\mathbf{t}_3\mu_{31}^{-1}\mu_{13}$ while $\mathbf{t}_1^* := \mathbf{t}_1$. Moreover, let μ_{ij}^* denote the coefficients in the representations of $\mathbf{t}_1^*$, $\mathbf{t}_2^*$ and $\mathbf{t}_3^*$ analogue to (2). Then holds $\mu_{21}^*+\mu_{12}^* = \mu_{31}^*+\mu_{13}^* = 0$ and therefore, as a consequence of $\mu_{12}^*\mu_{23}^*\mu_{31}^* = -\mu_{13}^*\mu_{21}^*\mu_{32}^*$, also $\mu_{32}^*+\mu_{23}^*=0$. Thus, the representation of the $\mathbf{t}_i^*$ satisfies the conditions in (1), and Theorem 4 confirms that the sextuple is Desarguesian. □

How can Desarguesian sextuples be characterized in terms of coordinates on the axis a? For this purpose we introduce homogeneous coordinates on a in the form $\mathbf{t}_i := (\tau_{i0},\tau_{i1})^T$ and $\mathbf{s}_j := (\sigma_{j0},\sigma_{j1})^T$. Note that from now on $\mathbf{t}_i$ and $\mathbf{s}_j$ stand for two-dimensional vectors over $\mathbb{F}$. In order to obtain a representation $\mathbf{t}_i = \mathbf{s}_j\mu_{ij}+\mathbf{s}_k\mu_{ik}$ for all cyclic permutations (i,j,k) of $(1,2,3)$, we use Cramer's rule and solve the system

$$\mu_{ij}\begin{pmatrix}\sigma_{j0}\\ \sigma_{j1}\end{pmatrix} + \mu_{ik}\begin{pmatrix}\sigma_{k0}\\ \sigma_{k1}\end{pmatrix} = \begin{pmatrix}\tau_{i0}\\ \tau_{i1}\end{pmatrix}$$

by

$$\mu_{ij} = \frac{\det(\mathbf{t}_i\,\mathbf{s}_k)}{\det(\mathbf{s}_j\,\mathbf{s}_k)},\ \mu_{ik} = \frac{\det(\mathbf{s}_j\,\mathbf{t}_i)}{\det(\mathbf{s}_j\,\mathbf{s}_k)}.$$

From (3) follows the characterization

$$\begin{aligned}&\det(\mathbf{t}_1\,\mathbf{s}_2)\det(\mathbf{t}_2\,\mathbf{s}_3)\det(\mathbf{t}_3\,\mathbf{s}_1)\\ =\ &\det(\mathbf{t}_1\,\mathbf{s}_3)\det(\mathbf{t}_2\,\mathbf{s}_1)\det(\mathbf{t}_3\,\mathbf{s}_2).\end{aligned} \tag{4}$$

For the sake of simplicity, let us assume that neither any τ_{i1} nor any σ_{j1} vanishes. Then we can use inhomogeneous coordinates $t_i = \tau_{i0}/\tau_{i1}$ for T_i and $s_j := \sigma_{j0}/\sigma_{j1}$ for S_j so that $\det(\mathbf{t}_i\,\mathbf{s}_j) = t_i - s_j$. Thus we can rewrite (4) as a product of affine ratios

$$\operatorname{ar}(S_2,S_3,T_1)\cdot\operatorname{ar}(S_3,S_1,T_2)\cdot\operatorname{ar}(S_1,S_2,T_3) = 1, \tag{5}$$

where $\operatorname{ar}(S_i,S_j,T_k) = (s_i-t_k)/(s_j-t_k)$. The equation (5) reminds on Menelaos's theorem characterizing the collinearity of three points T_1,T_2,T_3 on the respective side lines of the triangle $S_1S_2S_3$.
Finally, equation (5) is equivalent to[4]

$$\begin{aligned}(s_1+t_1)(s_2t_2-s_3t_3)+(s_2+t_2)(s_3t_3-s_1t_1)\\ +(s_3+t_3)(s_1t_1-s_2t_2) = 0.\end{aligned} \tag{6}$$

By the way, in (5) we may exchange S_i with T_i for some $i\in\{1,2,3\}$. This yields three other equivalent equations

$$\begin{aligned}&\operatorname{ar}(S_2,S_3,S_1)\cdot\operatorname{ar}(S_3,T_1,T_2)\cdot\operatorname{ar}(T_1,S_2,T_3)\\ =\ &\operatorname{ar}(T_2,S_3,T_1)\cdot\operatorname{ar}(S_3,S_1,S_2)\cdot\operatorname{ar}(S_1,T_2,T_3)\\ =\ &\operatorname{ar}(S_2,T_3,T_1)\cdot\operatorname{ar}(T_3,S_1,T_2)\cdot\operatorname{ar}(S_1,S_2,S_3) = 1.\end{aligned}$$

If the underlying plane is a Fano-plane, then the existence of an involution with $S_i \mapsto T_i$ for $i=1,2,3$ and a corresponding nontrivial symmetric bilinear form are equivalent to the condition

$$\det\begin{pmatrix}1 & s_1+t_1 & s_1t_1\\ 1 & s_2+t_2 & s_2t_2\\ 1 & s_3+t_3 & s_3t_3\end{pmatrix} = 0. \tag{7}$$

At the same token, the characterizations in (4), (5) or (6) could also be used to deduce the particular cases with additional admissible permutations as listed in Theorem 3.

[4] Desarguesian sextuples are a refinement of quadrangular sets (note Remark 1) due to the distinction between S- and T-points. By virtue of Theorem 1, this distinction becomes obsolete in Pappian planes. Therefore the equations (4), (5) and (6) can already be found in the literature as characterizations of quadrangular sets in Pappian Fano-planes, e.g., in [17, Sect. 8]. However, our approach is different.

References

[1] BALTUS, C., *Collineations and Conic Sections*, Springer, 2020, https://doi.org/10.1007/978-3-030-46287-1

[2] BLATTNER, J.W., *Projective Plane Geometry*, Holden-Day Inc., San Francisco, 1968.

[3] BOTTEMA, O., Eine Bemerkung über den Desarguesschen und den Pascalschen Satz, *Math. Ann.* **111** (1935), 68–70, https://doi.org/10.1007/BF01472203

[4] BRAUNER, H., *Geometrie Projektiver Räume I, II*, Bibliographisches Institut, Wien, Zürich, 1976.

[5] COXETER, H.S.M., *Projective Geometry*, Springer-Verlag, New York, 2003.

[6] CRONHEIM, A., A proof of Hessenberg's Theorem, *Amer. Math. Monthly* **4**(2) (1953), 219–221.

[7] GLAESER, G., STACHEL, H., ODEHNAL, B., *The Universe of Conics*, Springer Spektrum, Heidelberg, 2016.

[8] FAULKNER, J.R., Lines with quadrangle section, *J. Geom.* **22** (1984), 31–46, https://doi.org/10.1007/BF01230122

[9] FAULKNER, J.R., *The Role of Nonassociative Algebra in Projective Geometry*, American Mathematical Society, Providence, 2014.

[10] HARTSHORNE, R., *Foundations of Projective Geometry*, W.A. Benjamin Inc., New York, 1967.

[11] HESSENBERG, G., Beweis des Desarguesschen Satzes aus dem Pascalschen, *Math. Ann.* **61** (1905), 161–172.

[12] HILBERT, D., *Grundlagen der Geometrie*, (In Festschrift zur Enthüllung des Gauss-Weber Denkmals in Göttingen), B.G. Teubner, Leipzig (1899), Second edition: B.G. Teubner, Leipzig, 1903.

[13] MARCHISOTTO, E.A., The Theorem of Pappus: A Bridge Between Algebra and Geometry, *Amer. Math. Monthly* **109**(6) (2002), 497–516, https://doi.org/10.1080/00029890.2002.11919880

[14] PAMBUCCIAN, V., SCHACHT, C., The axiomatic destiny of the theorems of Pappus and Desargues, In: S.G. Dani, A. Papadopoulos (eds.), *Geometry in History*, 355–399, Springer, Cham, 2019, https://doi.org/10.1007/978-3-030-13609-3_8

[15] PEDOE, D., *An Introduction to Projective Geometry*, A Pergamon Press Book, Oxford, 1963.

[16] PICKERT, G., *Projektive Ebenen*, 2. Aufl., Springer-Verlag, Berlin, Heidelberg, New York, 1975, https://doi.org/10.1007/978-3-642-66148-8

[17] RICHTER-GEBERT, J., *Perspectives on Projective Geometry*, Springer-Verlag, Berlin, Heidelberg, 2011, https://doi.org/10.1007/978-3-642-17286-1

[18] SEIDENBERG, A., Pappus Implies Desargues, *Amer. Math. Monthly* **83**(3) (1976), 190–192, https://doi.org/10.2307/2977023

[19] VEBLEN, O., YOUNG, J.W., *Projective Geometry.* Vol. I, Ginn and Company, Boston, New York, Chicago, London, 1910.

[20] VOLKERT, K. (ED.), *David Hilbert – Grundlagen der Geometrie (Festschrift 1899)*, Springer-Spektrum, Berlin Heidelberg, 2015, https://doi.org/10.1007/978-3-662-45569-2

Konstantinos Myrianthis
orcid.org/0009-0000-8680-8948
e-mail: myrian@ath.forthnet.gr

58, Zan Moreas street, 15231 Athens, Greece

Hellmuth Stachel
orcid.org/0000-0001-5300-4978
e-mail: stachel@dmg.tuwien.ac.at

Vienna University of Technology
Wiedner Hauptstr. 8-10/104, 1040 Wien, Austria

https://doi.org/10.31896/k.28.2
Original scientific paper
Accepted 21. 8. 2024.

GUNTER WEISS
BORIS ODEHNAL

Miquel's Theorem and its Elementary Geometric Relatives

Miquel's Theorem and its Elementary Geometric Relatives

ABSTRACT

The elementary geometric Miquel theorem concerns a triangle $\triangle ABC$ and points R, S, T on its sides, and it states that the circles $k(ART)$, $k(BRS)$, $k(CST)$ have a common point M, the Miquel point to these givens. Choosing R, S, T in special ways one receives the so-called *beermat theorem*, the *Brocard theorems*, and the *Steiner Simson-Wallace theorem* as special cases of Miquel's theorem. Hereby facts connected with Brocard's theorem follow from properties of Miquel's theorem. If e.g. R, S, T fulfill the Ceva condition, Miquel's construction induces a mapping of the Ceva point to the Miquel point. We discuss this and other mappings, which are natural consequences of Miquel's theorem. Furthermore, if the points R, S, T run through the sides of $\triangle$ such that e.g. the affine ratios $\mathrm{ar}(ARB)$, $\mathrm{ar}(BSC)$, $\mathrm{ar}(CTA)$ are equal, then the corresponding Miquel points M run through the circumcircle of the triangle formed by the Brocard points and the circumcenter of $\triangle$. Besides these three remarkable points of $\triangle$, this circle contains several other triangle centers. Even though most of the presented topics are well-known, their mutual connections seem to be not yet considered in standard references on triangle geometry and therefore might justify an additional treatment.

Key words: Miquel's theorem, Brocard's theorems, theorems of Steiner and Simson-Wallace

MSC2010: 51M04, 51N15

Miquelov teorem i njegovi elementarnogeometrijski srodnici

SAŽETAK

Elementarnogeometrijski Miquelov teorem odnosi se na trokut $\triangle ABC$ i točke R, S, T na njegovim stranicama, i kaže da kružnice $k(ART)$, $k(BRS)$, $k(CST)$ imaju jednu zajedničku točku M, Miquelovu točku zadane figure. Posebnim odabirom točaka R, S, T dobivaju se takozvani *beermat teorem*, *Brocardovi teoremi* i *Steinerov Simson-Wallaceov teorem* kao specijalni slučajevi Miquelovog teorema. Stoga, činjenice vezane za Brocardov teorem slijede iz svojstava Miquelovog teorema. Ako npr. R, S, T zadavoljavaju Cevin uvjet, Miquelova konstrucija inducira preslikavanje Cevine točke u Miquelovu točku. Proučavamo ovo i druga preslikavanja koja su direktna posljedica Miquelovog teorem. Nadalje, kreću li se točke R, S, T stranicama trokuta tako da su npr. afini omjeri $\mathrm{ar}(ARB)$, $\mathrm{ar}(BSC)$, $\mathrm{ar}(CTA)$ jednaki, Miquelove točke M opisuju kružnicu opisanu trokutu čiji su vrhovi dvije Brocardove točke i središte opisane kružnice trokuta. Osim spomenutih triju posebnih točaka trokuta, na ovoj kružnici leži još nekoliko osobitih točaka trokuta. Iako je većina predstavljenih tema dobro poznata, čini se da njihove međusobne veze još nisu razmatrane u standardnoj literaturi iz geometrije trokuta i stoga bi mogle opravdati dodatnu obradu.

Ključne riječi: Miquelov teorem, Brocardovi teoremi, Steinerovi Simson-Wallaceovi teoremi

1 Introduction

In 1838 Auguste Miquel (1816-1851) published a theorem (see [10]), which later on was called after him and got the meaning of an important axiom in circle geometries, see e.g. [2]. (In [11] it is mentioned, that this remarkable incidence was known already since 1804.) The elementary geometric version of Miquel's theorem concerns a triangle $\triangle ABC$ and an inscribed triangle $\triangle RST$, and it states that the circles $k(ART)$, $k(BRS)$, $k(CST)$ have a common point M, the *Miquel point* to these givens, see Fig. 1. For M there exists a two-parametric set of possibilities, such that there is a one-parameter family of triplets R, S, T to a given point M. The consequences of this fact are properties of the Miquel configuration and *Miquel mappings*, which seemingly are not yet considered. This will be treated in Chapter 2.
Obviously, when choosing R, S, T dependent (e.g. collinear or infinitesimally close to the vertices A, B, C), the cor-

responding Miquel point M will get special meanings and connect Miquel's theorem to e.g. that of Steiner and Simson-Wallace resp. to Brocard's theorems. The well-known *beer-mat theorem* and it's reverse, the *three circle theorem*, is a relative of Miquel's theorem, too. We dedicate Chapter 3 to these rather well-known 2-dimensional cases.

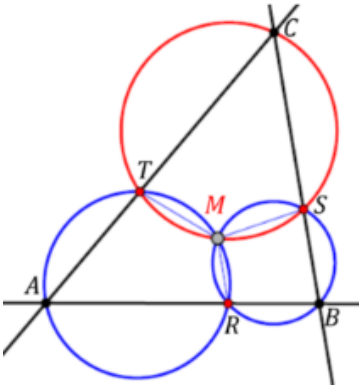

Figure 1: *Elementary geometric version of Miquel's theorem*

If the points R, S, T run through the sides of $\triangle$ such that e.g. the affine ratios $ar(ARB)$, $ar(BSC)$, $ar(CTA)$ are equal, then the corresponding Miquel points M run through the circumcircle of the triangle formed by the Brocard points and the circumcenter of $\triangle$. Besides these three remarkable points of $\triangle$, this circle contains several other triangle centers. This will be the content of Chapter 4. Here, we refrain from presenting further generalizations, as, for example, using congruent point series on the sides of $\triangle$ or cross ratios instead of the affine ratios. This will be treated at another occasion.

Finally, it is well-known that the theorem of Miquel holds in classical circle geometries, but it also holds in affine normed planes, while it is not true in an elliptic or hyperbolic plane. We show some examples in Chapter 5.

2 Properties of elementary geometric Miquel figures

2.1 Miquel stars to a given triangle

To an arbitrarily chosen point M, we construct the feet R, S, T on the sides of $\triangle ABC$. The Miquel circles $k(ART)$, $k(BRS)$, $k(CST)$ then are the Thales circles over segments $[MA]$, $[MB]$, $[MC]$, and M is indeed their common intersection. Therewith, as the lines RM, SM, TM are parallel to the altitudes of $\triangle ABC$, they include angles $\angle RMT = \pi - \alpha$, $\angle RMS = \pi - \beta$, $\angle SMT = \pi - \gamma$, see Fig. 2. Choosing another point $R' \in AB$ leads to Miquel circles $k(AR'M)$, $k(BR'M)$, which intersect BC in S' and CA in T', see Fig. 2.

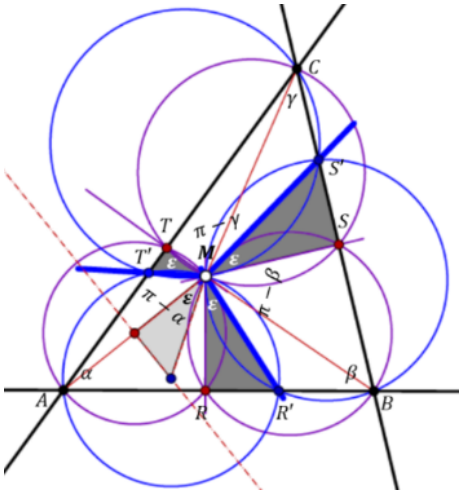

Figure 2: *The triples (R,S,T), (R',S',T'), belonging to a fixed Miquel point M define congruent Miquel stars.*

For quadrangles inscribed into these circles, opposite angles must sum up to π, and therefore $\sphericalangle RMR' = \sphericalangle SMS' = \sphericalangle TMT'$. In the following we use

Definition 1 *Let M be the Miquel point of a triangle $\triangle ABC$ to R', S', T'. The triplet of half-lines (MR', MS', MT') is called the Miquel star associated with the point M.*

For Miquel stars the following holds

Theorem 1 *If R' runs through AB, the Miquel star rotates about M with angle ε. The Miquel stars to different Miquel points are congruent, i.e. the angles enclosed by any pair of half-lines are equal.*

The content of Theorem 1 relates to generalizations of Wallace's theorem, see [11]. The vertex triplets R', S', T', belonging to a given Miquel-point M, form triangles, the sides of which envelop three parabolas with common focus M. (This follows from the projectivity between e.g. $R' \in AB \mapsto S' \in BC$.) The trilateral of vertex-tangents of the parabolas has the pedal points R, S, T of M for its vertices, and the directrices pass through the reflection images R'', S'', T'' of M in the sides of $\triangle ABC$, see Fig. 3. Therewith follows

Theorem 2 *Let M be given and let R' run through AB. Then the sides of $\triangle R'S'T'$ envelop three parabolas with common focus M. Their common chords form a complete quadrangle consisting of the incenter I and the excenters of $\triangle R''S''T''$. (R'', S'', T'' are the images of reflections of M in the sides of $\triangle ABC$, and $\triangle R''S''T''$ consists of the directrix lines of the above mentioned parabolas.)*

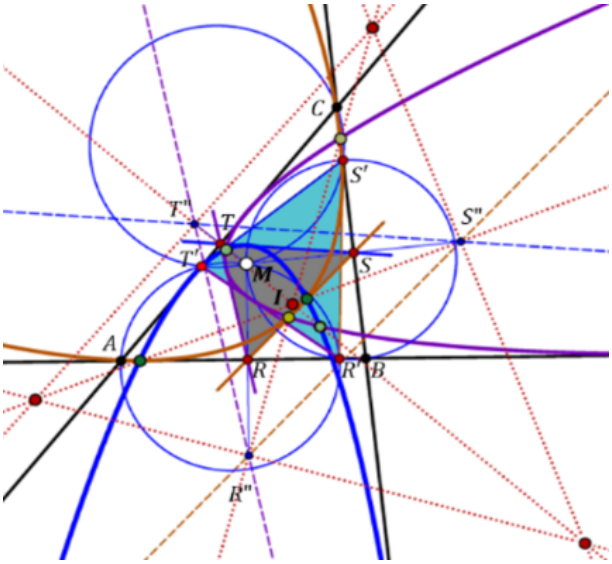

Figure 3: *The sides of $\triangle R'S'T'$ envelop three parabolas with common focus M. Their common cords form a complete quadrangle.*

2.2 A first Miquel mapping

The chords through the real intersection points of pairs of parabolas turn out to be the interior angle bisectors of triangle $R''S''T''$. Therefore, the common intersection point I of the three cords is the incenter of $R''S''T''$. As two parabolas intersect (in algebraic sense) in 4 points, there must exist, for our three parabolas, a complete quadrangle formed by six chords, see Fig. 3. It is near laying that the outer chords then must be the second angle bisectors of $R''S''T''$ and deliver the excenters. It makes sense to define a *first Miquel mapping*:

Definition 2 *Given a triangle $\triangle ABC$ and an arbitrarily given point M. Reflecting M in the sides of $\triangle ABC$ delivers a triangle $R''S''T'' =: \triangle''$. The first Miquel mapping μ_1 to $\triangle ABC$ maps the point M to the incenter I of the reflection triangle $\triangle''$ of M.*

Remark 1 *When we choose R, T, S as (collinear) ideal points, then the three degenerate Miquel circles consist of a side of $\triangle ABC$ together with the ideal line. The ideal line is therefore a common one-dimensional component and a Miquel point M is not defined. But when we choose an ideal point as Miquel point, points R'', S'', T'' are constructible, as reflections, extended to ideal points, act as harmonic homologies. Incenter and excenters to this degenerate ideal triangle $\triangle''$ are not defined. The triangle $\triangle''$ collapses, too, if M is a point of the circumcircle c of $\triangle ABC$. Let $M \in c\backslash\{A,B,C\}$, then $R'' \neq S'' \neq T'' \neq R''$ are collinear and define a segment bounded by two of the points R'', S'', T'', while the third, inner point, can act as limit of the incenter I of $\triangle''$. (The limits of the excenters E_i are the other two vertices plus the ideal point of the direction orthogonal to line $R''S''$. Therefore, the exceptional set for the first Miquel mapping μ_1 consist of $\{A,B,C\}$ alone.*

Without calculation, by arguments of elementary geometry and chains of projectivities, we find that

- the orthocenter O and the vertices A, B, C are fixed points of the first Miquel mapping μ_1,
- a point M at the circumcircle c of $\triangle$ is mapped to a point I on one of the circular arcs (AOB), (BOC), (COA) of circles congruent to c, (obviously, the triangles $\triangle''$ then collapse to lines through O), see Fig. 4,
- if M traverses through a side of $\triangle$, e.g. through AC, then I runs along conic arcs through A and C, see Fig. 5a. Here I and one excenter E_i swap their meaning for inner resp. outer points M of the segment $[A,C]$. The pairs (I,E_1), (E_2,E_3) run through two conics.

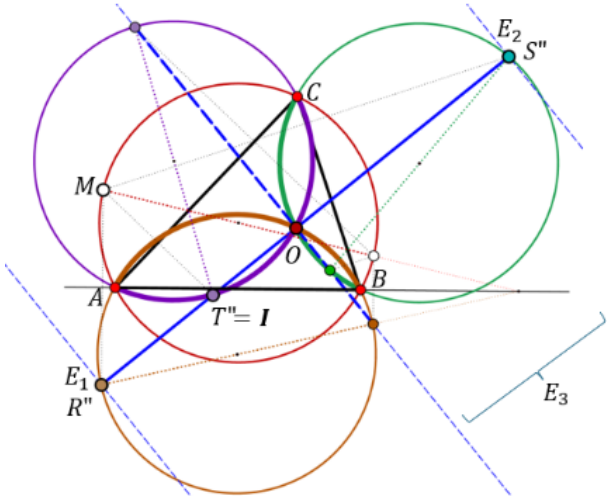

Figure 4: *The first Miquel-mapping μ_1 maps a point M on the circumcircle c to a point I on one of the circular arcs AOB, BOC, COA of circles congruent to c. The "excenters" trace the remaining arcs of these circles plus the ideal line. The orthocenter O and A, B, C are mapped to themselves.*

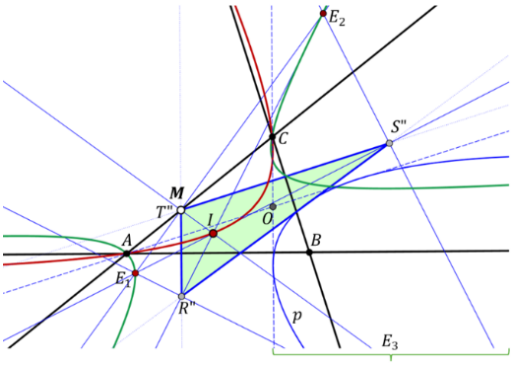

Figure 5a: *If M runs through a side of △ABC, e.g. through AC, then the incenters and excenters of △″ run through a pair of conics through A and C. The line R″S″ envelops a parabola p with focus B and touching the altitudes of △ABC through A, C.*

The following figures Fig. 5b and Fig. 5c show general cases of the mapping μ_1. It seems that, when M traces a line I, the orbits of I and E_i are parts of one algebraic curve.

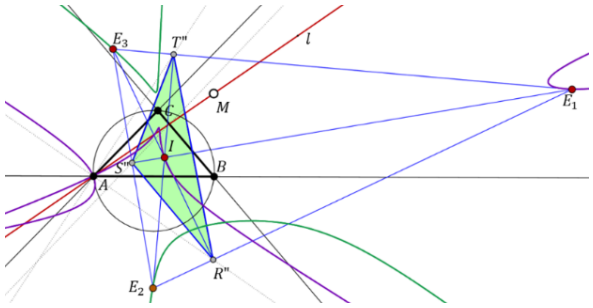

Figure 5b: *If M runs through a line l through A, then I and E_i to △″ run in pairs through two parts of an algebraic curve.*

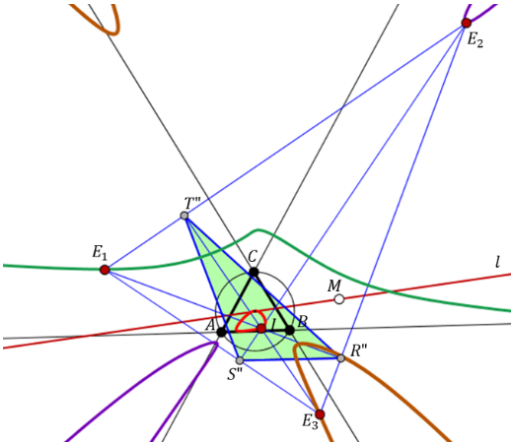

Figure 5c: *If M runs through a line l not passing through a vertex of △ABC, then I and E_i trace four distinct parts of an algebraic curve, such that the mapping $\mu_1 : M \mapsto I$ is independent of E_i. In the presented case, I traces even a closed curve.*

For an analytic description of μ_1 it seems adequate to connect a Cartesian frame with the triangle $\triangle ABC$ with origine A and unit point B on the x-axis. Thus, $\triangle ABC$ as also $\triangle AMB$ can be described by the angles α and β (fixed) resp. ξ and η (variable), see Fig. 6. With these angles the side lengths a, b are

$$a = \frac{\sin\alpha}{\sin(\alpha+\beta)},\quad b = \frac{\sin\beta}{\sin(\alpha+\beta)},\quad c = 1 \tag{1}$$

$$\begin{aligned}
|AM| &= \frac{\sin\eta}{\sin(\xi+\eta)},\\
|BM| &= \frac{\sin\xi}{\sin(\xi+\eta)},\\
|CM| &= \frac{\sin(\alpha-\eta)\sin\beta}{\sin(\xi+\eta)\sin\sphericalangle AMC},
\end{aligned} \tag{2}$$

$$(\cot\sphericalangle AMC = \tfrac{\sin\alpha\sin(\beta-\eta)+\cos(\xi+\eta)\sin\beta\sin(\alpha-\xi)}{\sin\beta\sin(\alpha-\xi)\sin(\xi+\eta)}),$$

$$\begin{aligned}
|R''T''| &= 2|AM|\sin\alpha,\\
|R''S''| &= 2|BM|\sin\beta,\\
|S''T''| &= 2|CM|\sin(\alpha+\beta),
\end{aligned} \tag{3}$$

$$\begin{aligned}
R'' &= |AM|\begin{pmatrix}\cos\xi\\ -\sin\xi\end{pmatrix},\\
T'' &= |AM|\begin{pmatrix}\cos(2\alpha-\xi)\\ -\sin(2\alpha-\xi)\end{pmatrix},\\
S'' &= |BM|\begin{pmatrix}1-\cos(2\beta-\eta)\\ \sin(2\beta-\eta)\end{pmatrix}.
\end{aligned} \tag{4}$$

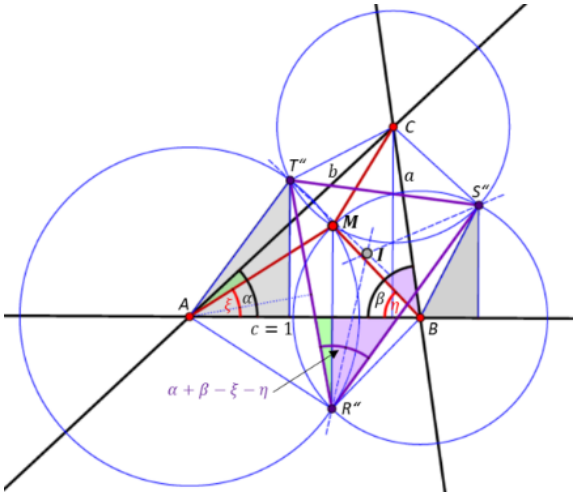

Figure 6: *Labeling used for calculating the analytic representation of the first Miquel mapping μ_1.*

When iterating $\mu_1 : M \mapsto I =: M^1 \mapsto I^1 =: m^2 \to \cdots$, we might suppose the following

Conjecture: The orthocenter O of $\triangle ABC$ is an attractor of μ_1^n, $(n \to \infty)$.

Remark 2 *Obviously, one could extend the first Miquel mapping to the quadrangle consisting of I and the excenters E_i of $\triangle''$. If M traces a line l, then each of the excenters traces a curve l_{E_i}. Thereby, dependent on the line l and similar as in Fig. 5b, the centers E_i can change their roles. The combination of these four orbits l_{E_i}, l_I seems to form a single algebraic curve.*

2.3 Miquel circles and their midpoints

In the following we consider the triangle formed by the centers of the Miquel circles $m_A = k(AR'T')$, $m_B = k(BR'S')$, $m_C = k(CS'T')$. Independent of the chosen points R', S', T' we find a property of the centers of m_A, m_B, m_C (see Fig. 2, Fig. 7, and [16]), which we formulate as

Theorem 3 *Given a triangle $\triangle ABC$ and a triangle $\triangle R'S'T'$ arbitrarily inscribed to it. The centers M_A, M_B, M_C of the three Miquel circles m_A, m_B, m_C form a triangle similar to $\triangle ABC$. The similarity factor is $1/2\cos\varepsilon$.*

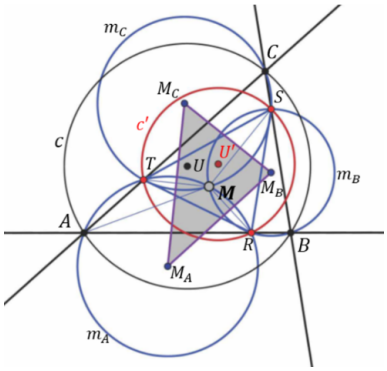

Figure 7: *The triangle of the Miquel circle centers is similar to the given triangle $\triangle ABC$.*

A proof of Theorem 3 can be read from Fig. 2. It follows that the sides of $\triangle M_AM_BM_C$ enclose a fixed angle with the sides $\triangle ABC$. We shall make use of Theorem 3 in the next chapters.

2.4 A second Miquel mapping

The circumcircle c' of triangle $\triangle RST$ intersects the sides of the initial triangle $\triangle ABC$ in additional points $\overline{R}$, $\overline{S}$, $\overline{T}$ see Fig. 8. This new triangle $\triangle\overline{RST} =: \overline{\triangle}$ gives rise to a new Miquel point $\overline{M}$, such that one can give:

Definition 3 *Given a triangle $\triangle ABC$ and arbitrarily chosen non collinear points R, S, T defining the Miquel point M. Let further $\overline{R}$, $\overline{S}$, $\overline{T}$ be the remaining intersections of the circumcircle c' of $\triangle RST$ with the sides of $\triangle ABC$, which define a new Miquel point $\overline{M}$, then we define the mapping $\mu_2 : M \mapsto \overline{M}$ as the second Miquel mapping.*

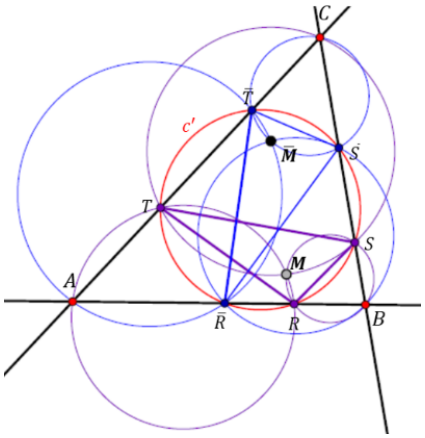

Figure 8: *Visualization of the second Miquel mapping $\mu_2 : M \mapsto \overline{M}$.*

If we consider the contact points $R = \overline{R}$, $S = \overline{S}$, $T = \overline{T}$ of in- and excircles of $\triangle ABC$ then it becomes obvious that the incenter and the excenters of $\triangle ABC$ are fixed points of the second Miquel mapping μ_2.

We collect some properties of μ_2, leaving the elementary but lengthy calculations to the reader.

A less obvious property, see Fig. 9, shall be formulated as

Theorem 4 *Let the triangles $\triangle RST$, $\triangle\overline{RST}$, both inscribed to $\triangle ABC$, have the same circumcircle c'. Thtouchinge midpoint triangles $\triangle_M := \triangle M_AM_BM_C$ and $\triangle_{\overline{M}} := \triangle\overline{M}_A\overline{M}_B\overline{M}_C$ of the therewith defined two triplets of Miquel circles are directly congruent with rotation center Z_2 and they are similar to the initial triangle $\triangle ABC$. Furthermore, the two Miquel points M, $\overline{M}$ are equidistant to Z_2 and the angle $\sphericalangle MZ_2\overline{M}$ is twice the rotation angle $M_A \to \overline{M}_A$.*

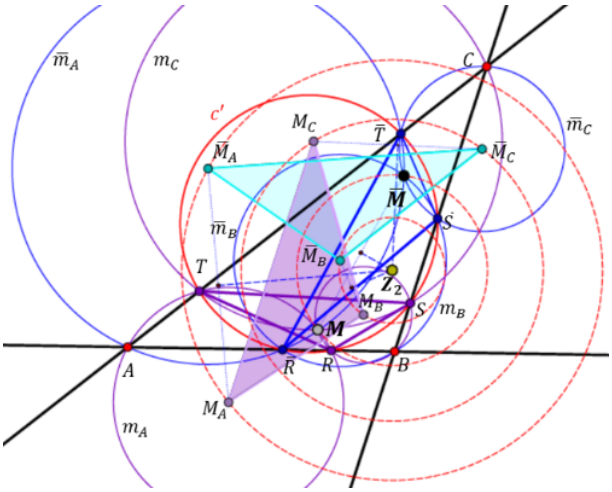

Figure 9: *The midpoint triangles $\triangle_M$ and $\triangle_{\overline{M}}$ are directly congruent (rotation center Z_2) and similar to the initial triangle $\triangle ABC$.*

When we start with a fixed (but arbitrarily chosen) Miquel point M and consider the one-parameter family of triangles, (in Fig. 10 represented by $\triangle RST$, $\triangle R'S'T'$), then we find the centers of their circumcircles on a line u, although these circles dot form a pencil. They intersect the sides of $\triangle ABC$ in an additional family of triangles of type $\triangle\overline{RST}$, $\triangle\overline{R}'\overline{S}'\overline{T}'$, which define a fixed Miquel point $\overline{M}$.

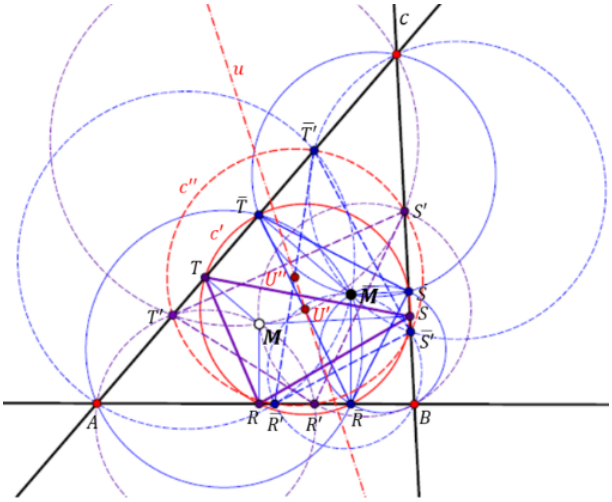

Figure 10: *To a fixed Miquel point M belongs a set of triangles $\triangle RST$ and, via their circumcircles, a set of triangles $\triangle\overline{RST}$, which again define a fixed Miquel point $\overline{M}$, such that $\mu_2 : M \mapsto \overline{M}$ is involutive.*

Remark 3 *For points M on the circumcircle $c = k(ABC)$ the points R, S, T are collinear and their circumcircle degenerates and splits to the line RS plus the ideal line ω, which defines the collinear triple $\overline{R}$, $\overline{S}$. $\overline{T}$. Therefore, as the circumcircles $k(A\overline{RT})$, $k(B\overline{RS})$, $k(C\overline{ST})$ are not defined, c is an exceptional set of points M.*

We can therefore conclude

Theorem 5 *The second Miquel mapping $\mu_2 : M \mapsto \overline{M}$ is involutoric. The in- and excenters of $\triangle ABC$ are fixed points of μ_2, the circumcenter c of $\triangle ABC$ is an exceptional set of points M.*

3 Special cases of Miquel's theorem

3.1 The Theorems of Brocard

The French mathematician Henri Brocard (1845-1922) stated that the three circles passing through a pair of vertices of a triangle $\triangle ABC$ and touching one of its sides have a common point. Due to the two possible orientations of $\triangle$ there are two triples of circles, and therefore two such points, which are called *first* and *second Brocard point* B_1, B_2, see e.g. [10]. They have many interesting properties and give rise to additional concepts, c.f. [7]. There is an interpretation in the sense of Miquel, if we choose R, S, T infinitely close to A, B, C. Then the Miquel circles will touch the sides of $\triangle$ at its vertices and become *Brocard-Miquel* circles see Fig. 11. The two possible Miquel points become the first and second Brocard point B_1, B_2. For these points, the Miquel stars pass through all three vertices of $\triangle$. Fig. 12 shows the situation for one of the Brocard points, but also for the altitude star.

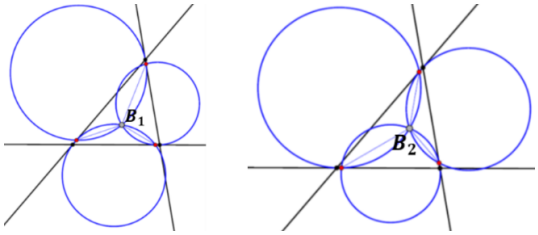

Figure 11: *Brocard-Miquel circles and Brocard points of a triangle, as limit cases of Miquel points.*

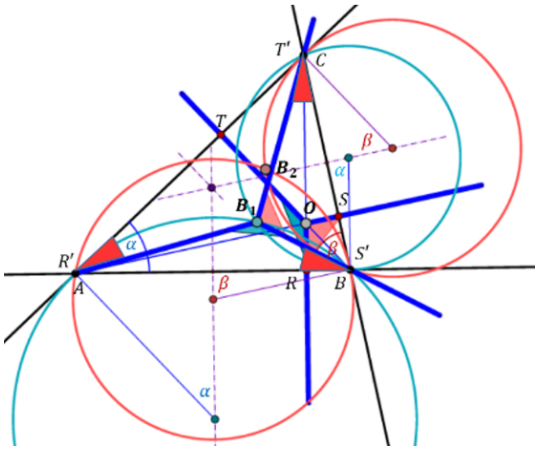

Figure 12: *The Miquel-star through the three vertices of a triangle $\triangle$ to Brocard point B_1 and to the orthocenter O.*

As the sides of each Miquel star intersect the sides of a triangle at equal angles (see Fig. 2), the theorem concerning the so-called *fixed Brocard-angle* follows as a trivial corollary.

As for one limit triangle $\triangle RST$ its circumcircle c' coincides with the circumcircle c of $\triangle$, we get the triangle $\triangle\overline{RST}$ mentioned in Chapter 2.2 as the 2nd limit triangle, such that the Miquel points B_1 and B_2 correspond in the second Miquel mapping μ_2. We formulate this as

Theorem 6 *The Brocard points B_1 and B_2 of a triangle $\triangle ABC$ correspond in the involutive Miquel mapping μ_2 of $\triangle ABC$.*

We consider now the midpoints of the two triads of Brocard-Miquel circles b_i^A, b_i^B, b_i^C, $(i=1,2)$, which intersect in the Brocard points B_i. As a consequence of Theorem 4 and by arguments of congruent angles, see Fig. 13 and 14, we can formulate

Theorem 7 *The centers Z_i^X, $(i=1,2;\ X=A,B,C)$, of the two triplets of Brocard Miquel circles b_i^X form two congruent triangles $\triangle_1$, $\triangle_2$, which are similar to the given triangle $\triangle ABC$. They are in Desargues-position with the circumcenter U of $\triangle$ as perspector and the bisector of the segment $[B_1,B_2]$ as perspectrix (passing through U). The centers Z_i^X of the 6 Brocard-Miquel circles b_i^X lay in pairs on circles, which are concentric with the circumcircle z of the isosceles triangle $\triangle B_1UB_2$.*

The proof of Theorem 7 can be performed by straight forward calculation similar to that of the first and second Miquel mappings. The similarity statement is a consequence of Theorem 3.

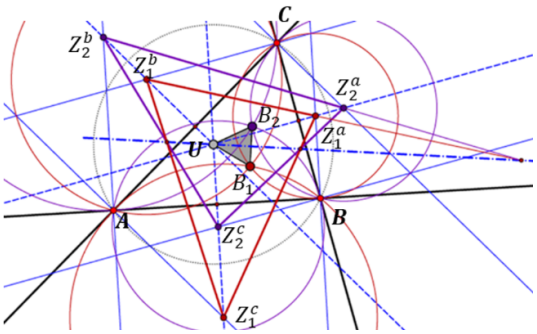

Figure 13: *The midpoints of the two triplets of Brocard-Miquel circles form two congruent triangles of a Desargues configuration. They are similar to the initial triangle.*

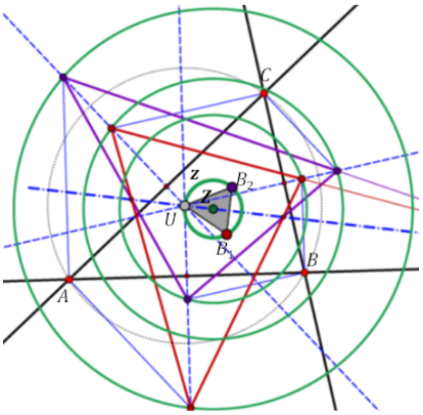

Figure 14: *The midpoints of the two triads of Brocard-Miquel circles are in pairs on concentric circles. Their common center is the center Z of the circumcircle z of $\triangle B_1UB_2$.*

Remark 4 *It turns out that the similarity factor σ for the midpoint triangles $\triangle_i' = \triangle Z_i^A Z_i^B Z_i^C$ with respect to $\triangle$ becomes $\sigma = \overline{UB_1} : \overline{B_1B_2}$. Consequently, one could construct the Brocard points for these triangles, and we must receive Brocard triangles similar to $\triangle B_1UB_2$. Fig. 15 shows the situation for the midpoint triangle $\triangle_i'$, which is directly similar to $\triangle$. Taking $\triangle ABC = \triangle A^0B^0C^0$ and $\triangle B_1UB_2 = \triangle B_1^0U^0B_2^0$ as the initial situation, the next step delivers $B_1^1 = U^0$, $B_2^1 = B_2^0$, and we get a chain of similar triangles with common vertex $B_2^0 = \cdots = B_2^n$. Constructing the Brocard points for both midpoint triangles at each stage gives a kind of a fractal structure based on a bifurcation process.*

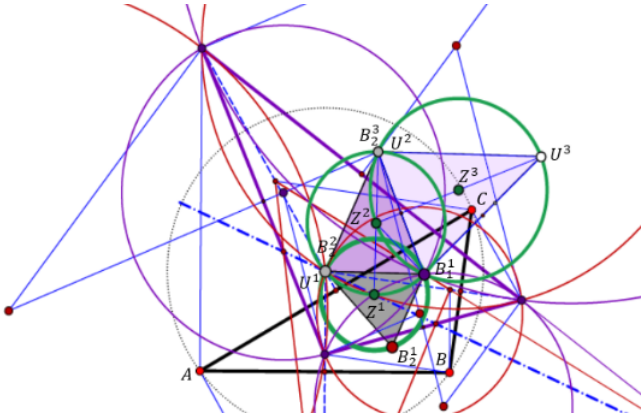

Figure 15: *The midpoint triangles $\triangle_1$, $\triangle_2$ are similar to the given triangle. The similarity factor σ turns out to be the ratio $\overline{UB_1} : \overline{B_1B_2}$.*

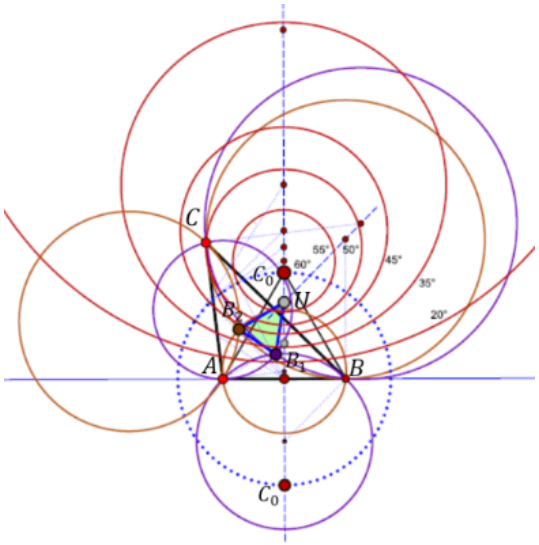

Figure 16: *Vertices C moving along circles of a hyperbolic pencil of circles, together with fixed vertices A, B, form triangles with similar triangles $\triangle B_1UB_2$.*

Remark 5 *As a triangle $\triangle$ needs three parameters to be described, while $\triangle B_1UB_2$ is isosceles, there must be a one-parameter family of triangles to a given triangle $\triangle B_1UB_2$. We formulate the result when keeping the vertices A and B fixed and C movable such that the corresponding triangles $\triangle B_1UB_2$ are similar, see Fig. 16:*

Theorem 8 *The vertices C to fixed vertices A, B move along two circles symmetric to the line AB if we demand that the corresponding triangles $\triangle B_1UB_2$ shall be similar. The circles $c(\varphi)$ to different angles $\varphi = \sphericalangle B_1UB_2$ belong to a hyperbolic pencil of circles, the degenerate circles of which are the two possible vertices C forming equilateral triangles $\triangle ABC$ over the segment $[AB]$.*

We omit the proof, which is straight forward calculation similar to that for μ_1 and μ_2. A consequence of Theorem 8 is that $0^\circ < \varphi < 60^\circ$. Therefore, only for equilateral triangles $\triangle$ the triangles $\triangle_1$, $\triangle_2$ coincide and are congruent to $\triangle$.

3.2 The points *R*, *S*, *T* fulfill the Menelaos condition

As a second special case we choose collinear points *R*, *S*, *T*. In other words, *R*, *S*, *T* fulfill *Menelaos's condition*. Now $\triangle RST =: \triangle'$ is degenerate and the, in general, three parabolas (Fig. 3) coincide in a single one with the Miguel point *M* as focus, see Fig. 17.

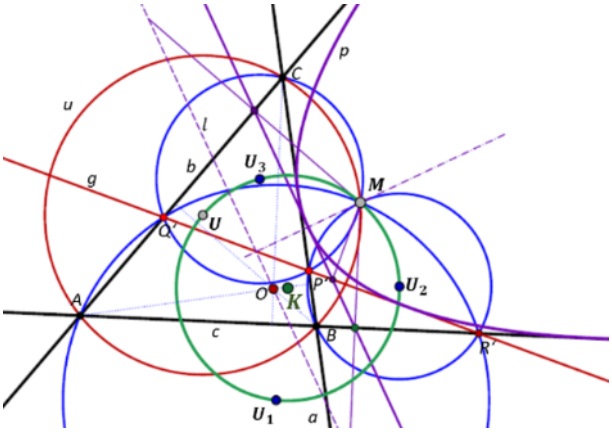

Figure 17: *Collinearly chosen points R, S, T lead to the theorems of Steiner and Simson-Wallace and of Kantor.*

J. Steiner interpreted the line *RS* as the fourth line of a quadrilateral and stated that the four circumcircles of its four partial triangles intersect in one point, namely the focus of the single parabola *p* touching all four lines. In the sense of Miquel, all possible Miquel triangles $\triangle R'S'T'$ to *M* must be degenerate and *M* is a point of the circumcircle of $\triangle$. The pedal points of *M* at the sides of $\triangle ABC$ are therefore collinear with the vertex tangent of the parabola *p*, which means that the theorem of Simson-Wallace (see [4]) becomes an obvious consequence. As the Miquel points are restricted to the circumcenter of $\triangle$, i.e. a one-parameter set, while for the line *RS* there is a two parameter set of possibilities, there must be a one-parameter set of lines belonging to the same Miquel point *M*. Indeed, this set consists of the tangents of the single parabola mentioned above. Of course, one again could define a kind of Miquel mapping $\mu^\star : g \to M$, which now is singular with image $\mathrm{img}(\mu^\star) = u$ and the tangent sets of parabolas as fibers.

Remark 6 *It seems worth mentioning a theorem by S. Kantor* [9]*, which states that the centers U, U_1, U_2, U_3 of the four circumcircles of the partial triangles of a quadrilateral and their common intersection, (the Miquel point M) are concyclic. In Fig. 17 the center of this Kantor circle is labelled by K. Kantor considered the five partial quadrilaterals of a five-lateral and states that the centers of the five Kantor circles are again concyclic, delivering a new center. K. Hirano* [6] *considers these new centers of a six-lateral and found that they again are concyclic. Finally, Ch. J. Hsu* [17] *extended these results step by step to n-laterals, stating that concyclicity prevails in each step. Furthermore, a connection of Steiner's and Miquel's theorems is applied in* [11] *to define so-called Steiner-Miquel mappings.*

3.3 The points *R*, *S*, *T* fulfill Ceva's condition

Now, we choose *R*, *S*, *T* such that *RC*, *SA*, and *TB* meet at a point *X*, which means that they fulfill the "Ceva condition". Even though this case looks somehow dual to the former case and can be related to it via the *triangle polarity* to $\triangle ABC$, it has quite different properties.

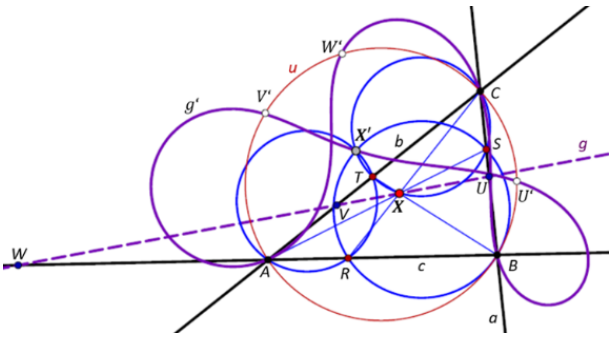

Figure 18a: *The 2^nd Miquel-mapping $\mu_2 : X \mapsto X'$ maps a line g to a curve g' of degree 6. If g coincides with a side of $\triangle$, then its μ_2-locus is the circumcircle u of $\triangle ABC$.*

Now, a mapping of some point *X* to the Miquel point $M =: X'$ is induced in a natural way which is algebraic of degree 6. In the following, we give a description of what shall be called *third Miquel-mapping* $\mu_3 : X \mapsto X'$. It turns

out that points on the sides of $\triangle ABC$ are mapped to points of the circumcircle of this triangle $\triangle$, see Fig. 18a.

In the view of circle geometry, which usually considers both lines and circles as Möbius circles within a projective line over complex numbers, and which is modeled as the Gauss plane π and/or the Riemannian sphere, we present here a slight modification of this approach: We replace the Riemannian sphere by a paraboloid of revolution and an axis normal to the plane of the triangle $\triangle$. The standard *stereographic projection* of the Riemann sphere becomes then the orthogonal projection onto what shall be called *Riemann paraboloid* Ψ described by the Cartesian equation

$$\Psi: \; x^2+y^2=z. \tag{5}$$

For a convenient calculation, we embed the Euclidean space into its projective closure and use homogeneous coordinates $(x,y,z)\mapsto(x_0,x_1,x_2,x_3)\mathbb{R}$. Let the Euclidean planar coordinate representation of the vertices of triangle $\triangle$ and of the points R, S, T be $A:=(0,0)$, $B:=(1,0)$, $C:=(u,v)$, $R:=(r,0)$, $S:=(1+(u-1)s,vs)$, $T:=(ut,vt)$.

They are mapped by the *inverse stereographic projection* $p:\pi\to\Psi$ to points $A^p,\ldots,T^p\in\Psi$. The representation in homogeneous coordinates of these image points reads therefore as

$$\begin{aligned}
A^p &= (1,0,0,0)\mathbb{R}\\
B^p &= (1,1,0,1)\mathbb{R},\\
C^p &= (1,u,v,u^2+v^2)\mathbb{R}\\
R^p &= (1,r,0,r^2)\mathbb{R}\\
T^p &= (1,ut,vt,(u^2+v^2)t^2)\mathbb{R}\\
S^p &= (1,1+u_{-1}s,vs,(1+u_{-1}s)^2+v^2s^2)\mathbb{R}, \quad (u_{-1}:=u-1).
\end{aligned} \tag{6}$$

The planes $A^pR^pT^p$, $B^pS^pR^p$, $C^pT^pS^p$ represent the three Miquel circles, and, because of Miquel's theorem, their intersection point M^p must be a point of Ψ.

As there is a one-parameter family of triplets R, S, T to a given Miquel point X', we can expect, that at least one of those triples fulfills Ceva's condition, such that it is possible to define the inverse mapping $\mu_2^{-1}: X'\to X$ in a geometric way, see Fig. 18b. Starting with an arbitrarily given triple R', S' T', we construct a *Ceva trilateral* with sides AS', BT', CR' and its vertices U', V', W'. When rotating the Miquel star (Fig. 2), these vertices trace conics with a common point X, the Ceva point of X'.

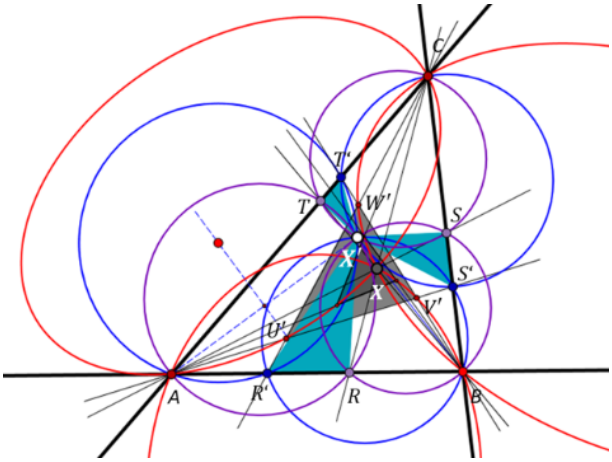

Figure 18b: *Reconstruction of the Ceva point X to a given Miquel point X'.*

Theorem 9 *The Ceva-Miquel mapping $\mu_3: X\mapsto X'$ maps a Ceva point to a Miquel point. It is invertible and has the orthocenter of $\triangle ABC$ as fixed point.*

4 Orbits of Miquel points for special sets of Miquel triangles $\triangle RST$

In the earlier Chapter 3.3, Fig. 15, we considered a special kind of dependencies of the point triples (R,S,T) caused by the fact that the corresponding Ceva points X are bound to a line g. In this chapter, we shall look for other and simpler kind of dependencies. As there are too many quite interesting cases, they shall be treated in a separate paper. Here, we restrict ourselves to present the case of R, S, T running through similar point series on the sides of $\triangle ABC$, see Fig. 19. This shall mean that the ratios, in cyclic order, are equal, i.e. $\mathrm{ar}(ARB)=\mathrm{ar}(BSC)=\mathrm{ar}(CTA)=:t\in\mathbb{R}$. We formulate

Theorem 10 *The Miquel points M to triplets (R,S,T) at sides of a triangle $\triangle ABC$ fulfilling the ratio equality $ar(ARB)=ar(BSC)=ar(CTA)=:t\in\mathbb{R}$ trace the 1^{st} Brocard circle, which is the circumcircle of the triangle formed by the circumcenter U and the two Brocard points B_1, B_2 of $\triangle$.*

It turns out that this Brocard circle contains the triangle centers X_i with the following Kimberling numbers i (see [10]):
$i\in\{3,\ 6,\ 1083,\ 1316,\ 1670,\ 1671,\ 2555,\ 2556,\ 2557,\ 32481,\ 32482,\ 5091,\ 5108,\ 6232,\ 6322,\ 6795,\ 8429,9129,\ 11650,\ 13414,\ 13415,\ 13511,\ 13515,\ 13516,\ 14685,18332,\ 18338,\ 24279,\ 35901,\ 43765,\ 46407,\ 46410,\ 53719,\ 59781,\ 59782,\ 59783,\ 59784,\ 59785,\ 59786,\ 59787,\ 59788,\ 59789,\ 59790,\ 59791,\ 59792,\ 59793,\ 59794,\ 59795,\ 59796\}$.

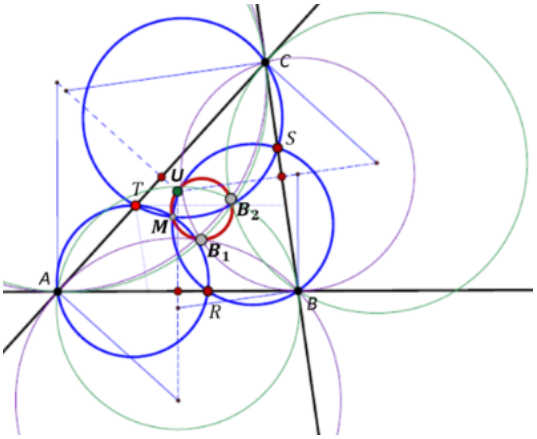

Figure 19: *The set of triplets R, S, T with* $ar(ARB) = ar(BSC) = ar(CTA) =: t \in \mathbb{R}$ *has its Miquel points on the Brocard circle of* $\triangle ABC$.

In addition we found (see Fig. 20)

Theorem 11 *The cases of dependencies of R, S, T, with* $ar(ARB) = t \in \mathbb{R}$, *and* $ar(BSC) = f_S(t)$, $ar(CTA) = f_T(t)$, *where the linear functions* $f_S(t)$, $f_T(t)$ *lead to circles as loci of Miquel points.*

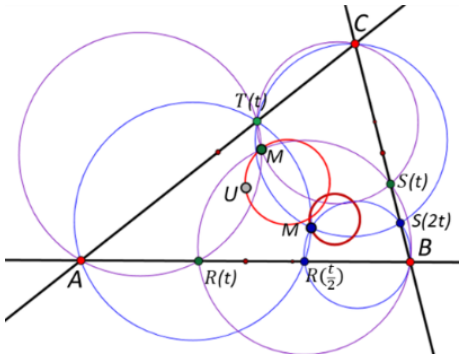

Figure 20: *The set of triples R, S, T with* $ar(ARB) = t$, $ar(BSC) = f_S(t)$, $ar(CTA) = f_T(t)$, *where* $f_S(t)$, $f_T(t)$ *are linear functions, causes the Miquel points to lie on a circle.*

5 Miquel's theorem in circle geometries and Minkowski planes

5.1

It is near to consider the classical version of the Theorem of Miquel in the Möbius-Gauss plane and use it as an axiom for certain ring geometries, see [2]. There is an interpretation as a $(6_4, 8_3)$-configuration of 6 Möbius circles, each containing four points, and eight Möbius points, each on three Möbius circles. Via stereographic projection onto the Riemann sphere, these eight points can be seen as the vertices of a right prism, e.g., a cube, while its six faces act as the planes of the circumcircles of face rectangles, see Fig. 21a.

Similarly, the four (congruent) circles of the so-called *beermat theorem* (Fig. 21b, left), in some sense also a relative to Miquel's configuration, form a $(4_3, 4_3)$-configuration and can be interpreted as an image of a tetrahedron, see Fig. 21b. The beermat theorem states that, if one marks three points A, B, C on a circle c and draws congruent circles c_1, c_2, c_3 through any pair of these points, then these three circles have a common point which turns out to be the orthocenter of $\triangle ABC$.

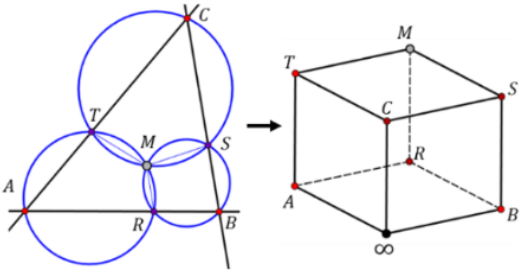

Figure 21a: *The* $(6_4, 8_3)$*-configuration of a Miquel figure is interpreted as vertices and faces of a cube.*

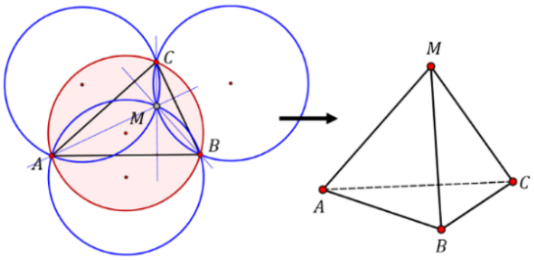

Figure 21b: *The* $(4_3, 4_3)$*-configuration of a beermat figure can be interpreted as vertices and faces of a tetrahedron.*

Remark 7 *If we choose R, S, T as the feet of the altitudes of* $\triangle ABC$, *then the orthocenter O becomes the corresponding Miquel point. We can say that this combines somehow the beermat configuration with Miquel's configuration. In addition to the altitudes r, s, t, which now contain 4 points, also the Thales circles over* $[AB]$, $[BC]$ *and* $[CA]$ *pass through 4 points, see Fig. 22. This gives rise to a* $(12_4, 8_6)$*-configuration which allows an interpretation as the 8 vertices of a cube, its 6 faces and 6 diagonal planes. In Fig. 22 the altitudes r, s, t are mapped to diagonal planes* ρ, σ, τ *through the vertex labelled as* ∞. *This shows that the standard interpretation of Miquel's configuration by a cube can only be a metaphor, as the cube automatically*

has additional planes through four vertices, and this would mean six additional Möbius circles containing four points also in the general Miquel figure.

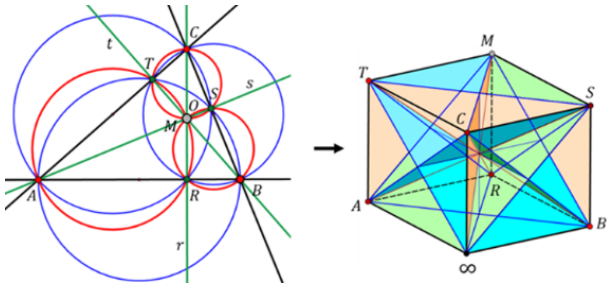

Figure 22: *The* $(12_4, 8_6)$*-configuration of the special Miquel figure with the orthocenter as Miquel point can be interpreted as vertices and faces and diagonal planes of a cube.*

Steiner's configuration with its 4 straight Möbius circles and 4 Miquel-Möbius circles is therefore an $(8_4, 8_4)$-configuration. Here, no proper interpretation of a polyhedron in 3-space with quadrangular faces / diagonal planes is possible. One could still use a cube and 8 tetrahedra, the four vertices of which symbolizing concyclic point quadruples, see Fig. 23a.

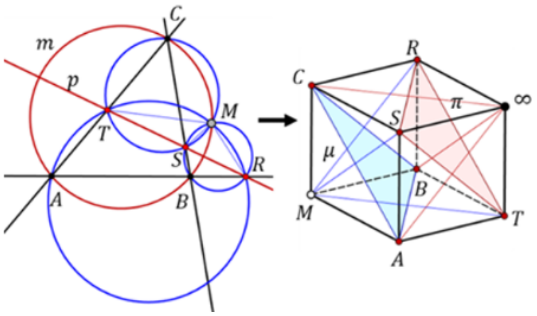

Figure 23a: *The* $(8_4, 8_4)$*-configuration of the Steiner figure could be interpreted as the 8 vertices of a cube with 8 partial tetrahedra, the vertices of which correspond to concyclic point quadruples.*

Each of the two Brocard figures Fig. 11 show a degenerate situation, where three points, the vertices of $\triangle ABC$, count twice (and lead to parabolic pencils of circles), while two points are always distinct. In this case we can no longer speak of a configuration. We get six Möbius circles and five points, and a 3D-interpretation could be the six planes and five points of a three-sided double pyramid, see Fig. 23b.

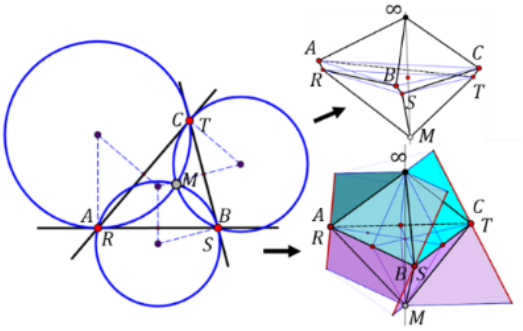

Figure 23b: *"Limit situation" for one of the Brocard figures. It is no longer a con figuration, it can be interpreted as a 3-sided double-pyramid.*

5.2

Affine planes with a norm are called *Minkowski* planes. Here, a centrally symmetric and convex curve or polygon acts as *unit circle u* with radius of length 1 and all circles are centric similar or translates to *u*, see e.g. [1] and [15]. Therewith, the question arises, if there are analogs to the classical figure of Miquel and its relatives, see e.g. [1] and [14]. Note that the norm depends on an additionally given (affine) coordinate frame, see Fig. 24, while the (geometric) distance measure is already well-defined by *u* alone.

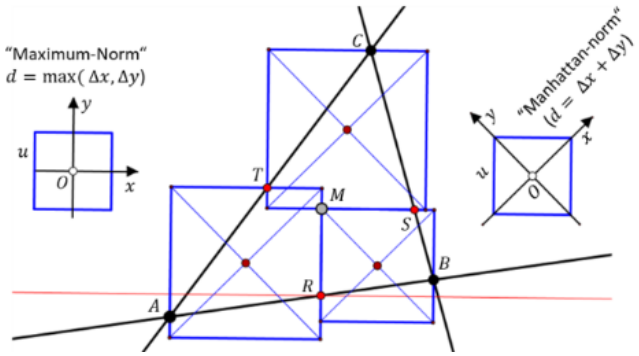

Figure 24: *Miquel figure for a parallelogram as unit circle u. Dependent on the affine coordinate frame, it allows an interpretation in a plane with maximum norm or with Manhattan norm.*

For the beermat theorem to remain valid, central symmetry of *u* is a sufficient condition. For some triples *R*, *S*, *T*, one of the three beermats through *R*, *S* or *S*, *T* or *T*, *R* is identical with the basic beermat *u*. Fig. 25a and 25b show this for beermats being regular hexagons, decagons, and pentagons.

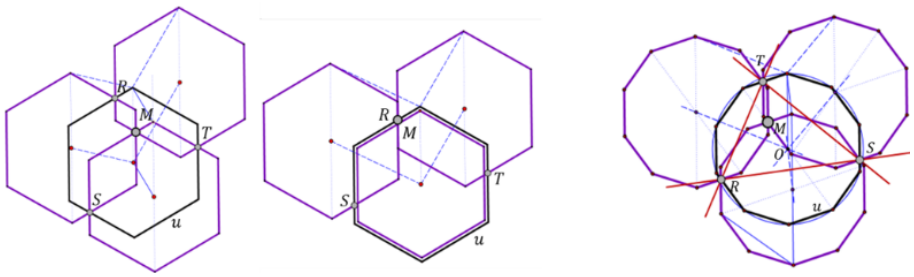

Figure 25a: *The beermat theorem is valid in Minkowski planes.*

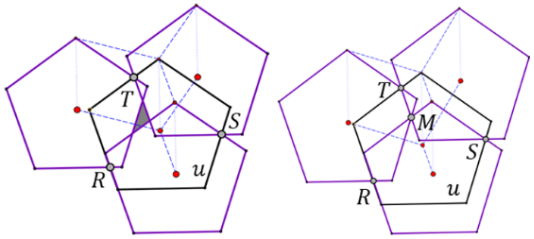

Figure 25b: *If the beermats are not centrally symmetric, the three congruent beermats through $R,S,T \in$ have, in general, no common point, but there exist triplets R, S, T such that they can have a common point M.*

It turns out that there is, in general, no analogon for the Steiner-Wallace-Simson figure in Minkowski planes with a unit circle u different from an ellipse. The same is true also for Brocard's theorem. To translate a Brocard figure into a Minkowski plane the unit circle u should be strictly convex and smooth, such that e.g. the left-orthogonality of Birkhoff [3] becomes a (1,1)-relation. In general, the three Brocard-Miquel circles to a given triangle $\triangle ABC$ have no common point, see Fig. 26a, but there are triangles $\triangle ABC$ and unit circles u, such that they can be concurrent, see Fig. 26b.

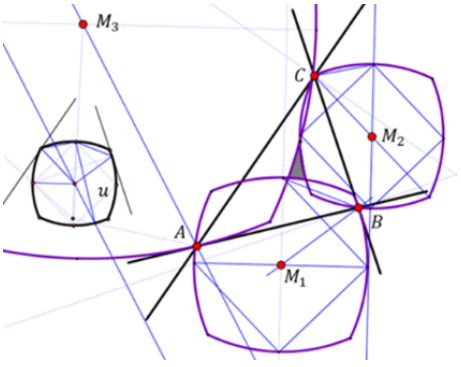

Figure 26a: *A general case for a Brocard figure in a Minkowski plane with unit circle u. The three Brocard-Miquel circles have no common point.*

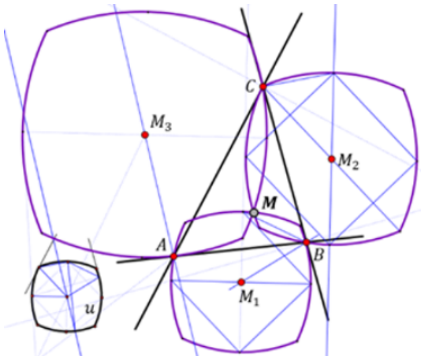

Figure 26b: *A special case of a Brocard figure, where the three Brocard-Miquel circles pass through one point M.*

5.3

Finally, we shortly point to some classical Cayley-Klein planes, thus generalizing the Euclidean case in an obvious direction. As long as we deal with pseudo-Euclidean and isotropic planes the place of action is a projectively extended affine plane and we can expect that Miquel's theorem and its relatives remain valid. For example, the isotropic case of a Miquel figure is shown in Fig. 27a, while Fig. 27b shows an isotropic version of the Steiner-Wallace-Simpson figure.

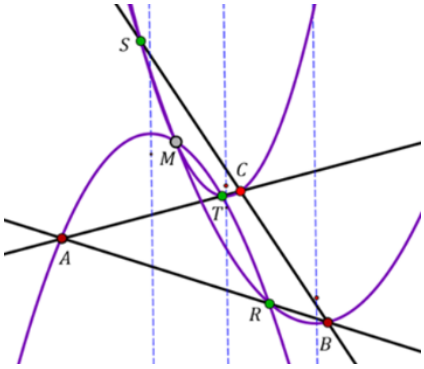

Figure 27a: *A Miquel figure in an isotropic plane.*

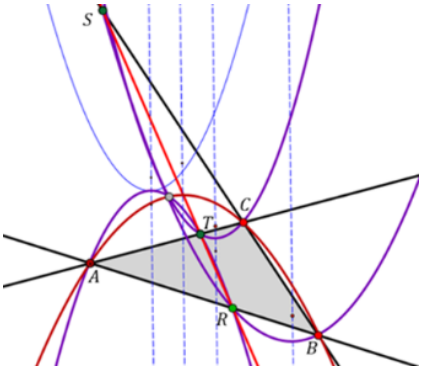

Figure 27b: *A "Steiner figure" with collinear points R, S, T.*

In an elliptic or hyperbolic plane a triangle has four circumcircles. A Miquel figure in such a plane consists of the triangle $\triangle ABC$, the triplet R, S, T on its sides, and the four times three circumcircles of partial triangles. It is well-known that there are, in general, no common points for triplets of such circles, such that Miquel's Theorem is not true in such planes.

Also the beermat theorem, dealing with congrtuent circles, is not true in elliptic or hyperbolic planes, as can be seen in Fig. 28: The three congruent circles through R, S resp. S, T resp. T, R, ($R \neq S \neq T$ arbitrarily chosen points of a fixed circle c), have no common point, and they do not pass through the orthocentre of $\triangle RST$.

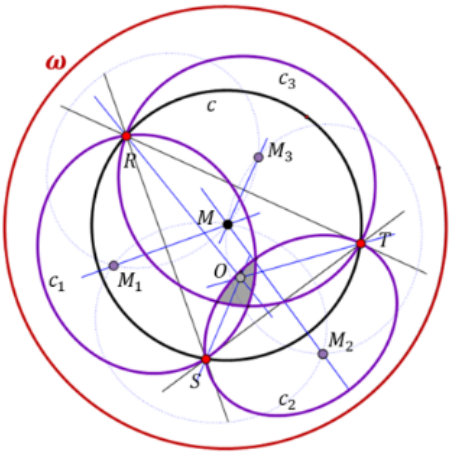

Figure 28: *Four hyperbolic congruent circles c_i forming a beermat figure visualized in the Klein model of a hyperbolic plane with absolute conic* ω.

6 Final remarks

Some of the material treated here is more or less common knowledge. However, we shall emphasize the connections between several elementary geometric theorems, and their interpretation as special cases of Miquel's Theorem. This leads, on one hand, to some Miquel mappings, which are seemingly new, and on the other to a more detailed understanding of those standard theorems.

The figures in this paper are generated with the graphics freeware *Cinderella* [5], an effective tool for planar geometry in Euclidean, hyperbolic and elliptic geometry.

Acknowledgments
The authors thank the reviewers for valuable comments and proposed improvements.

References

[1] ASPLUND, E., GRÜNBAUM, B., On the Geometry of Minkowski planes, *Enseign. Math.* **6** (1960), 299–306.

[2] BENZ, W., *Vorlesungen über Geometrie der Algebren*, Springer, Berlin, 1973, https://doi.org/10.1007/978-3-642-88670-6

[3] BIRKHOFF, G., Orthogonality in linear metric spaces, *Duke Math. J.* **1**(2) (1935), 169–172, https://doi.org/10.1215/S0012-7094-35-00115-6

[4] BLAŽEK, J., PECH, P., Generalization of Simson–Wallace theorem: planar and spatial formulation, *J. Geom.* **114**, 5 (2023), https://doi.org/10.1007/s00022-022-00665-z

[5] CINDERELLA, *Die interaktive Geometrie-Software Cinderella*, *Multiscale Modeling & Simulation*, https://cinderella.de/tiki-index.php (last access August 2024)

[6] HIRANO, K., On some center circles and their relations, *Sugaku* **8** (1956/57), 210–211.

[7] HONSERGER, R., The Brocard angle, *Episodes in Nineteenth and Twentieth Century Euclidean geometry*, Math. Assoc. of America 1995, 101–106, https://doi.org/10.5948/UPO9780883859513

[8] HSU, CH. J., On systems of center-circles derived successively from that of Steiner-Kantor-Morley, *Soochow J. Math. Natur. Sci.* **3** (1977), 17–34.

[9] KANTOR, S., Über das vollständige Fünfseit, *Sb. Österr. Akad. Wiss.* **78** (1878), 1–9.

[10] KIMBERLING, C., *Encyclopedia of Triangle Centers*, https://faculty.evansville.edu/ck6/encyclopedia/etc.html (last access June 2024)

[11] MACKAY, J.S., The Wallace line and the Wallace point, *Proc. Edinb. Math. Soc.* **9** (1890), 83–91, https://doi.org/10.1017/S001309150003087X

[12] MIQUEL, A., Théorèmes sur les intersections des cercles et des spheres, *J. Math. Pures Appl.* **3** (1838), 517–522.

[13] ODEHNAL, B., A Miquel-Steiner Transformation, *KoG* **27** (2023), 14–24, https://doi.org/10.31896/k.27.2

[14] SPIROVA, M., On Miquel's theorem and inversions in normed planes, *Monatsh. Math.* **161** (2010), 335–345, https://doi.org/10.1007/s00605-009-0153-8

[15] THOMPSON, A.C., *Minkowski Geometry*, Cambridge University Press, 1996, https://doi.org/10.1017/CBO9781107325845

[16] DE VILLIERS, M., A variation of Miquel's theorem and its generalization, *Math. Gaz.* **98**(542) (2014), 334–339, https://doi.org/10.1017/S002555720000142X

[17] WEISS, G., 3D-Versions of Theorems related to Miquel's Theorem, *Proceedings of the Slovak-Czech Conference on Geometry and Graphics 2023* (Kremnica, Slovakia, Sept. 11-14, 2023), Bratislava 2023, 195–202.

Gunter Weiss
orcid.org/0000-0001-9455-9830
e-mail: weissgunter@gmx.at

University of Technology Vienna
Karlsplatz 13, 1040 Vienna, Austria

University of Technology Dresden
Helmholtzstrße 10, 01069 Dresden, Germany

Boris Odehnal
orcid.org/0000-0002-7265-5132
e-mail: boris.odehnal@uni-ak.ac.at

University of Applied Arts Vienna
Oskar-Kokoschka-Platz 2, 1010 Vienna, Austria

https://doi.org/10.31896/k.28.3
Original scientific paper
Accepted 1. 10. 2024.

BORIS ODEHNAL

Universal Porisms and Yff Conics

Universal Porisms and Yff Conics

ABSTRACT

The Yff circumellipse and the Yff inellipse of a triangle allow for a poristic family of triangles (henceforth called Yff porism), since the initial triangle is already an interscribed triangle. Surprisingly, the Yff porism can be parametrized by means of rational functions, and thus, it delivers a porism in Universal Geometry. This also allows us to give explicit examples of poristic triangle families over finite fields. Considering the Yff inellipse and Yff circumellipse as the basis of an exponential pencil of conics, we can iterate the construction of the porism and find an infinite sequence (and thus infinitely many) nested rational triangle porisms over the real (and complex) number field or a finite closed chain of porisms in the case of a finite field.

Key words: porism, inellipse, circumellipse, triangle, rational porism, rational parametrization, finite field, finite projective plane

MSC2010: 14A25, 51N15

Univerzalne porizme i Yff konike

SAŽETAK

Yff opisana elipsa i Yff upisana elipsa trokuta dopuštaju poristični familiju trokuta (odsada zvanu Yff porizma), budući da je polazni trokut već upisan prvoj, a opisan drugoj elipsi. Iznenađujuće, Yff porizma se može parametrizirati pomoću racionalnih funkcija i stoga daje porizmu u univerzalnoj geometriji. To nam također omogućuje da damo eksplicitne primjere poristični familija trokuta nad konačnim poljima. Promatrajući Yff upisanu elipsu i Yff opisanu elipsu kao bazu eksponencijalnog pramena konika, možemo ponavljati konstrukciju porizme i pronaći beskonačan niz (a time i beskonačno mnogo) ugniježđenih racionalnih porizmi trokuta nad realnim (i kompleksnim) poljem brojeva ili konačni zatvoreni lanac porizmi u slučju konačnog polja.

Ključne riječi: porizma, upisana elipsa, opisana elipsa, trokut, racionalna porizma, racionalna parametrizacija, konačno polje, konačna projektivna ravnina

1 Introduction

Porisms have attracted the interest of geometers in the past years anew. An exhausting overview of this topic and newer as well as many classical results can be found in [3] and [4]. Certain subproblems, dealing with a detailed analysis of CHAPPLE's porism (the most prominent one cf. [1]) were studied in [19] and inspired further investigations of orbits and invariants in relation to porisms in [5, 6, 7]. The isotropic version of CHAPPLE's porism was investigated in [13]. Not only orbits of points and centers related with the moving triangles have gained interest. The closely related topic of billiards within ellipses, and in conics in general, was enriched with new results. To mention only a few, see for example [8] and a study on Poncelet grids in [22]. Projective invariants of Poncelet closure figures are presented in [24, 27], the motions induced by Poncelet closure figures are studied in [25], the diagonals in Poncelet grids are the subject of interest in [26], and focal billiards are described in [23].

In the vast majority, and especially in the case of CHAPPLE's porism, explicit analytical descriptions of Poncelet triangle families involve algebraic (and by no means rational) expressions (cf. [6, 7, 19, 21]). This limits direct symbolic computations, and sometimes, even graphical representations. Even the (from the computational point of view) simple case of the isotropic Chapple porism studied in [13] needs square roots in order to describe the vertices of the moving triangles. Now, the question is near: Are there porisms that allow for rational (or, in terms of homogeneous coordinates, even polynomial) parametrizations? Such porisms would then also exist in *Universal Rational Trigonometry* (as defined in [28]) and would also be well-defined in planes over finite fields.

In this article, we shall present porisms that can be described by rational (or polynomial) functions. Sec. 2 is devoted to the basic setting and notations. In this section, it is further shown that the tritangent and the circumconic allow for certain porisms in general. Then, in Sec. 3

the parametrization of the poristic triangle families interscribed between Yff conics are derived and some examples in planes over finite fields are given in order to show different phenomena that can occur in various exotic planes. Sec. 4 shows how to find more such rational porisms based on the Yff porism. Finally and for the sake of completeness, Sec. 5 collects some results in the Euclidean plane.

2 Porisms interscribed between the Yff ellipses

In the plane of the initial triangle $\Delta = ABC$, we describe points and lines by homogeneous trilinear coordinates. Thus, the vertices of Δ have the coordinates

$$A = 1:0:0,\ B = 0:1:0,\ C = 0:0:1. \tag{1}$$

Circumconics, *i.e.*, conics which pass through all three vertices of Δ, are given by a homogeneous equation of the form

$$\mathcal{C}:\ pyz + qzx + rxy = 0, \tag{2}$$

where $p,q,r \in \mathbb{F}\setminus\{0\}$ and $\mathbb{F}$ is some commutative field. The conics $\mathcal{C}$ are always regular if neither of p, q, r vanishes, since $\det \mathrm{H}\,\mathcal{C} = 2pqr$, provided that $\mathrm{char}\,\mathbb{F} \neq 2$. Here, and in the following $\mathrm{H}\,Q$ shall denote the Hessian matrix of a (trivariate) form Q.
In the beginning, $\mathbb{F}$ shall be the real or complex number field. Later, we also consider finite fields $\mathbb{F}$ of order q, which we shall denote by $\mathrm{GF}(q)$. The order q can be a prime or a prime power. Projective planes of order q shall be denoted by $\mathrm{PG}(2,q)$.
A conic inscribed into Δ, or simply, an inconic of Δ touches all side lines of Δ. An inconic should rather be termed *tritangent conic*, since the contact points with the sides of Δ may also be exterior points. We use the term inconic or inscribed just as a simplification, though we know that such conics are not necessarily inscribed into Δ in the elementary geometric sense.
The inconics of Δ in the aforementioned sense can be given by equations of the form

$$\mathcal{D}:\ l^2x^2 + m^2y^2 + n^2z^2 - 2lmxy - 2mnyz - 2nlzx = 0, \tag{3}$$

where $l,m,n \in \mathbb{F}\setminus\{0\}$. Note that the conics $\mathcal{D}$ are regular if neither of l, m, n vanishes, since $\det \mathrm{H}\,\mathcal{D} = 2l^2m^2n^2$, again provided that $\mathrm{char}\,\mathbb{F} \neq 2$. It is worth pointing at the characteristic of the underlying field as we shall see later.
The conics in the pencil spanned by $\mathcal{C}$ and $\mathcal{D}$ are called *Yff conics* (cf. [15]) among them, we also find the *permutation conics* (see [16, 20]). The existence of a poristic triangle family interscribed between $\mathcal{C}$ and $\mathcal{D}$ is obvious, since there exists already one interscribed triangle, namely Δ. We shall call this family the *Yff porism*.

Now, we shall return to the case of $\mathrm{char}\,\mathbb{F} = 0$ (*e.g.*, $\mathbb{F} \cong \mathbb{R},\mathbb{C}$). Any two regular conics $\mathcal{C}$, $\mathcal{D}$ with equations (2) and (3) allow for poristic families of certain polygons:

Theorem 1 *The pair $(\mathcal{C},\mathcal{D})$ of conics circumscribed to and inscribed into Δ allows for a poristic family of $3n$-gons for $n \in \mathbb{N}\setminus\{0\}$.*

Proof. The conics in the pencil spanned by $\mathcal{C}: \mathbf{x}^{\mathrm{T}}\mathbf{C}\mathbf{x} = 0$ and $\mathcal{D}: \mathbf{x}^{\mathrm{T}}\mathbf{D}\mathbf{x} = 0$ have the equations $\mathbf{x}^{\mathrm{T}}(t\mathbf{C}+\mathbf{D})\mathbf{x} = 0$. In order to apply the Cayley criterion (cf. [9, p. 432]), we expand $\sqrt{\det(\mathrm{H}(\mathbf{tC}+\mathbf{D}))}$ in a power series $S(t) = a_0 + a_1t + a_2t^2 + \ldots$. With the abbreviations $\lambda := lmn$, $\pi := pqr$, and $\omega := lp + mq + nr$, we find

$$S(t) = \mathrm{i}\sqrt{2}\left(4\lambda - \omega t + \mathbf{0}\cdot t^2 - \frac{1}{8}\frac{\pi}{\lambda}t^3 - \frac{1}{32}\frac{\pi\omega}{\lambda^2}t^4 - \frac{1}{128}\frac{\pi\omega^2}{\lambda^3}t^5 + \ldots\right).$$

Hence, $\delta_3 = a_2 = 0$, $\delta_4 = a_3 = \frac{\mathrm{i}\sqrt{2}}{8}\frac{\pi}{\lambda}$,

$$\delta_5 = \begin{vmatrix} a_2 & a_3 \\ a_3 & a_4 \end{vmatrix} = -\tfrac{1}{32}\tfrac{\pi^2}{\lambda^2},\ \delta_6 = \begin{vmatrix} a_3 & a_4 \\ a_4 & a_5 \end{vmatrix} = 0,$$

$$\delta_7 = \begin{vmatrix} a_2 & a_3 & a_4 \\ a_3 & a_4 & a_5 \\ a_4 & a_5 & a_6 \end{vmatrix} = \tfrac{-\mathrm{i}\sqrt{2}}{2^{14}}\tfrac{\pi^4}{\lambda^5},\ \delta_8 = \begin{vmatrix} a_3 & a_4 & a_5 \\ a_4 & a_5 & a_6 \\ a_5 & a_6 & a_7 \end{vmatrix} = \tfrac{-\mathrm{i}\sqrt{2}}{2^{20}}\tfrac{\pi^5}{\lambda^7},$$

$$\delta_9 = 0, \ldots,$$

and $\delta_{3k} = 0$ for all $k \in \mathbb{N}$ which confirms the statement. □

The Cayley criterion uses the complex number field. However, the equations (2) and (3) can be considered as conics in projective planes over arbitrary commutative fields and the criterion can be used to test pairs of conics whether or not they allow for poristic polygons interscribed in between. The square root of the cubic polynomial can be expanded in a power series $S(t)$ anyhow. In [2], the Cayley criterion was used in order to count possible cases of conic pairs allowing for triangle porisms. This does neither answer the question whether such porisms exist nor what they look like if they exist.
As is clear from the proof of Thm. 1, the pair $(\mathcal{C},\mathcal{D})$ of conics will never allow for interscribed quadrilaterals according to the assumptions made on the coefficients in their equations.

3 Parametrizing the poristic family

3.1 Basic properties

Two conics that merely fulfill the Cayley criterion will not immediately lead to an explicit description of the poristic triangle family interscribed between them. In order to give an explicit example which later will even allow for a generalization, we choose $p = q = r = l = m = n = 1$ which yields the Yff circumellipse $\mathcal{M}$ and the Yff inellipse $\mathcal{N}$.

The resulting two conics are indeed triangle conics because of the cyclic symmetry of their equations, and of course, they are Yff conics (cf. [15]). Their equations in terms of homogeneous trilinear coordinates do not depend on Euclidean notions such as the side lengths or the interior angles of the triangle Δ:

$$\begin{aligned} \mathcal{M} &: xy+yz+zx=0, \\ \mathcal{N} &: x^2+y^2+z^2-2(xy+yz+zx)=0. \end{aligned} \tag{4}$$

From the elementary (affine) point of view, these conics are ellipses, the Yff ellipses. They span a pencil of the third kind considered as a pencil of the real or complex projective plane. The point $X_1 = 1:1:1$ is the common pole and the antiorthic axis $\mathcal{L}_1 = 1:1:1$ (or with the homogeneous equation $x+y+z=0$) is the common polar of all regular conics in the pencil (see Fig. 1). Here and in the following, the labelling of points (centers) and lines (central lines) related to triangles follows the labelling in [14, 17]. (Later, in Sec. 5, this will be of more significance.) We shall also use shorthand X_1 for the point defined by $1:1:1$ and the symbol $\mathcal{L}_1$ if we mean the line $x+y+z=0$ even if they are not the incenter and the antiorthic axis in the elementary geometric sense.

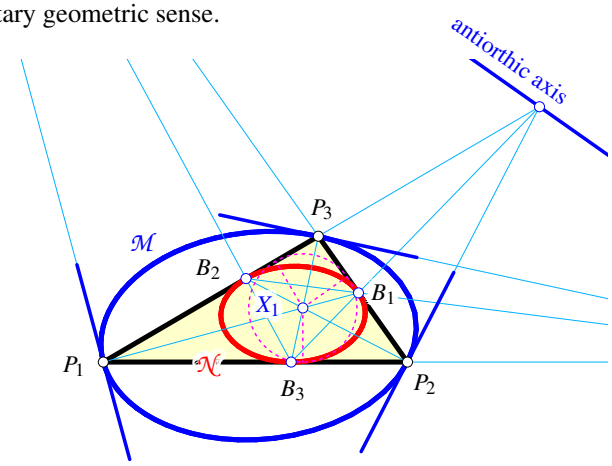

Figure 1: *The Yff conics $\mathcal{M}$ and $\mathcal{N}$ in the real plane.*

In PG$(2,\mathbb{C})$, the conics $\mathcal{M}$ and $\mathcal{N}$ share the pair of complex conjugate points $1:\varepsilon:\varepsilon^2$ and $1:\varepsilon^2:\varepsilon$ on $\mathcal{L}_1$ (with ε being a non-trivial cube root of unity), hence $\mathcal{M}\cap\mathcal{N}=\emptyset$ in the real projective plane. However, in some finite planes, their intersection is not empty.

In order to describe the vertices P_1, P_2, P_3 of the triangles in the poristic family, we start with the homogeneous and polynomial parametrization of $\mathcal{M}$ given by

$$P_1 = -uv : u(u+v) : v(u+v),\ u:v \neq 0:0. \tag{5}$$

Note that the parametrization (5) of $\mathcal{M}$ makes sense over any field.

In order to find the remaining vertices P_2 and P_3, we determine the polar line of P_1 with respect to $\mathcal{N}$ which meets $\mathcal{N}$ in the contact points

$$\begin{aligned} B_2 &= u^2 : (u+v)^2 : v^2, \\ B_3 &= v^2 : u^2 : (u+v)^2, \end{aligned} \tag{6}$$

of the tangents from P_1 to $\mathcal{N}$. Note that the homogeneous representations of the contact points are also polynomial, *i.e.*, they do not involve square roots. This cannot be the case in CHAPPLE's porism (see, *e.g.*, [19, 9]). Now, we intersect the tangents $t_2 = [P_1, B_2]$ and $t_3 = [P_1, B_3]$ with the Yff circumellipse $\mathcal{M}$ and find the remaining vertices P_2, P_3 of the moving triangle as

$$\begin{aligned} P_2 &= v(u+v) : -uv : u(u+v), \\ P_3 &= u(u+v) : v(u+v) : -uv. \end{aligned} \tag{7}$$

For the sake of completeness, we determine the contact point B_1 of $[P_2, P_3]$ and $\mathcal{N}$, which has the homogeneous coordinates

$$B_1 = (u+v)^2 : v^2 : u^2. \tag{8}$$

By virtue of (6) and (8), we see that the homogeneous coordinate representation of B_1, B_2, and B_3 can be obtained from each other by applying cyclic shifts to the coordinate functions. The same holds true for the vertices P_1, P_2, and P_3 of the triangles in the poristic family. The fact that all coordinate functions of the vertices and the contact points are polynomial has the following consequence:

Theorem 2 *The Yff porism, that is the family of triangles interscribed between the Yff inellipse $\mathcal{N}$ and Yff circumellipse $\mathcal{M}$ given in* (4) *contains triangles whose vertices allow for rational parametrizations. The Yff porism is also well-defined over arbitrary fields $\mathbb{F}$ with positive characteristic not equal to 2.*

Proof. The rationality is obvious: The homogeneous coordinates of the vertices $P_i \in \mathcal{M}$ (5) and (7) as well as the contact points B_i (6) and (8) are polynomial. All polynomials are well-defined over any field. □

The case $\mathrm{char}\,\mathbb{F} = 2$ is excluded in Thm. 2 since the construction of the triangles in the poristic family uses the polar system of $\mathcal{N}$. In planes of characteristic 2, polarities are null polarities at the same time, and therefore, they are singular and all tangents of a conic pass through one point, the nucleus.

It makes sense to call the Yff porism a *unsiversal porism* in the sense of [28] for the vertices of the triangles (as well as the contact points) are given in terms of rational functions. Thus, they are defined over any finite field.

Depending on the characteristic of the underlying field $\mathbb{F}$, we can prove:

Theorem 3 *In any finite field* $\mathbb{F}$ *with* $\operatorname{char}\mathbb{F} \neq 2$*, the Yff porism contains at most two degenerate triangles. In the case* $\operatorname{char}\mathbb{F} = 3$*, the Yff porism contains a single degenerate triangle.*

Proof. The vertices (5) and (7) of the triangles in the Yff porism are at least collinear if, and only if, $\det(\mathbf{p}_1, \mathbf{p}_2, \mathbf{p}_3) = 0$ which is equivalent to

$$\delta^3 := (u^2 + uv + v^2)^3 = 0 \tag{9}$$

(where $\mathbf{p}_i$ is a coordinate vector of P_i) vanishes for some parameter $u : v \neq 0 : 0$, *i.e.*, $\delta = u^2 + uv + v^2 = 0$. This is obviously a quadratic equation in $u : v$, and depending on the underlying field, it may have 0, 1, or 2 zeros.
If $\operatorname{char}\mathbb{F} = 3$, then $1 = -2$, and thus, $u^2 + uv + v^2 = u^2 - 2uv + v^2 = (u - v)^2$ which yields the single solution $u : v = 1 : 1$ (with multiplicity two). □

In Thm. 3, we did not explicitly state that the order of the underlying field is a prime, say p, different from a prime power p^k with $k \in \mathbb{N} \setminus \{0, 1\}$. It is clear that the number of degenerate triangles in an Yff porism will not exceed 2. If in $\mathrm{PG}(2, p)$ the Yff porism already has a degenerate triangle, then $\omega(x) = x^2 + x + 1$ already has at least one solution in $\mathrm{GF}(p)$ and $\omega(x)$ cannot be used for a quadratic field extension and no additional zeros will show up with a proper field extension.
We shall have a look at the following examples:
(1) If the underlying field $\mathbb{F}$ is a quadratic extension of $\mathrm{GF}(p)$, the number of zeros of δ may increase if $\mathbb{F} \cong \mathrm{GF}(p)[x]/(x^2 + x + 1)$. For example, there exists a unique quadratic extension of $\mathrm{GF}(2)$ in order to obtain $\mathrm{GF}(4)$, since $x^2 + x + 1$ is the only quadratic polynomial that has no zeros in $\mathrm{GF}(2)$. Hence, in $\mathrm{PG}(2, 4)$ the Yff porism contains two degenerate triangles, while in $\mathrm{PG}(2, 2)$ the Yff porisms consists of regular triangles only. We shall come back to $\mathrm{PG}(2, 4)$ in Sec. 3.2.3.
(2) The quadratic polynomial $x^2 + x + 1$ has a single zero of multiplicity two in $\mathrm{GF}(3)$. Therefore, it cannot be used for a quadratic extension of $\mathrm{GF}(3)$ in order to create $\mathrm{GF}(9)$. However, $x^2 + 1$ is suitable for the desired quadratic extension and its zeros are not zeros of δ from (9). Thus, in $\mathrm{GF}(9)$ the Yff porism still has a single degenerate triangle inherited from $\mathrm{GF}(3)$. For details, we refer to Sec. 3.2.6.
(3) The example of $\mathrm{GF}(5)$ is to show that there do exist quadratic field extensions so that the Yff porism shows both, degenerate and non-degenerate triangles. Both polynomials $\omega_1(x) = x^2 + x + 1$ and $\omega_2(x) = x^2 + x + 2$ have no zeros in $\mathrm{GF}(5)$. Since $\omega_1(x)$ is an inhomogeneous version of (9), the extension with $\omega_1(x)$ delivers two degenerate triangles, while the extension with $\omega_2(x)$ does not.
We will come back to field extensions and the thus created planes in Sec. 3.2.

The regularity condition for the contact triangle $B_1B_2B_3$ equals $2\delta = 0$. This shows again that the case $\operatorname{char}\mathbb{F} = 2$ plays an exceptional role.
Further, we can say:

Theorem 4 *If the Yff porism contains a degenerate triangle, then this triangle is a single point.*

Proof. According to Thm. 3, the matrix $\mathbf{P} := (\mathbf{p}_1, \mathbf{p}_2, \mathbf{p}_3)$ is singular if, and only if, (9) holds, *i.e.*, $\delta = 0$, or, likewise, $\operatorname{rk}\mathbf{P} \leq 2$. A triangle of the Yff porism becomes a single point if $\mathbf{P}$ is of rank 1 which is the case if, and only if, all 2×2 submatrices of $\mathbf{P}$ are singular. The determinants of the non-trivial 2×2 submatrices of $\mathbf{P}$ evaluate to one of the following polynomials (up to the coefficient -1, not playing a role even if $\operatorname{char}\mathbb{F} = 2$):

$$uv\delta, \;\; u(u+v)\delta, \;\; v(u+v)\delta,$$

which vanish all, if δ does. This is not the case if only one of the following is true $u : v = 1 : 0$, $u : v = 0 : 1$, or $u + v = 0$. The only larger minor is already singular by assumption, and therefore, it does not have to be taken into account. □

In Thm. 4, a distinction of the underlying field is not necessary. Once $\delta = 0$, the Yff porism contains at least one degenerate triangle, no matter, if $\delta = 0$ is caused by a field extension or not.
Common points of $\mathcal{M}$ and $\mathcal{N}$ and degenerate triangles do not enter the scene independently:

Theorem 5 *A degenerate triangle in the Yff porism is necessarily a common point of* $\mathcal{M}$ *and* $\mathcal{N}$*, and* vice versa*.*

Proof. Assume that there is a parameter $u : v \neq 0 : 0$ (with $u, v \in \mathbb{F}$) such that (9) is annihilated. Then, according to Thm. 3, $P_1 = P_2 = P_3$, *i.e.*, a pose with a degenerate triangle is reached. Inserting (5) and (7) into (4), we see that both equations are also fulfilled.
On the other hand, common points of $\mathcal{M}$ and $\mathcal{N}$ can be found by eliminating one variable, say, *e.g.* z, from both equations in (4). This yields $(x^2 + xy + y^2)^2 = 0$, which is fulfilled by any of the parametrizations of (5) and (7) if, and only if, $u^2 + uv + v^2 = 0$, *i.e.*, the points P_i coincide. □

For the following 80 prime integers less than 1000 (which are in total 168), (9) has two solutions in $\mathrm{GF}(p)$:

7, 13, 19, 31, 37, 43, 61, 67, 73, 79, 97, 103, 109, 127,
139, 151, 157, 163, 181, 193, 199, 211, 223, 229, 241,
271, 277, 283, 307, 313, 331, 337, 349, 367, 373, 379,
397, 409, 421, 433, 439, 457, 463, 487, 499, 523, 541,
547, 571, 577, 601, 607, 613, 619, 631, 643, 661, 673,
691, 709, 727, 733, 739, 751, 757, 769, 787, 811, 823,
829, 853, 859, 877, 883, 907, 919, 937, 967, 991, 997.

Thus, in $\mathrm{PG}(2, p)$ with one of the above p, the Yff porism contains two degenerate triangles and quadratic field extensions have to be constructed with a polynomial different from $x^2 + x + 1$ in any case. If $p = 3$, the polynomial

x^2+x+1 is not suitable for a quadratic field extension, since then it is a full square. For any other $p \neq 3$ and not in the above list, a quadratic field extension with x^2+x+1 would add two degenerate triangles to the Yff porism.
Field extensions $\mathrm{GF}(p^k)$ with arbitrary $k>2$ do not cause more degenerate triangles in the Yff porism as long as x^2+x+1 is not a divisor of the extension polynomial.
The chosen conics $\mathcal{M}$ and $\mathcal{N}$ with equation (4) have rather simple equations because of their relative position with respect to the underlying coordinate system. More general forms of rational and universal porisms can be obtained by applying collineations to $\mathcal{M}$, $\mathcal{N}$, and the family of interscribed triangles:

Theorem 6 *The totality of universal Yff porisms in a projective plane* $\mathrm{PG}(2,p)$ *can be obtained by applying the full group of regular projective transformations to the Yff porism determined by* $\mathcal{M}$ *and* $\mathcal{N}$*. In the projective plane* $\mathrm{PG}(2,p)$*, there exist* $p^3(p^3-1)(p^2-1)$ *collinear copies of the initial Yff porism.*

Proof. According to [10, p. 298], the number of 3×3 matrices $\mathbf{K}$ with entries from $\mathrm{GF}(p)$ and $\det\mathbf{K}=1$ equals $p^3(p^3-1)(p^2-1)$. Since non-zero multiples of $\mathbf{K}$ describe the same collineation, it is admissible to normalize the transformation matrices such that their determinants are equal to unity. □

3.2 Examples of Yff porisms in small planes

In the following, we shall describe the universal porisms in some finite projective planes of low order, *i.e.*, in small planes. For details and basic information on finite projective planes, we refer to [12].
The points (1) appear as poses of the vertices P_1, P_2, P_3 of the triangles in the poristic family in any projective plane over any (finite) field. Since for any prime p (5) and (7) evaluate to multiples of the canonical basis vectors, we shall use the labels of the vertices of the initial triangle Δ for those poses of the points P_i.
The vertices P_i of the triangles have the coordinate representations $\mathbf{p}_i(u_0,v_0)$ with $i\in\{1,2,3\}$ and the homogeneous parameter $(u,v)\neq(0,0)$ always traces the projective line $\mathrm{PG}(1,\mathbb{F})$, *i.e.*,

$$(u,v)\in\{(1_\mathbb{F},0_\mathbb{F}),(1_\mathbb{F},1_\mathbb{F}),\ldots,(0_\mathbb{F},1_\mathbb{F})\}.$$

Note that the parameter pairs are normalized, *i.e.*, the first coordinate is set to unity (except the last one) which can always be achieved. So, they are ordered numerically. This has no geometric meaning and is done just in order not to lose a point.

3.2.1 The minimal projective plane

The minimal projective plane is the unique projective plane with seven points and seven lines sometimes referred to as the Fano plane. (Despite not showing the Fano property: Here, the three diagonal points of a quadrilateral are collinear.) Its algebraic model is erected over $\mathrm{GF}(2)$. Although we have emphasized at several places that the case $\mathrm{char}\,\mathbb{F}=2$ has to be excluded or at least to be handled with care (polarities are null polarities at the same time), we find that the parametrizations (5) and (7) of the points P_i evaluate to meaningful expressions, whence we shall have a look at it.

There is only one triangle in the family: It is the standard triangle that plays its role in a threefold way and it is the only non-trivial triangle in this particular poristic family. We collect the triangles depending on the homogeneous parameter $u:v$ in a table:

$u:v$	1 : 0	1 : 1	0 : 1
triangle	*BCA*	*ABC*	*CAB*

Fig. 2 tries to illustrate the three poses of the moving triangle.

Note that in the minimal plane the conic $\mathcal{M}$ has a singular equation, since the determinant of the coefficient matrix vanishes:

$$\mathcal{M}: xy+yz+zx=\mathbf{x}^{\mathrm{T}}\underbrace{\begin{pmatrix}0&1&1\\0&0&1\\0&0&0\end{pmatrix}}_{=:\mathbf{M}}\mathbf{x}=0,$$

hence $\det\mathbf{M}=0$ and $\mathrm{rk}\,\mathbf{M}=2$. Here, we shall point out that the usual way of extracting the coefficient matrix from a quadratic form fails: We cannot multiply coefficients by 2.

However, the three points on $\mathcal{M}$ are not collinear as should be the case with conics.

In comparison, $\mathcal{N}$ whose equation simplifies due to the speciality of the underlying field according to

$$\mathcal{N}:\ x^2+y^2+z^2=0$$

is regular, but contains the three collinear points

$$B_1=1:1:0,\ \ B_2=1:0:1,\ \ B_3=0:1:1.$$

They also lie on the line $\mathcal{L}_1$. Hence, $\mathcal{N}$ and $\mathcal{L}_1$ agree as sets of points. Note that there is no contact between the sides of Δ and $\mathcal{N}$, since all tangents of $\mathcal{N}$ pass through its nucleus.

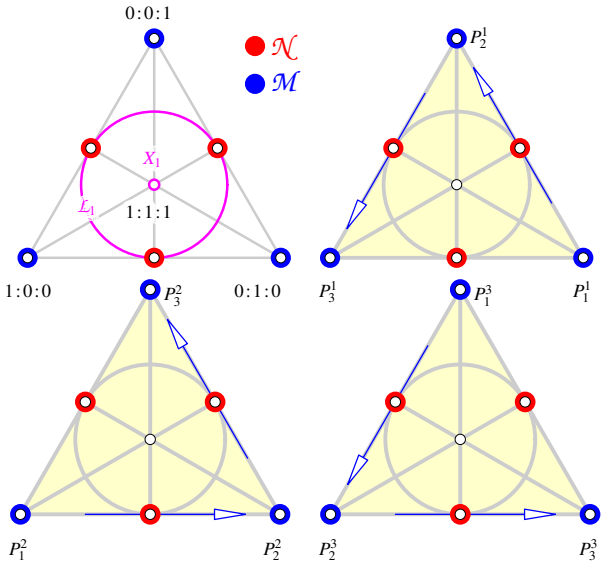

Figure 2: *The projective plane* PG(2,2) *with its seven points and lines and the two conics* $\mathcal{M}$ *and* $\mathcal{N}$*. A special feature can be observed here: The inconic* $\mathcal{N} = \mathcal{L}_1$ *consists of three collinear points. Superscripts denote the pose.*

3.2.2 The thirteen point plane

The unique projective plane of order three has thirteen points and lines. It can be modeled over GF(3). An incidence graph and the coordinatization that we use are shown in Fig. 3. In the thirteen point plane PG(2,3), the two conics $\mathcal{M}$ and $\mathcal{N}$ are regular. They share precisely one point, *i.e.*, X_1 and have the line $\mathcal{L}_1$ as common tangent there.

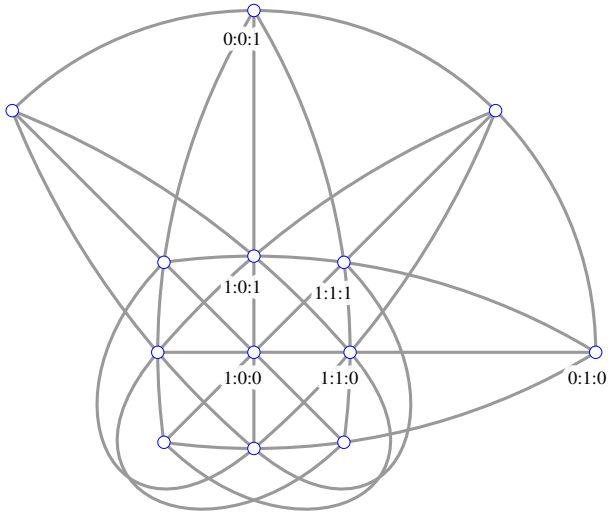

Figure 3: *The plane of order 3 with 13 points and lines is isomorphic to the projective plane* PG(2,3).

Again, the standard triangle plays a threefold role for the parameter values

$$u : v = 1 : 0, \quad u : v = 1 : 2, \quad u : v = 0 : 1.$$

According to Thm. 3, the Yff porism in PG(2,3) contains a single degenerate triangle corresponding to δ's single (double) root $u : v = 1 : 1$. The degenerate triangle equals the point X_1, which is the only point of intersection of $\mathcal{M}$ and $\mathcal{N}$. This holds true in any plane over GF(3^k) with positive k.

Fig. 4 illustrates the position of $\mathcal{M}$ and $\mathcal{N}$ in PG(2,3) relative to each other. Fig. 5 is given in order to illustrate the poristic family in PG(2,3).

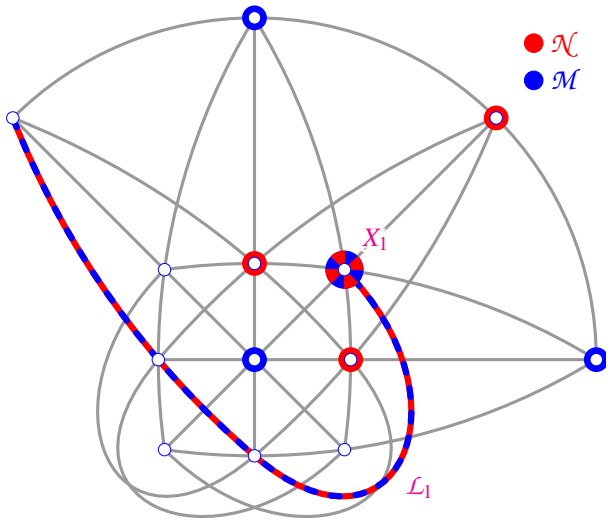

Figure 4: *Both Yff conics consist of four non-collinear points, they intersect in* X_1 *and share the tangent* $\mathcal{L}_1$ *there.*

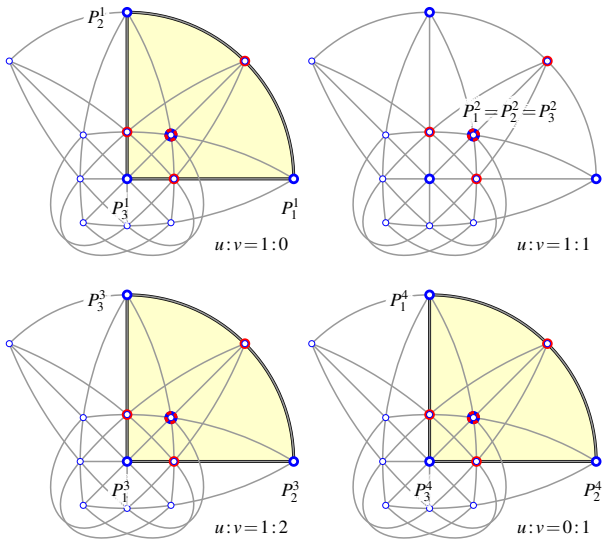

Figure 5: *The Yff porism in the 13 point plane shows a single degenerate triangle corresponding to* $u:v=1:1$ *and all three vertices fall into the point* $1:1:1$ *(see top right).*

In order to track the triangle while it moves through the poristic family, we collect the different poses of $P_1P_2P_3$ in

the following table:

$u:v$	$1:0$	$1:1$	$1:2$	$0:1$
triangle	BCA	$1:1:1$	ABC	CAB

3.2.3 The projective plane of order 4

The projective plane $\mathrm{PG}(2,4)$ of order 4 consists of 21 points and lines. The underlying field $\mathrm{GF}(4)$ is obtained from $\mathrm{GF}(2)$ by the unique quadratic field extension $\mathrm{GF}(4)=\mathrm{GF}(2)[x]/(x^2+x+1)$. This clearly shows that the Yff porism in $\mathrm{PG}(2,4)$ contains two degenerate triangles (since the polynomial used for the extension is an inhomogeneous version of δ from (9)). However, $\mathrm{PG}(2,4)$ inherits all properties from $\mathrm{PG}(2,2)$ including the singularity and regularity of conics. Only the order of the underlying field changes, not so the characteristic.

The field $\mathrm{GF}(4)$ is obtained from $\mathrm{GF}(2)$ by the quadratic field extension with the *only* quadratic polynom $\omega(x)=x^2+x+1$ that has no zeros over $\mathrm{GF}(2)$. If we label the elements of $\mathrm{GF}(4)$ by $\{0,1,a,1+a\}$, then we compute modulo 2 and simplify sums and products according to $a^2+a+1=0$. Fig. 6 shows an incidence diagram of $\mathrm{PG}(2,4)$ with the coordinatization used in this section.

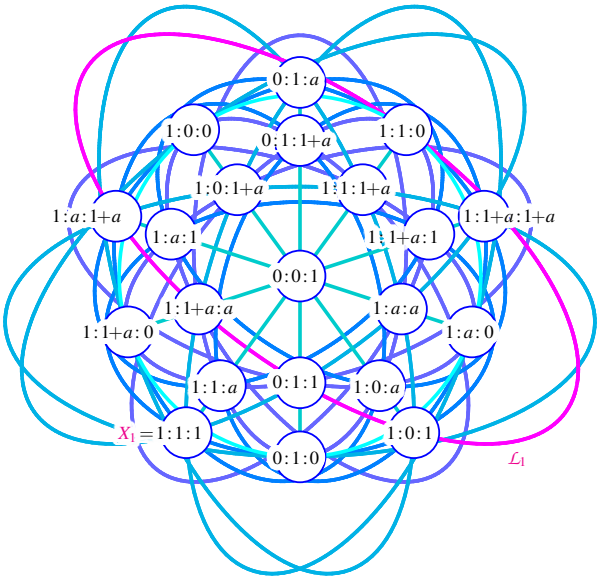

Figure 6: *The 21 point plane modeled over* $\mathrm{GF}(4)$ *contains Fano-subplanes, and therefore, it doesn't have the Fano property: The diagonal points of quadrilaterals are collinear mirroring the property of the algebraic model based on the field* $\mathrm{GF}(4)$ *whose characteristic equals 2.*

The conic $\mathcal{M}$ has a singular equation in $\mathrm{PG}(2,4)$ (like in the case of $\mathrm{GF}(2)$ and for the same reasons) and consists of the five points

$$0:1:0,\quad 1:0:0,\quad 1:a:1+a,\\ 1:1+a:a,\quad 0:0:1,$$

of which no three are collinear, while the conic $\mathcal{N}$ has a regular equation and consists of the five collinear points

$$1:1:0,\quad 1:0:1,\quad 0:1:1,\\ 1:a:1+a,\quad 1:1+a:a.$$

Obviously, the two Yff conics intersect in

$$S_1=1:a:1+a \quad\text{and}\quad S_2=1:1+a:a.$$

The diagram in Fig. 7 illustrates the relative position of the two conics $\mathcal{M}$ and $\mathcal{N}$ in $\mathrm{PG}(2,4)$.

The quadratic form $\delta=u^2+uv+v^2$ equals ω if we substitute $u=1$ and $v=x$. Hence, the two new elements in the extension $\mathrm{GF}(4)$ of $\mathrm{GF}(2)$ are zeros of δ. Thus, in $\mathrm{GF}(4)$, the Yff porism contains two degenerate triangles. The parameters $u:v=1:a$ and $u:v=1:1+a$ deliver the two degenerate triangles in the Yff porism, which coincide with the points S_1 and S_2 (the intersections of $\mathcal{M}$ and $\mathcal{N}$).

By virtue of (5) and (7), we find the vertices of the triangles in the poristic family as

$u:v$	$1:0$	$1:1$	$1:a$
triangle	BCA	ABC	$1:a:1+a$
$u:v$	$1:1+a$	$0:1$	
triangle	$1:1+a:a$	CAB	

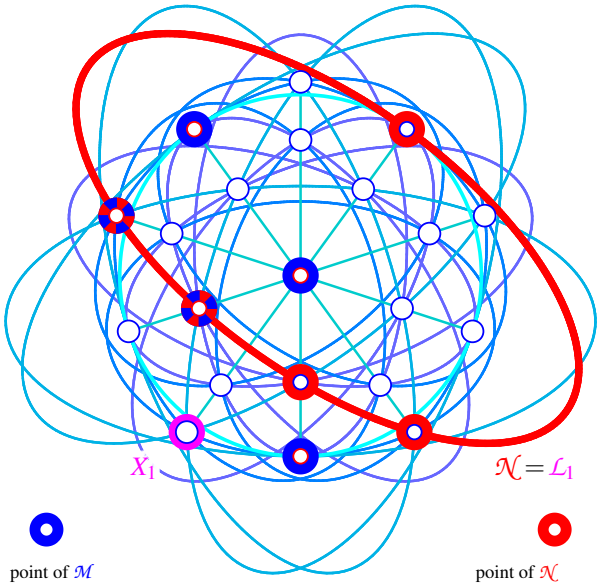

Figure 7: *In* $\mathrm{PG}(2,4)$*, the* circumconic $\mathcal{M}$ *is regular, while the* inconic $\mathcal{N}$ *consists of five collinear points. Further,* $\mathcal{M}$ *and* $\mathcal{N}$ *share two points playing the role of the degenerate triangles in the poristic family.*

3.2.4 The planes over GF(5) and GF(7)

We shall treat the two planes over GF(5) and GF(7) simultaneously which helps simplifying the comparison. In Figs. 8 and 9, we have illustrated an affine version of the respective Yff porisms.

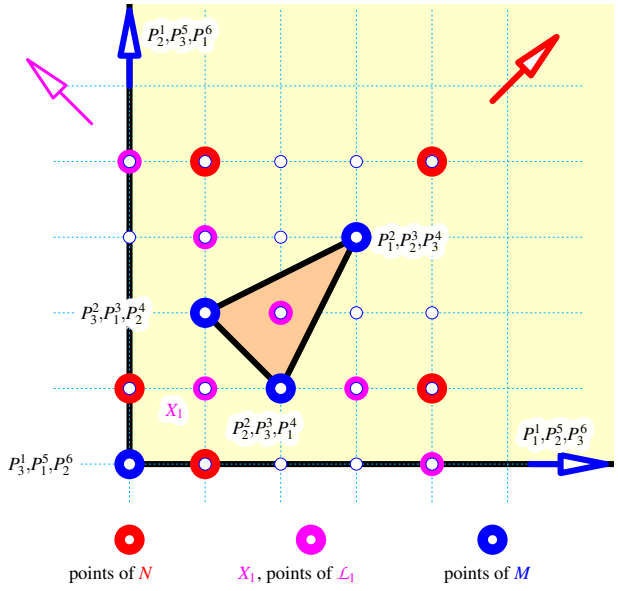

Figure 8: *The Yff porism in an affine part of the plane* PG(2,5)*:* $\mathcal{M}\cap\mathcal{N}=\emptyset$ *and the Yff porism contains only non-degenerate triangles each playing a threefold role.*

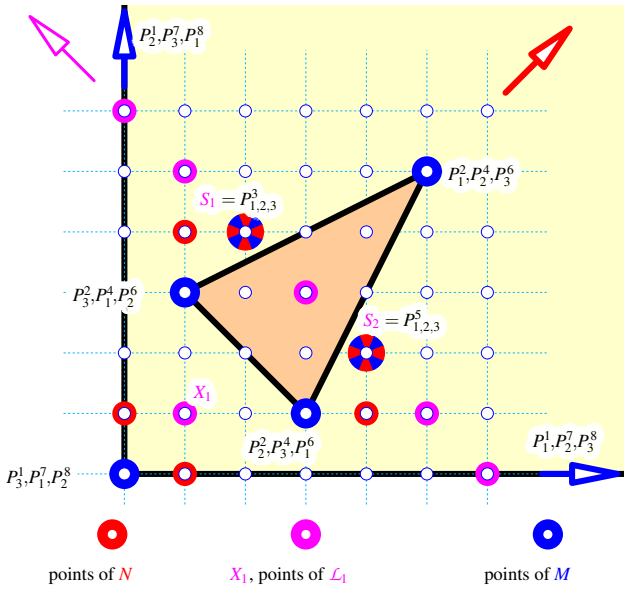

Figure 9: *The Yff porism in an affine part of the plane* PG(2,7)*:* $\mathcal{M}\cap\mathcal{N}=\{S_1,S_2\}$ *and the two degenerate triangles fall into the points* S_1 *and* S_2*.*

In both planes PG(2,5) / PG(2,7), both Yff conics have regular equations and consist of 6 / 8 points where no three of them are collinear. While $\mathcal{M}$ and $\mathcal{N}$ do not intersect in PG(2,5), they share the two points

$$S_1=1:2:4 \quad\text{and}\quad S_2=1:4:2$$

in PG(2,7). Further, $\mathcal{M}$ and $\mathcal{N}$ share the tangents S_1 and S_2. Thus, in PG(2,7), the pencil spanned by $\mathcal{M}$ and $\mathcal{N}$ resembles a pencil of the third kind as we know it from the case $\mathbb{F}=\mathbb{C}$.
The two intersection points S_1 and S_2 of $\mathcal{M}$ and $\mathcal{N}$ in PG(2,7) serve as the degenerate triangles in the Yff porism. On the contrary, degenerate triangles are missing in the Yff porism over GF(5).

3.2.5 A cubic field extension: the projective plane over GF(8)

The field GF(8) shall be constructed from GF(2) by the cubic field extension with the roots of $\omega(x)=x^3+x+1$ which is irreducible in GF(2). This means computations are performed modulo 2 and modulo ω. The elements of GF(8) shall be denoted by

$$\{0,1,a,1+a,a^2,1+a^2,a+a^2,1+a+a^2\}.$$

The triangle $P_1P_2P_3$ with the parametrization (5) and (7) reaches the following poses while the homogeneous parameter $u:v$ traverses PG(1,8):

$u:v$	$1:0$	$1:1$	$1:a$
triangle	BCA	ABC	$R_1S_1T_1$
$u:v$	$1:1+a$	$1:a^2$	$1:1+a^2$
triangle	$R_2S_2T_2$	$S_1T_1R_1$	$T_2R_2S_2$
$u:v$	$1:a+a^2$	$1:1+a+a^2$	$0:1$
triangle	$T_1R_1S_1$	$S_2T_2R_2$	CAB

where we have set

$$R_1=1:a^2:1+a,\quad S_1=1:a:1+a+a^2,$$
$$T_1=1:a+a^2:1+a^2,$$
$$R_2=1:1+a+a^2:a,\quad S_2=1:1+a:a^2,$$
$$T_2=1:1+a^2:a+a^2.$$

There is no degenerate triangle in the Yff porism in PG(2,8), since (9) has no zeros in GF(8). The poristic orbit of the triangle *ABC* splits into three suborbits and the *moving* triangle changes the orbits more or less irregularly, for it is not possible to establish an ordering in GF(8).

3.2.6 The only Desarguesian plane of order 9

Among the four non-isomorphic projective planes of order 9, only the plane PG(2,9) is Desarguesian. Because of the commutativity of GF(9), the projective plane PG(2,9) is also Pappian, and thus, the study of conics makes sense there (cf. [9]), whence it makes sense to consider this particular plane of order 9. (Note that any Pappian plane is

Desarguesian, but on the contrary, not any Desarguesian plane is Pappian, cf. [9]).
The field GF(3) shall be extended to GF(9) by adding the roots of $\omega(x)=x^2+1$ (which do not exist in GF(3)). It is well-known that any other quadratic polynomial (without zeros in GF(3)) leads to an isomorphic copy of the field of order 9. We label the nine elements of GF(9) by

$$\{0,1,2,a,1+a,2+a,2a,1+2a,2+2a\}$$

and calculate modulo 3 and modulo ω. Then, (5) and (7) yield the following triangles:

$u:v$	1:0	1:1	1:2	1:a
triangle	BAC	1:1:1	ACB	$R_1S_1T_1$
$u:v$	1:1+a	2+a	2a	1+2a
triangle	$S_1T_1R_1$	$R_2S_2T_2$	$T_1R_1S_1$	$T_2R_2S_2$
$u:v$	2+2a	0:1		
triangle	$S_2T_2R_2$	CAB		

where we have used the abbreviations

$$R_1=1:2+a:2+2a,\quad S_1=1:a:1+a,$$
$$T_1=1:1+2a:2a,$$
$$R_2=1:2a:1+2a,\quad S_2=1:1+a:a,$$
$$T_2=1:2+2a:2+a,$$

There is only one degenerate triangle in the poristic family. The degenerate triangle corresponds to the parameter $u:v=1:1$ and is inherited from GF(3), and as such, rather a feature of GF(3), than of GF(9). However, $\operatorname{char}\mathrm{GF}(9)=\operatorname{char}\mathrm{GF}(3)=3$.

4 More universal porsims

4.1 The tangent triangle

For the case of CHAPPLE's porism (triangles with common incircle and circumcircle), it is shown that the vertices of the tangent triangle Δ_t, *i.e.*, the triangle of tangents to the circumcircle at Δ's vertices, move on an ellipse which is of course traced thrice, while Δ traverses the poristic family (see [19]).
For the tangent triangle of $\mathcal{M}$ in the Yff porism, we can show:

Lemma 1 *In any projective plane* $\mathrm{PG}(2,\mathbb{F})$ *with* $\operatorname{char}\mathbb{F}\neq 2$*, the vertices of the tangent triangle of* $\mathcal{M}$ *trace a single conic* $\mathcal{T}$*, while the initial triangle traverses the Yff porism.* $\mathcal{T}$ *is the image of* $\mathcal{N}$ *under the harmonic homology with center* X_1 *and axis* $\mathcal{L}_1$*.*

Proof. When determining the vertices T_i of the tangent triangle Δ_t, we observe that the tangents t_i of $\mathcal{M}$ at P_i have homogeneous coordinate vectors proportional to those of B_i given in (8) and (6). Then, for example, $T_1=t_2\cap t_3$ is given by

$$T_1=u^2+3uv+v^2:-u^2-uv+v^2:u^2-uv-v^2$$

and the others are obtained by permuting the coordinate functions of the latter. Now, the implicitization of the parametrization of T_1 yields

$$\mathcal{T}:\ \sum_{\text{cyclic}} x^2+3yz=0 \tag{10}$$

and confirms that T_1 runs on a conic. It is easily verified that the points T_2 and T_3 also trace $\mathcal{T}$ while Δ and Δ_t move through the Yff porism.
We can check that $\operatorname{cr}(P_i,B_i,X_1,T_i)=-1$ for all $i\in\{1,2,3\}$. Furthermore, by the initial construction, it is elementary to verify that $[B_i,B_j]\cap t_j=[P_i,P_j]\cap t_k\in\mathcal{L}_1$ for $(i,j,k)\in\{(1,2,3),(2,3,1),(3,1,2)\}$. Hence, the harmonic homology $\rho_{X_1,\mathcal{L}_1}$ (with center X_1 and axis $\mathcal{L}_1$) sends B_i to T_i and maps the respective tangents of $\mathcal{N}$ and $\mathcal{T}$ onto each other. □

Lem. 1 is in particular valid in the real and in the complex projective plane. In planes of characteristic two (or equivalently, in planes over fields of characteristic two), the construction of the tangent conic must fail for two reasons:
(1) The tangents of a conic pass through a single point (the nucleus). If the characteristic of the underlying plane (or field) equals 3, we have $\mathcal{T}:\ \sum_{\text{cyclic}} x^2=0$.
(2) In the planes of characteristic 2 there are no harmonic homologies.

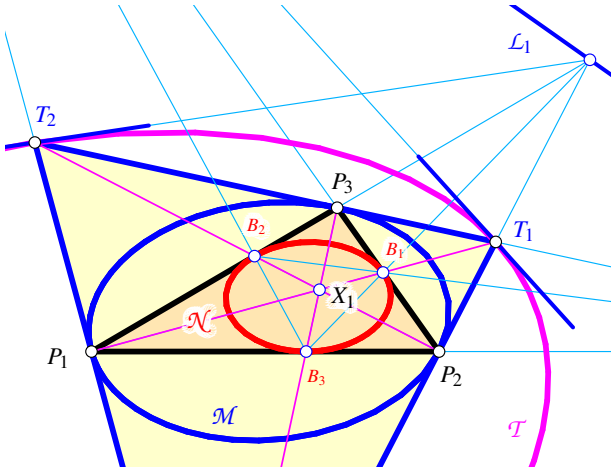

Figure 10: *Iterating the Yff porism can yield infinitely many universal porisms.*

Fig. 10 illustrates the geometric relations between pairs of subsequent conics and the orbits of tangent triangles in the Yff pencil.
If **M**, **N**, and **T** denote the coordinate matrices of the homogeneous equations of the conics $\mathcal{M}$, $\mathcal{N}$, and $\mathcal{T}$, then $\mathbf{T}=5\cdot\mathbf{M}+2\cdot\mathbf{N}$. Hence, $\mathcal{T}$ is also an Yff conic (cf. [15]).

4.2 A linear family of matrices

The coefficient matrices of the conics $\mathcal{M}$, $\mathcal{N}$, and $\mathcal{T}$ belong to the special family of matrices that can be parametrized by

$$\mathbf{L}(p,q) = \begin{pmatrix} p & q & q \\ q & p & q \\ q & q & p \end{pmatrix}, \tag{11}$$

with entries $p,q \neq 0$ from some commutative field $\mathbb{F}$. The linear one-parameter family of matrices (11) forms a straight line in the eight-dimensional projective space of 3×3 matrices. Note that the coefficient matrices of these triangle conics do also not depend on Euclidean notions such as the side lengths of Δ.

For the sake of simplicity (and since non-zero multiples do not count), we shall assume $\gcd(p,q) = 1$ (in the underlying field under consideration). The matrices $\mathbf{L}(p,q)$ are regular if, and only if,

$$p^3 - 3pq^2 + 2q^3 = (p-q)^2(p+2q) \neq 0,$$

i.e., $p:q \neq 1:1$ and $p:q \neq -2:1$. The two singular matrices in the family (11) are $\mathbf{L}(1,1)$ and $\mathbf{L}(-2,1)$. While $\operatorname{rk}\mathbf{L}(1,1) = 1$ and $\ker\mathbf{L}(1,1) = [(1,-1,0),(1,0,-1)]$, we have $\operatorname{rk}\mathbf{L}(-2,1) = 2$ and $\ker\mathbf{L}(-2,1) = (1,1,1)$.

The regular matrices (11) form a commutative group, since the multiplication obeys the rule

$$\begin{gathered}\mathbf{L}(p_1,q_1)\cdot\mathbf{L}(p_2,q_2) = \\ = \mathbf{L}(p_1p_2 + 2q_1q_2, p_1q_2 + p_2q_1 + q_1q_2),\end{gathered}$$

the inverses are

$$\mathbf{L}(p,q)^{-1} = \mathbf{L}\left(p+q,-q\right)/(p^2+pq-2q^2)$$

(provided that $p^2+pq-2q^2 \neq 0$, *i.e.*, $\mathbf{L}(p,q)$ is regular), and $\mathbf{L}(1,0)$ is the neutral element.

4.3 More tangent triangles

The coefficient matrices of $\mathcal{M}$ and $\mathcal{N}$ of the Yff conics in (4) are $\mathbf{M} = \mathbf{L}(0,1)$ and $\mathbf{N} = \mathbf{L}(1,-1)$. For the coefficient matrix of $\mathcal{T}$ from (10), we find $\mathbf{T} = \mathbf{L}(2,3)$. Moreover, the respective matrices in (4) satisfy

$$\mathbf{M}\cdot\mathbf{N} = -2\mathbf{I}_3 \tag{12}$$

as long as $\operatorname{char}\mathbb{F} \neq 2$. Further, we can easily verify that

$$\mathbf{T} = \mathbf{M}(\mathbf{N}^{-1}\mathbf{M})^1 = -\frac{1}{2}\mathbf{M}^3. \tag{13}$$

Since $\mathcal{T}$ is the polar conic of the dual conic $\mathcal{N}^\star$ (the set of tangents of $\mathcal{N}$) with respect to $\mathcal{M}$, $\mathcal{T}$ is a successor of $\mathcal{N}$ and $\mathcal{M}$ in the exponential pencil of conics spanned by $\mathcal{N}$ and $\mathcal{M}$ (cf. [11]).

According to [11], the conics in the exponential pencil spanned by two regular conics $\mathcal{C}_0 : \mathbf{x}^{\mathrm{T}}\mathbf{C}_0\mathbf{x} = 0$ and $\mathcal{C}_1 : \mathbf{x}^{\mathrm{T}}\mathbf{C}_1\mathbf{x} = 0$ have equations of the form $\mathbf{x}^{\mathrm{T}}\mathbf{C}(t)\mathbf{x} = 0$ with

$$\mathbf{C}(t) = \mathbf{C}_1\cdot\left(\mathbf{C}_0^{-1}\cdot\mathbf{C}_1\right)^{t-1}, \quad t\in\mathbb{F}.$$

Again, the case $\operatorname{char}\mathbb{F} = 2$ has to be excluded, since there $\mathbf{M}$ is singular. In [11], the coordinate t in the exponential pencil was assumed to be real. By virtue of Lem. 1, $t\in\mathbb{F}$ it makes sense.

With $\mathbf{C}_0 = \mathbf{N}$ and $\mathbf{C}_1 = \mathbf{M}$ and by virtue of (12), the coefficient matrices of the conics' equations in the thus defined exponential pencil are

$$\mathbf{C}(t) = (-\tfrac{1}{2})^{t-1}\mathbf{M}^{2t-1} = (-2)^u\mathbf{N}^{1-2u}, \tag{14}$$

where $t+u = 1$. Here, it is more obvious that fields $\mathbb{F}$ with $\operatorname{char}\mathbb{F} = 2$ do not play a role.

Defining the matrices $\mathbf{C}_i$ the other way around, *i.e.*, $\mathbf{C}_1 = \mathbf{N}$ and $\mathbf{C}_0 = \mathbf{M}$, means to trace the pencil of conics in the opposite direction.

In the case $\mathbb{F}\cong\mathbb{R}$, we can describe the limit conics in the exponential pencil: For $t\to\infty$, the matrices $\mathbf{C}(t)$ converge towards the singular matrix $\mathbf{L}(1,1)$ which describes $\mathcal{L}_1$ as a repeated line. The limit $t\to-\infty$ yields $\mathbf{L}(2,-1)$ corresponding to X_1 as the intersection of the pair of complex conjugate tangents

$$\sum_{\text{cyclic}} x^2 - yz = (x+\varepsilon y+\varepsilon^2 z)(x+\varepsilon^2 y+\varepsilon z) = 0,$$

(where ε is a non-trivial third root of unity) common to all conics in the linear and the exponential pencil (in the case of $\mathbb{F} = \mathbb{C}$). Obviously, $\mathbf{C}(2)$ evaluates to the coefficient matrix of the conic $\mathcal{T}$ in (10), *i.e.*, $\mathbf{C}(2) = -\frac{1}{2}\mathbf{L}(2,3)$.

We can repeat the construction of the tangent triangle now applied to $\mathcal{T}$ and the triangles $T_1T_2T_3$ and, by virtue of Lem. 1, we can state:

Theorem 7 *Any pair of subsequent conics in the exponential pencil spanned by $\mathcal{N}$ and $\mathcal{M}$ allows for a universal porism of $3n$-gons, provided there are sufficiently many points and conics in the plane under consideration and the exponential parametrization is evaluated only at integers.*

We can also give a more synthetic generation of the sequence of pairs of conics allowing for rational porisms:

Theorem 8 *Any conic in the exponential pencil together with its tangent triangle (including the contact points) is the image of its pre-predecessor under a harmonic homology with center X_1 and axis $\mathcal{L}_1$.*

4.4 The chain of universal porisms

The triangle $B_1B_2B_3$ is perspective with $P_1P_2P_3$ and both are perspective with $T_1T_2T_3$. The common perspector for any pair of triangles is the point X_1. Any two out of the three triangles share the perspectrix, the line $\mathcal{L}_1$.

According to Thm. 7, this is true for any pair of triangles in the infinite chain of contact and tangent triangles. In this way, we find infinitely many nested Desargues configurations with the perspector X_1 and perspectrix $\mathcal{L}_1$. The same holds true for the contact triangle. These Desargues configurations are more special than those constructed in [18].

Subsequent contact and tangent triangles are mapped to their successors by means of a harmonic homology. Further, the coefficients of equations of all conics in the pencil contain only elements of the underlying field and (especially in the Euclidean case) do not depend on the triangle's side lengths, we have:

Theorem 9 *Independent of the underlying field* $\mathbb{F}$ *(with* $\operatorname{char}\mathbb{F} \neq 2$*), the exponential pencil of conics spanned by* $\mathcal{N}$ *and* $\mathcal{M}$ *contains at most as many poristic* $3n$*-gon families as there are pairs of subsequent conics in the exponential pencil of conics.*

The number of poristic triangle families in the Yff pencil is equal to the number of points on a line if $\mathbb{F} \cong \mathbb{R}, \mathbb{C}$. In the case of finite fields we have to distinguish several cases:

(1) If $\operatorname{char}\mathbb{F} = 2$, the Yff pencil consists of three conics with the coefficient matrices $\mathbf{N} = \mathbf{L}(1,0)$, $\mathbf{M} = \mathbf{L}(0,1)$, $\mathbf{T} = \mathbf{L}(1,1)$ of rank 3, 2, 1. The *conic* $\mathcal{T}$ is the repeated line $\mathcal{L}_1$, which agrees with $\mathcal{N}$ as point set. In $\mathrm{PG}(2,2)$, tangent conics do not exits, to be more precise the tangent triangle of $\mathcal{M}$ collapses to a point as can be seen by evaluating the parametrization of $\mathcal{T}$ given prior to (10). So, there is only a triad of triangles forming the one and only poristic family. (as explained in Section 3.2.1).

(2) If $\operatorname{char}\mathbb{F} = 3$, the Yff pencil contains the four conics defined by the coefficient matrices $\mathbf{N} = \mathbf{L}(1,2)$, $\mathbf{M} = \mathbf{L}(0,1)$, $\mathbf{T} = \mathbf{L}(1,0)$, and further $\mathbf{L}(1,1)$. The latter is of rank 1 and corresponds to the repeated line $\mathcal{L}_1$ as a singular conic. The tangent triangle of $\mathcal{M}$ moves on $\mathcal{T}$ and passes one instant of degeneracy, which is again the point X_1 corresponding to $u : v = 1 : 1$. Since there are only 3 regular conics in the pencil, we find only 3 different Yff porisms in $\mathrm{PG}(2,3)$ (up to collineations). Fig. 11 shows one particular pose in each of the three nested poristic families.

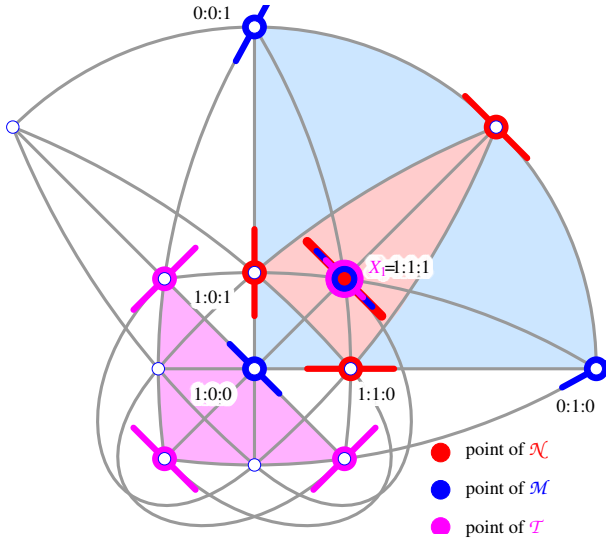

Figure 11: *The chain of Yff porisms in* $\mathrm{PG}(2,3)$ *contains three poristic triangle families: (i) between* $\mathcal{N}$ *and* $\mathcal{M}$*, (ii) between* $\mathcal{M}$ *and* $\mathcal{T}$*, and (iii) between* $\mathcal{T}$ *and* $\mathcal{N}$*. The point* X_1 *plays the role of the degenerate triangle in each porism. The line* $\mathcal{L}_1$ *(with multiplicity two) is a degenerate conic in the discrete exponential pencil.*

(3) Let us now assume that $\operatorname{char}\mathbb{F} \neq 2,3$ is a prime p. Then it is rather elementary to verify that the coefficient matrices of the conics in the pencil are matrices proportional to

$$\mathbf{L}\left(\frac{1}{6}(4^k-4), \frac{1}{6}(4^k+2)\right), \quad k \in \mathbb{F}.$$

(Note the denominator.) The base $4_{\mathbb{F}}$ can never be a generator of the multiplicative group in some $\mathrm{GF}(p)$, for odd powers of $2_{\mathbb{F}}$ cannot be reached. Hence, the number of conics in the Yff pencil is at most $\frac{1}{2}(p-1)$.

In Tab. 1, we have collected those primes $17 \leq p \leq 2011$ for which in $\mathrm{PG}(2,p)$ the number y of conics in the discrete exponential pencil and of Yff porisms is less than $\frac{1}{2}(p-1)$.

In the case of a prime $p = F(k) = 2^{2^k} + 1$, we have observed that $y(p) = 2^k$ if $k \in \{1,2,3,4\}$. Unfortunately, the projective plane of order $F(0) = 3$ does not fit. Since no prime $F(k)$ with $k > 5$ is known (as to October 2024), it is therefore also unclear, whether there do exist further finite projective planes of Fermat prime order $F(k)$ that allow for only 2^k Yff porisms.

Applying Thm. 6 to all results in this section leads to all possible variants of chains of rational Yff porisms in finite planes. Thms. 7, 8, and 9 remain valid if we apply any regular projective transformation to $\mathcal{N}$, $\mathcal{M}$, and the interscribed triangle family.

p	17	31	41	43	73	89	97	109	113
y	4	5	10	7	9	11	24	18	14
p	127	137	151	157	193	223	229	233	241
y	7	34	15	26	48	37	29	12	38
p	251	257	277	281	283	307	313	331	337
y	25	8	47	35	47	51	78	15	21
p	353	397	401	409	431	433	439	449	457
y	44	22	100	102	43	36	73	112	38
p	499	521	569	571	577	593	601	617	631
y	83	130	142	57	72	74	25	77	45
p	641	643	673	683	691	727	733	739	761
y	42	107	24	11	115	121	122	123	190
p	769	809	811	827	881	911	919	929	937
y	192	202	135	214	55	91	153	232	117
p	953	971	977	997	1009	1013	1021	1033	1049
y	34	97	244	166	252	46	170	129	131
p	1051	1069	1093	1097	1103	1129	1153	1163	1181
y	175	170	182	137	29	282	144	83	118
p	1193	1201	1217	1249	1289	1297	1321	1327	1361
y	149	150	76	78	161	324	30	221	340
p	1399	1409	1423	1429	1433	1459	1471	1481	1489
y	233	352	237	42	179	243	245	185	372
p	1553	1579	1597	1601	1609	1613	1627	1657	1697
y	97	263	266	200	201	26	271	46	424
p	1699	1709	1721	1723	1753	1777	1789	1801	1811
y	283	122	215	287	73	37	298	25	181
p	1831	1873	1889	1913	1933	1993	1999	2003	2011
y	305	468	236	239	322	498	333	143	201

Table 1: *Orders p of planes* $\mathrm{PG}(2,p)$ *in which the number y of subsequent regular conics and porisms in the discrete exponential Yff pencil is less than* $\frac{1}{2}(p-1)$.

5 Some Euclidean properties of the Yff porism

For the sake of completeness, we shall end the study of the Yff pencil and Yff porism by adding some results concerning the Euclidean plane. We restrict ourselves to a small number of moving points.

5.1 Some central orbits

With the parametrization of the triangles in the poristic family from (5) and (7) we can immediately determine the orbits of triangle centers. Many of them turn out to be centers which still does not answer the question raised in [5] why there are so many elliptic orbits. Of course, since each triangle vertex takes the role of any other vertex, the orbits of centers are traced three times by the corresponding center. We can state:

Theorem 10 *The orbits of the triangle centers X_i of a triangle Δ traversing the Yff porism in the Euclidean plane with Kimberling indices $i = \{2,3,4,5,6\}$ are ellipses.*

Proof. The centroid X_2 is the harmonic conjugate of the ideal line $\omega := a : b : c$, *i.e.*, the pole of ω with respect to Δ. Hence, we obtain a parametrization of the one-parameter family of centroids with triangle center function

$$\begin{aligned}
&bc(u^6+v^6)+3bcuv(u^4+v^4)\\
&+(b-c)(b+c-2a)(v^4-u^4)uv\\
&-(3a^2-8ab+2ac+b^2-4c^2)u^4v^2\\
&-(3a^2+2ab-8ac-4b^2+c^2)u^2v^4\\
&-(6a^2-6ab-6ac-3b^2+5bc-3c^2)v^3u^3,
\end{aligned}$$

i.e., the second and third coordinate function can be obtained by cyclically replacing a, b, c, while we keep the parameters u and v in their place.
Implicitization of the latter parametrization yields the quadratic trivariate form

$$\begin{aligned}
O_2 :\ &\sum_{\text{cyclic}} a(a+b+c)x^2\\
&-(2a(b+c)-b^2+bc-c^2)yz=0,
\end{aligned}$$

which is the equation of a conic centered at the yet unknown triangle center with the generating trilinear center function

$$\begin{aligned}
&2(b+c)a^2-(3b^2+5bc+3c^2)a\\
&+(b+c)(b^2-3bc+c^2).
\end{aligned}$$

The orbits of the circumcenter, the orthocenter, the nine-point center, and the symmedian point are determined in the same way, once a parametrization of the respective centers is known. The circumcenter X_3 is the center of the circumircle $\mathcal{U}$ of $\Delta = P_1P_2P_3$ with the equation

$$\begin{aligned}
\mathcal{U}\colon &\sum_{\text{cyclic}} x^2auv(u+v)\Big(bc(b-c)(u^3-v^3)\\
&+\big((b+c)a^2-abc-b^3+2b^2c-bc^2-c^3\big)u^2v\\
&+\big((b+c)a^2-abc-b^3-b^2c+2bc^2-c^3\big)uv^2\Big)\\
&+\Big(a^2bc(u^2+v^2)(u^4-u^2v^2+v^4)\\
&+a\big((b+c)a^2+3abc-(b-c)(b^2+c^2)\big)u^5v\\
&-a\big((b+c)a^2-3abc-(b-c)(b^2+c^2)\big)uv^5\\
&-\big(a^4-(3b-2c)a^3-2(b^2+c^2)a^2\\
&+(3b^3-4b^2c+bc^2-2c^3)a+(b^2-c^2)^2\big)u^4v^2\\
&-\big(a^4+(2b-3c)a^3-2(b^2+c^2)a^2\\
&-(2b^3-b^2c+4bc^2-3c^3)a+(b^2-c^2)^2\big)u^2v^4\\
&-\big(+2a^4-(b+c)a^3-(4b^2-5bc+4c^2)a^2\\
&(c+b)(b^2-4bc+c^2)a+2(b^2-c^2)^2\big)u^3v^3\Big)yz.
\end{aligned}$$

Now, it is rather elementary to determine the center of $\mathcal{U}$ as the pole of ω with respect to $\mathcal{U}$. We omit writing down the rather lengthy parametrization of the circumcenters. The elimination of the homogeneous parameter $u : v \neq 0 : 0$

yields the equation of an ellipse centered at the unknown triangle center

$$C_3 = a\big((b+c)a^4-(2b^2+5bc+2c^2)a^3+ 4bc(b+c)a^2+ (2b^4+b^3c-4b^2c^2+bc^3+2c^4)a -(b-c)^2(b+c)^3\big) ::$$

The orthocenter X_4 is the intersection of Δ's altitudes. Note that in terms of trilinear coordinates, the homogeneous trilinear coordinates of the altitudes are found as

$$\mathbf{h}_k = \mathbf{p}_k \times \mathbf{G}(\mathbf{p}_i \times \mathbf{p}_j)$$

with $(i,j,k) \in J_3$, where

$$J_3 := \{(1,2,3),(2,3,1),(3,1,2)\},$$

and $\mathbf{p}_i$ are homogeneous coordinate vectors of the vertices P_i, and $\mathbf{G}$ is the singular 3×3 matrix

$$\mathbf{G} = \begin{pmatrix} 1 & -\cos C & -\cos B \\ -\cos C & 1 & -\cos A \\ -\cos B & -\cos B & 1 \end{pmatrix}$$

ruling the orthogonality in Δ's plane (cf. [14, p. 29]). We recall that the cosines of Δ's interior angles can be expressed in terms of its side lengths as rational functions:

$$\cos A = (b^2+c^2-a^2)/(2bc) \ \text{(cyclic)}.$$

The intersection of any two altitudes results in a rather lengthy homogeneous parametrization of the orthocenter's trace, which after implicitization, again results in a conic $\mathcal{C}_4$ with the equation

$$\mathcal{C}_4 : \sum_{\text{cyclic}} x^2a(a^2-b^2-c^2) \big(a^3-(b+c)a^2-(b^2+c^2)a+(b+c)(b-c)^2\big) -\big((b^2+bc+c^2)a^4 -2(b^2-c^2)^2a^2+(b^2-bc+c^2)(b^2-c^2)^2\big)yz=0$$

centered at the yet unknown triangle center with the trilinear center function

$$C_4 = (b^2-bc+c^2)a^4-2(b+c)(b^2-bc+c^2)a^3 +2bc(b-c)^2a^2 +2(b+c)(b^2-bc+c^2)(b-c)^2a -(b^2-3bc+c^2)(b^2-c^2)^2 :: .$$

In order to verify the statement for X_5, we recall that the nine-point center is the circumcenter of the medial triangle $\Delta_m = M_1M_2M_3$ with M_i being the midpoint of the segments M_jM_k (again with $(i,j,k) \in J_3$). Note that the midpoint of the segment M_jM_k is the harmonic conjugate of the ideal point of the line $[M_j,M_k]$ with respect to M_j and M_k.

The symmedian point X_6 is the perspector of Δ and its tangent triangle $\Delta_t = T_1T_2T_3$ whose vertices T_i are the intersections of the tangents t_j and t_k of the circumcircle $\mathcal{U}$ at P_j and P_k. □

In a similar way, we can show that X_{75} (the isotomic conjugate of X_1) traces the conic

$$\mathcal{C}_{75} : \sum_{\text{cyclic}} x^2a^2(a^2+b^2+c^2) - \big((b^2+c^2)a^2 +2bc(b+c)a-bc(b^2-bc+2c^2)\big)yz=0$$

which is centered at $X_9 = b+c-a$ ::.

Triangle centers of the initial triangle that lie on $\mathcal{M}$ trace $\mathcal{M}$ three times. These are the 124 triangle centers X_i with Kimberling indices (<63000)

$i \in \{88,100,162,190,651,653,655,658,660,662,673,771,$
$799,823,897,1156,1492,1821,2349,2580,2581,3257,$
$4598,4599,4604,4606,4607,8052,20332,23707,24625,$
$27834,29059,32680,34085,34234,36083-36102,$
$37128-37143,37202-37223,38340,40110,43069,$
$43192,43757-43764,45875,46116-46122,55321,$
$55325,55328,55331,60055-60057,61240,62535\}.$

The same holds true for the inconic $\mathcal{N}$, where the following 24 triangle centers with Kimberling numbers (<63000) orbit three times:

$i \in \{244,678,2310,2632,2638,2643,3248,4094,$
$4117,10501,24012,41211,42074-42084,52302$

Further, 204 centers lie on the antiorthic axis $\mathcal{L}_1 : x+y+z=0$ which have the following Kimberling indices (<63000):

$i \in \{44,649,650,652,654,656,657,659,661,672,770,798,$
$822,851,896,899,910,1155,1491,1575,1635,1755,$
$2173,2182,2183,2225,2227-2240,2243-2247,$
$2252-2254,2265,2272,2290,2312-2315,2348,$
$2483,2484,2503,2509,2511,2515,2516,2522,2526,$
$2578,2579,2590,2591,2600,2610,2624,2630,2631,$
$2635,2637,2641,2642,3000,3013,3287,3330,3768,$
$4394,4724,4782,4784,4790,4813,4893,4979,7655,$
$7659,8043,8061,9356,9360,9393,9404,9508,9511,$
$10495,13401,14298,14299,14300,15586,17410,17418,$
$17420,18116,20331,20979,21127,21894,22108,22443,$
$23503,24533,24750,25143,29357,29361,30600,38472,$
$39690,40109,40137,40338,44151,44319,45877,$
$45881-45886,46380-46393,47777,47810,47811,$
$47826-47828,47842,48019-48033,48160,48162,$
$48193,48194,48213,48226,48244,48544,48572,50328,$
$50335,50336,50349,50350,50358,50359,50454,50455,$
$50505,50525,53300,54258,54277,54278,55216,57164,$
$58288,58374,58773,58842\}.$

Fig. 12 (top) shows the orbits of X_1, …, X_6 in the Euclidean Yff porism. The bottom of Fig. 12 shows a close-up of the central orbits together with the envelope of the Euler lines, which is a sextic curve.

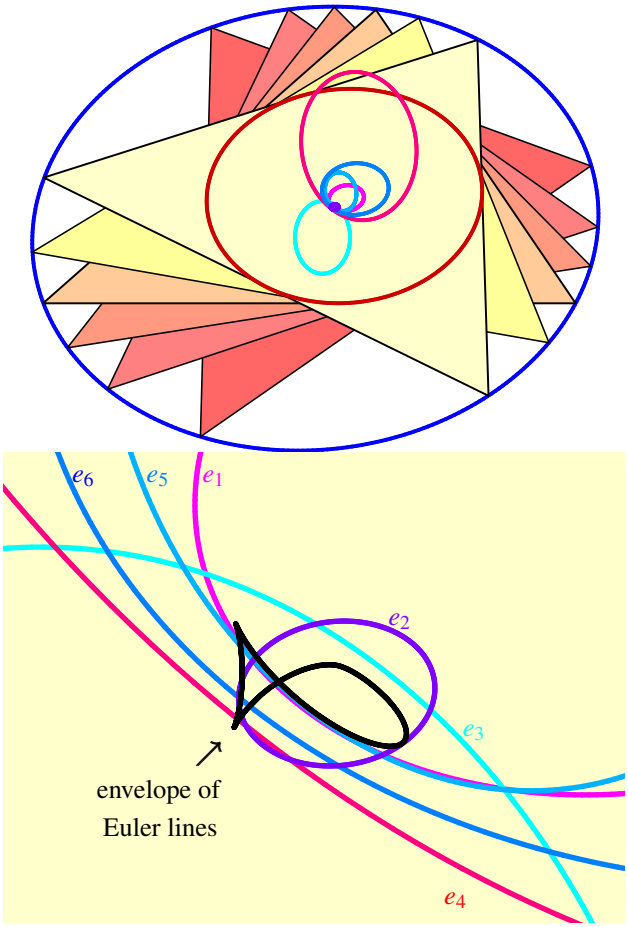

Figure 12: *Top: Some triangles in the Euclidean Yff porism and the traces of the triangle centers $X_1,\ldots,X_6$.*
Bottom: Close-up of the top figure including the envelope of the Euler lines.

6 Final remarks

The construction of further Yff porisms by means of tracing the exponential pencil (14) or by applying harmonic homologies to existing pairs of conics leaves open, whether field extensions enrich the family of Yff porisms or not. The number of points, lines, and even conics in the extended plane is definitely raised. This does not necessarily mean that the exponential pencil contains more members. In principle, the parametrization of the exponential pencil (14) can be evaluated at any value taken from the underlying field. However, it is unclear if matrix powers evaluate to meaningful matrices if we insert elements from the extension of a finite field, since discrete logarithms evaluate only to integers.

Acknowledgments
I have to express my sincere thanks to the careful and competent reviewer for valuable comments.

References

[1] CHAPPLE, W, An essay on the properties of triangles inscribed in and about two given circles, *Misc. Curiosa Math.* **4** (1746), 117–124.

[2] CHIPALKATTI, J., On the Poncelet triangle condition over finite fields, *Finite Fields Appl.* **45** (2017), 59–72, https://doi.org/10.1016/j.ffa.2016.11.014

[3] DEL CENTINA, A., Poncelet's Porism: a long story of renewed discoveries I, *Arch. Hist. Exact Sci.* **70** (2016), 1–122, https://doi.org/10.1007/s00407-015-0163-y

[4] FLATTO, L., *Poncelet's theorem*, American Mathematical Society, Providence, RI, 2008, https://doi.org/10.1090/mbk/056

[5] GARCIA, R., KOILLER, J., REZNIK, D., Loci of 3-periodics in an Elliptic Billiard: Why so many ellipses?, *J. Symb. Comp.* **114** (2023), 336–358, https://doi.org/10.1016/j.jsc.2022.06.001

[6] GARCIA, R.A., ODEHNAL, B., REZNIK, D., Poncelet porisms in hyperbolic pencils of circles, *J. Geom. Graph.* **25**(2) (2021), 205–225.

[7] GARCIA, R, ODEHNAL, B., REZNIK, D., Loci of Poncelet Triangles in the General Closure Case, *J. Geom.* **113**:17 (2022), https://doi.org/10.1007/s00022-022-00629-3

[8] GARCIA, R., REZNIK, D., STACHEL, H., HELMAN, M., Steiner's Hat: a Constant-Area Deltoid Associated with the Ellipse, *KoG* **24** (2020), 12–28, https://doi.org/10.31896/k.24.2

[9] GLAESER, G., STACHEL, H., ODEHNAL, B., *The Universe of Conics. From the ancient Greeks to 21st century developments*, Springer, Berlin, 2016.

[10] HACHENBERGER, D., JUNGNICKEL, D., *Topics in Galois Fields,* Algorithms and Computation in Mathematics 29, Springer Cham, 2020, https://doi.org/10.1007/978-3-030-60806-4

[11] HALBEISEN, L., HUNGERBÜHLER, N., The exponential pencil of conics, *Beitr. Algebra Geom.* **59** (2018), 549–571, https://doi.org/10.1007/s13366-017-0375-1

[12] HIRSCHFELD, J.W.P., *Projective Geometries over Finite Fields*, Clarendon Press, Oxford, second edition, 1998.

[13] JURKIN, E., Poncelet Porisms and Loci of Centers in the Isotropic Plane, *Mathematics* **12**(4) (2024), 618, https://doi.org/10.3390/math12040618

[14] KIMBERLING, C., *Triangle Centers and Central Triangles*, Congressus Numerantium 129, Utilitas Mathematica Publishing, Winnipeg, 1998.

[15] KIMBERLING, C., Yff Conics, *J. Geom. Graph.* **12** (1) (2008), 23–34.

[16] KIMBERLING, C., Permutation Ellipses, *J. Geom. Graph.* **24**(2) (2020), 233–247.

[17] KIMBERLING, C., *Encyclopedia of Triangle Centers*, https://faculty.evansville.edu/ck6/encyclopedia/ETC.html (Last accessed: 6/2024).

[18] ODEHNAL, B., Mixed intersections of Cevians and perspective triangles, *Proceedings of the 15th International Conference on Geometry and Graphics*, 2012, Montreal, Canada, article no. 089

[19] ODEHNAL, B., Poristic loci of triangle centers, *J. Geom. Graph.* **15**(1) (2011), 45–67.

[20] ODEHNAL, B., From Permutation Points to Permutation Cubics, *J. Geom. Graph.* **26**(2) (2022), 253–269.

[21] ODEHNAL, B., REZNIK, D., Circumparabolas in Chapple's porism, *ICGG 2022 - Proceedings of the 20th International Conference on Geometry and Graphics*, L.-Y. Cheng (ed.), *Lecture Notes on Data Engineering and Communications Technologies* **146**, 47–58.

[22] STACHEL, H., The Geometry of Billiards in Ellipses and their Poncelet Grids, *J. Geom.* **112**, 40 (2021), https://doi.org/10.1007/s00022-021-00606-2

[23] STACHEL, H., Isometric Billiards in Ellipses and Focal Billiards in Ellipsoids, *J. Geom. Graph.* **25**(1) (2021), 97–118.

[24] STACHEL, H., Billiard Motions in Ellipses - Invariants of Projective Nature, *Proceedings of the Slovak-Czech Confonference on Geometry and Graphics 2021*, Kočovce, Slovakia 2021, 143–148.

[25] STACHEL, H., On the Motion of Billiards in Ellipses, *Eur. J. Math.* **8**(4) (2022), 1602–1622, https://doi.org/10.1007/s40879-021-00524-2

[26] STACHEL, H., *On the Diagonals of Billiards*, In: L.-Y. Cheng (ed): *ICGG 2022 - Proceedings of the 20th International Conference on Geometry and Graphics*, São Paulo, Brazil 2022, Springer Nature Switzerland, 2023, 19–33.

[27] STACHEL, H., A Triple of Projective Billiards, *KoG* **26** (2022), 44–51, https://doi.org/10.31896/k.26.4

[28] WILDBERGER, N.J., *Divine Proportions: Rational Trigonometry to Universal Geometry*, Wild Egg Pty. Ltd., Australia, 2005.

Boris Odehnal
orcid.org/0000-0002-7265-5132
e-mail: boris.odehnal@uni-ak.ac.at

University of Applied Arts Vienna
Oskar-Kokoschka-Platz 2, A-1010 Vienna, Austria

https://doi.org/10.31896/k.28.4
Original scientific paper
Accepted 4. 11. 2024.

DOMINIQUE LAURAIN
PETER MOSES
DAN REZNIK

Cramer-Castillon on a Triangle's Incircle and Excircles

Cramer-Castillon on a Triangle's Incircle and Excircles

ABSTRACT

The Cramer-Castillon problem (CCP) consists in finding one or more polygons inscribed in a circle such that their sides pass cyclically through a list of N points. We study this problem where the points are the vertices of a triangle and the circle is either the incircle or one of the excircles. We find that (i) in each case there is always a pair of solutions (total of 8 new triangles and 24 vertices); (ii) each pair shares all Brocard geometry objects, (iii) barycentric coordinates are laden with the golden ratio; and (iv) simple operations on the barycentrics of a single vertex out of the 24 yield all other 23.

Key words: Golden ratio, triangle, Brocard, symmedian

MSC2020: 51M04, 51N20, 51N35

Cramer-Castillonov problem u slučaju trokutu upisane i pripisanih kružnica

SAŽETAK

Cramer-Castillonov problem (CCP) se sastoji u traženju jednog ili više mnogokuta upisanih u kružnicu tako da njihove stranice ciklički prolaze kroz N točaka. Ovaj problem proučavamo u slučaju kada su točke vrhovi trokuta, a kružnica ili njegova upisana ili jedna od pripisanih kružnica. Dokazujemo da (i) u svakom slučaju uvijek postoji par rješenja (ukupno 8 novih trokuta i 24 vrha); (ii) svaki par dijeli sve objekte Brocardove geometrije; (iii) u baricentričnim koordinatama se pojavljuje zlatni rez; i (iv) jednostavnim operacijama na baricentričnim koordinatama se iz jednog od 24 vrha mogu dobiti preostala 23.

Ključne riječi: zlatni rez, trokut, Brocard, simedijana

1 Introduction

The Cramer-Castillon problem (CCP) consists in finding one or more N-gons inscribed in a circle $\mathcal{C}$ such that their sides pass cyclically through a set of points P_i, $i = 1 \cdots N$. In Figure 1 this is illustrated for the $N = 3$ case. The solutions to CCP are given[1] by the roots of a quadratic equation (see [7, Section 6.9], [10]), i.e., there can be 0, 1, or 2 real solutions. Geometric conditions for solution existence, though not germane to this article, are described in the aforementioned references.

Referring to Figure 2, we investigate the CCP for the case where the P_i are the vertices A, B, C of a reference triangle and $\mathcal{C}$ is the incircle or one of the excircles. Our findings include:

- For any triangle, the CCP on either the incircle or an excircle has exactly two solutions (total of 8 new triangles and 24 new vertices).
- We derive barycentric coordinates for the 4 pairs of solutions and notice they are laden with the golden ratio $\phi = (\sqrt{5}+1)/2$.
- Each pair shares circumcenter, symmedian point, and all "Brocard geometry" objects [4], e.g., the Brocard points, Brocard circle and inellipse, Lemoine and Brocard axis, isodynamic points, etc.
- The four distinct Brocard axes shared by each pair concur on the de Longchamps point [11] of the reference triangle.
- Given barycentrics for a single vertex out of the 24 newly generated, all other 23 can be obtained with simple cyclic substitutions.
- Solving the CCP for a triangle's arbitrary inconic is equivalent to solving it (via a projectivity) for the incircle case.

[1] In the hyperbolic plane, corresponding sides of the two solutions are polar-orthogonal with respect to the ideal circle [1].

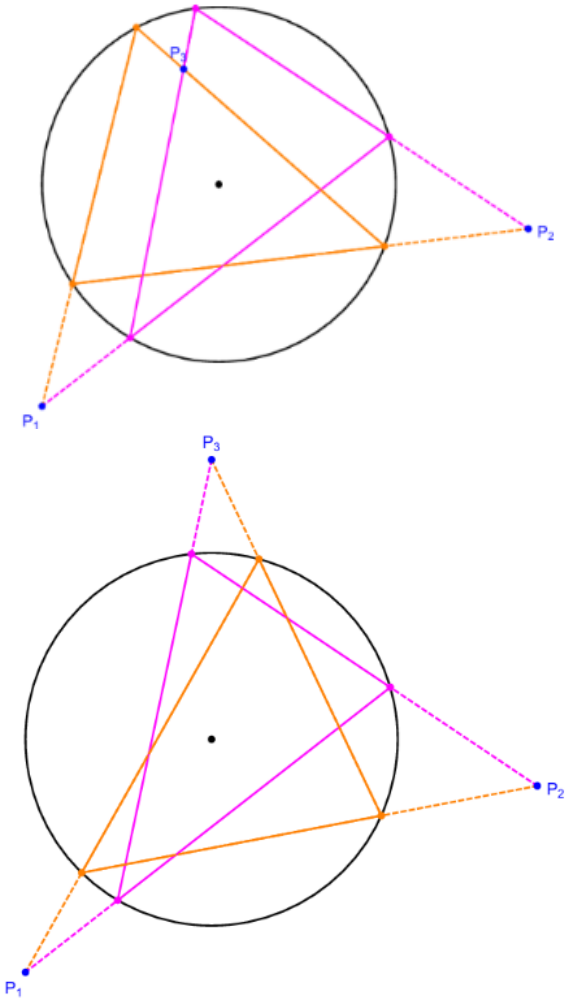

Figure 1: *The Cramer-Castillon problem (CCP) in the $N = 3$ case. In the top (resp. bottom) picture, two points are exterior and one is interior (resp. all exterior) to the target circle. In each case, two solutions are shown (magenta and orange).*

Article organization

The Cramer-Castillon Problem (CCP) on the incircle is covered in Section 2. Its shared Brocard objects are examined in Section 3. The CCP on the excircles are analyzed in Section 4. In Appendix A we provide a list of correspondences between triangle centers in the incircle CCP solutions and the reference triangle.

Notation

We shall use barycentric coordinates [11] and refer to triangle centers using Kimberling's notation X_k [5].

2 Cramer-Castillon on the Incircle

Referring to Figure 2, consider a triangle $T = ABC$ with the sidelengths a, b, c and $s = (a+b+c)/2$ its semiperimeter. Below we use ϕ to denote the golden ratio, $\phi = (1+\sqrt{5})/2$.

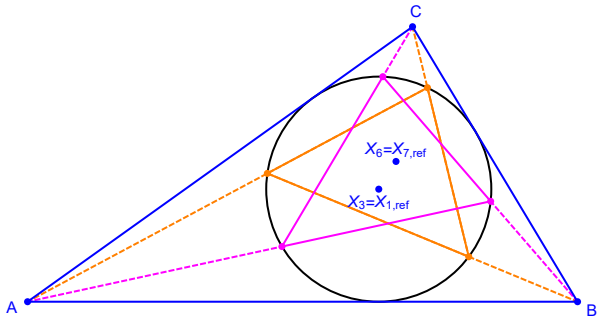

Figure 2: *The two solutions of CCP (orange, magenta) on the incircle $\mathcal{C}$ of a triangle $T = ABC$. Since both are inscribed in $\mathcal{C}$, they share their circumcenter X_3 (at the incenter $X_{1,ref}$ of the reference). Also shared is the symmedian point X_6, which coincides with the Gergonne $X_{7,ref}$ of the reference.*

Proposition 1 *The CCP on a triangle T and its incircle $\mathcal{C}$ admits exactly two solutions T_1 and T_2, whose barycentric vertex matrices with respect to T are given by:*

$$T_1 = \begin{bmatrix} (1-\phi)^2 vw & uw & (2-\phi)^2 uv \\ (2-\phi)^2 vw & (1-\phi)^2 uw & uv \\ vw & (2-\phi)^2 uw & (1-\phi)^2 uv \end{bmatrix}$$

$$T_2 = \begin{bmatrix} (1-\phi)^2 vw & (2-\phi)^2 uw & uv \\ vw & (1-\phi)^2 uw & (2-\phi)^2 uv \\ (2-\phi)^2 vw & uw & (1-\phi)^2 uv \end{bmatrix}$$

where $u = (s-a)$, $v = (s-b)$, $w = (s-c)$.

Proof. While barycentric entries in T_1, T_2 can be obtained as roots of a quadratic equation [7, Section 6.9], we also provide a synthetic construction for the vertices.

Referring to Figure 3, define three paths (A_1,A_2,A_3,A_4), (B_1,B_2,B_3,B_4) and (C_1,C_2,C_3,C_4). Cramer-Castillon requires that A_iA_{i+1} (or B_iB_{i+1} or C_iC_{i+1}) be a circle chord.

The points B_1, C_1 are tangent points of $\mathcal{C}$ with AC and AB while A_1 is the reflection of a tangent point with BC with respect to X_1.

The three paths are non-closing: A_4, B_4 and C_4 are respectively different from A_1, B_1 and C_1.

Intersect the two pairs of segments (A_1B_4, A_4B_1) and (A_1C_4, A_4C_1) to get points H_1 and H_2 on their perspectrix.

Intersecting the homography line with $\mathcal{C}$ gives M_1 and M_4, two vertices of the solution triangles $M_1M_2M_3$ and $M_4M_5M_6$. □

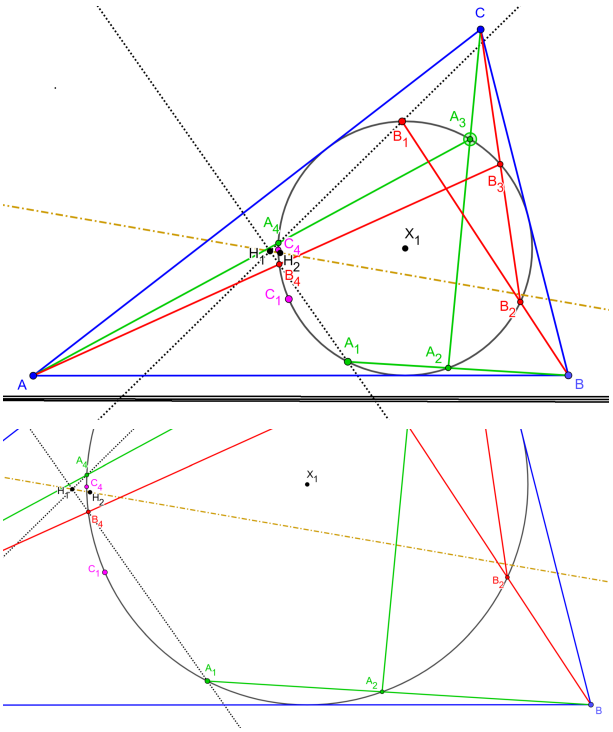

Figure 3: ***top**: The construction for the two points H_1 and H_2 which define the homography axis used in Proposition 1. The sequence $C_1,...C_4$ is not shown, but is as $A_1...A_4$ and $B_1...B_4$. **bottom**: a slight zoom-in on the region where H_1 and H_2 are.*

By definition, both solutions share their circumcenter X_3, located at the incenter X_1 of the reference. Interestingly:

Proposition 2 *The two solutions T_1 and T_2 have a common symmedian point X_6 which coincides with the Gergonne point X_7 of T.*

Proof. Using a CAS, we obtain $[1/(s-a) : 1/(s-b) : 1/(s-c)]$ as barycentrics for the symmedian point of T_1, T_2 with respect to T, which are precisely those of the Gergonne X_7 of T [5]. □

3 Shared Brocard objects

Recall (i) the Brocard circle of a triangle has segment X_3X_6 as diameter, and (ii) the Brocard axis is the line that passes through said diameter [11].

Since by definition T_1, T_2 share their circumcenter X_3, and per Proposition 2 their symmedian as well:

Corollary 1 *T_1 and T_2 share their Brocard axis and Brocard circles.*

Let $\delta = |X_6 - X_3|$. The Brocard angle ω to a triangle is given by [2, Prop. 3, p. 209]:

$$\tan\omega = \frac{\sqrt{3}}{3}\sqrt{1-\left(\frac{\delta}{R}\right)^2}$$

Corollary 2 *T_1 and T_2 have the same Brocard angle ω.*

Referring to Figure 4, recall the two Brocard points of a triangle lie on the Brocard circle and the line joining them is perpendicular to the Brocard axis X_3X_6. In [9] the following formula is given for the distance between the two Brocard points Ω_1, Ω_2 which only depends on the circumradius R and the Brocard angle ω:

$$|\Omega_1 - \Omega_2|^2 = 4c^2 = 4R^2\sin^2\omega(1-4\sin^2\omega)$$

Corollary 3 *T_1 and T_2 share their Brocard points Ω_1 and Ω_2.*

Proposition 3 *The shared Brocard points Ω_1 and Ω_2 of T_1 and T_2 are triangle centers of T given by the following barycentric coordinates:*

$$\Omega_1 = [\alpha/u : \beta/v : \gamma/w], \quad \Omega_2 = [\gamma/u : \alpha/v : \beta/w]$$

where:

$$\alpha = (a-b)^2 - (a+b)c$$
$$\beta = (b-c)^2 - (b+c)a$$
$$\gamma = (c-a)^2 - (c+a)b$$

and u, v, w are as in Proposition 1.

Let a, b be the semi-axes of the Brocard inellipse of a triangle (whose foci are the Brocard points). The following relation was derived in [8, Lemma 2]:

$$[a,b] = R\left[\sin\omega, 2\sin^2\omega\right]$$

Corollary 4 *T_1, T_2 share their Brocard inellipses.*

Recall the two isodynamic points X_{15} and X_{16} are the limiting points of the *Schoute pencil* [3], defined by the circumcircle and the Brocard circle (and orthogonal to the Apollonius circles), whose radical axis is the Lemoine axis.

Corollary 5 *T_1 and T_2 share their isodynamic points X_{15} and X_{16} and Lemoine axis.*

The intersection of the Lemoine axis with the Brocard axis is X_{187} [5].

Corollary 6 *T_1 and T_2 share their X_{187}.*

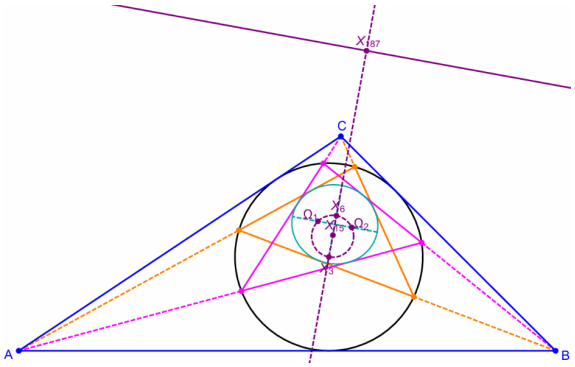

Figure 4: *The two solutions (orange, magenta) of CCP on a triangle's incircle (black) share all Brocard geometry objects, to be sure: their Brocard points Ω_1, Ω_2, Brocard circle and axis (dashed purple), Brocard inellipse (light blue) whose foci are the Brocard points, the two isodynamic points X_{15}, and X_{16} (not shown) and the Lemoine axis (solid purple).*

Generalizing the CCP to any inconic

Referring to Figure 5 (top), let I be some inconic of a triangle $T = ABC$.

Proposition 4 *The CCP of A, B, C on I has two solutions which circumscribe a single inconic $\mathcal{B}$.*

Proof. The CCP is projectively-invariant since only incidences are involved. Let T' be the image of T under a projectivity Π that sends I to a circle $\mathcal{C}'$, see Figure 5 (bottom). Clearly, $\mathcal{C}'$ is the incircle or an excircle of T'. Per Proposition 1 and Corollary 4, the CCP on $(T', \mathcal{C}')$ has two solutions with a common Brocard inellipse $\mathcal{B}'$. Thus $\mathcal{B}$ is the latter's pre-image under Π, with all tangencies preserved. □

Proposition 5 *Consider a general inconic I with perspector $[p, q, r]$. The two solutions T_1 and T_2 of the CCP on I have A-vertices given by:*

$$T_1(A\text{-vertex}) = [(2-\phi)p, q, (1+\phi)r]$$
$$T_2(A\text{-vertex}) = [(2-\phi)p, (1+\phi)r, q]$$

Corollary 7 *If I is the Steiner inellipse (perspector X_2), the two A-vertices are given by:*

$$T_1(A\text{-vertex}) = [2-\phi, 1, 1+\phi]$$
$$T_2(A\text{-vertex}) = [2-\phi, 1+\phi, 1]$$

Notice that if I is the incircle, whose perspector is the Gergonne point $X_7 : [1/(s-a) : 1/(s-b) : 1/(s-c)]$, we recover Proposition 1.

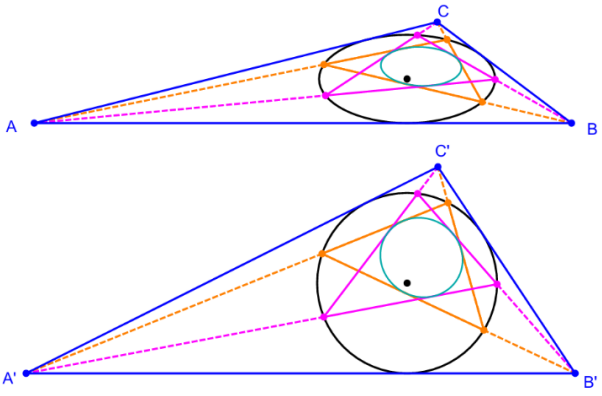

Figure 5: *Since the CCP is projectively-invariant, its solution on a ABC (top) with respect to a generic inconic(black) can be regarded as the pre-image of a perspectivity Π which sends said inconic to a circle (black, bottom). Clearly, this circle is an incircle of the new triangle $A'B'C'$. This implies that the two solutions in the original case will envelop a conic (light blue, top) which is the pre-image of the Brocard inellipse (light blue, bottom) under Π.*

4 Cramer-Castillon on the Excircles

In this section we extend the CCP to the excircles of a given triangle T. Referring to Figure 6:

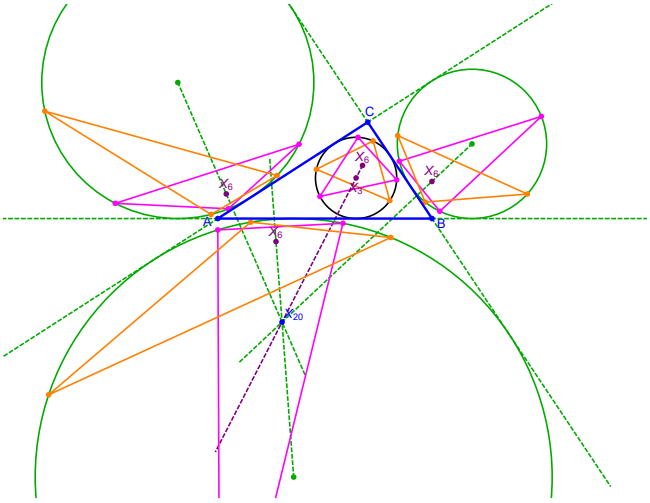

Figure 6: *The CCP applied both to the incircle and the excircles (green). In each of the four circles the symmedian (and all Brocard objects) are shared. The four Brocard axes concur on the de Longchamps point X_{20} of the reference triangle.*

Proposition 6 *The first and second solutions $T_{1,exc}$ and $T_{2,exc}$ of the CCP on the A-excircle are given by the following barycentric vertex matrices:*

$$T_{1,exc} = \begin{bmatrix} -vw(\phi-1)^2 & sv & sw(\phi-2)^2 \\ -vw(\phi-2)^2 & sv(\phi-1)^2 & sw \\ -vw & sv(\phi-2)^2 & sw(\phi-1)^2 \end{bmatrix}$$

$$T_{2,exc} = \begin{bmatrix} -vw(\phi-1)^2 & sv(\phi-2)^2 & sw \\ -vw & sv(\phi-1)^2 & sw(\phi-2)^2 \\ -vw(\phi-2)^2 & sv & sw(\phi-1)^2 \end{bmatrix}$$

where u,v,w are as in Proposition 1.

Proposition 7 *The symmedian X_6 of the A-excircle is shared by the two solution and is the A-exversion of the reference's Gergonne X_7, i.e., its barycentrics are given by $[-vw,sv,sw]$, coinciding with the Gergonne point X_7 of the "outer" contact triangle inscribed in the A-excircle.*

Corollary 8 *Each pair of solutions of the CCP on an excircle shares all of their Brocard objects.*

Proposition 8 *The Brocard axis of the incircle-CCP as well as the 3 Brocard axes of the excircle-CCP solutions concur on the de Longchamps point X_{20} of the reference.*

Proof. The shared Brocard axis of the incircle-CCP solutions contains, by definition, X_3 and X_6 of either solution triangle. We saw above these correspond to X_1 and X_7 of the reference, i.e., it is the Soddy line of the reference [6], which is known to pass through X_{20}. The Brocard axis shared by the A-excircle solutions are the A-exversion ($a \to -a$) of the incircle Brocard axis, and similarly for the B- and C-excircles. It can be shown these 4 lines meet at X_{20}. □

Twenty-three from one

There are a total of 4 pairs of triangles which are solutions to the CCP on both incircle and excircle, i.e., there are eight triangles and a total of 24 vertices.

Proposition 9 *Twenty-three of said vertices can be directly derived from a single vertex of a solution triangle of the CCP in the incircle.*

Proof. As seen in Proposition 1, the A-vertex of the first solution T_1 on the incircle is given by:

$$\left[(1-\phi)^2(s-b)(s-c),(s-a)(s-c),(2-\phi)^2(s-a)(s-b)\right]$$

Perform a bicentric substitution, i.e., $b \to c$ and $c \to b$, and swap postions 2 and 3 to arrive at:

$$\left[(\phi-1)^2(s-b)(s-c),(\phi-2)^2(s-a)(s-c),(s-a)(s-b)\right]$$

i.e., the A-vertex of T_2. The other vertices can be computed cyclically. Now, derive the A-excircle solution from the incircle one by performing an "A-exversion", i.e., changing every $a \to -a$, obtaining the T_1 A-vertex of the A-excircle:

$$\left[(\phi-1)^2(b-s)(s-c),(s-b)s,(\phi-2)^2(s-c)s\right].$$

For the B-vertex of the A-excircle, we first perform a cyclic substitution, then the exversion $a \to -a$, obtaining:

$$\left[(\phi-1)^2(s-b)(s-c),(s-a)(s-c),(\phi-2)^2(s-a)(s-b)\right]$$

which leads to:

$$\left[(\phi-2)^2(s-b)(s-c),(\phi-1)^2(s-a)(s-c),(s-a)(s-b)\right]$$

and then:

$$\left[(\phi-2)^2(s-b)(s-c),(\phi-1)^2s(b-s),s(c-s)\right]$$

The remaining vertices can be obtained similarly. □

Acknowledgements

We would like to thank Arseniy Akopyan and Ronaldo Garcia for useful discussions.

5 Appendix A. Center Correspondences

Let $[i,k]$ indicate that X_i of either solution of the incircle CCP coincides with X_j of the reference triangle. The following is a list of corresponding pairs: [3,1], [6,7], [15,3638], [16,3639], [32,10481], [182,5542], [187,1323], [371,482], [372,481], [511,516], [512,514], [575,43180], [576,30424], [1151,176], [1152,175], [1350,390], [1351,4312], [1384,21314], [2076,14189], [3053,279], [3098,30331], [3311,1373], [3312,1374], [3592,21169], [5017,42309], [5023,3160], [5085,11038], [5585,31721], [5611,10652], [5615,10651], [6200,31538], [6221,1371], [6396,31539], [6398,1372], [6409,17805], [6410,17802], [6419,21171], [6425,31601], [6426,31602], [6431,21170], [6437,17804], [6438,17801], [6449,17806], [6450,17803], [11824,31567], [11825,31568], [12305,30333], [12306,30334], [14810,43179], [15815,5543], [21309,20121], [31884,8236], [43118,30342], [43119,30341], [43120,31570], [43121,31569].

References

[1] ARNOLD, M., FUCHS, D., IZMESTIEV, I., TABACHNIKOV, S., Cross-ratio Dynamics on Ideal Polygons, *Int. Math. Res. Not.* **2022**(9) (2022), 6770–6853, https://doi.org/10.1093/imrn/rnaa289

[2] CASEY, J., *A sequel to the first six books of the Elements of Euclid*, Hodges, Figgis & Co., Dublin, Fifth edition, 1888.

[3] JOHNSON, R.A., Directed Angles and Inversion with a Proof of Schoute's theorem, *Am. Math. Monthly* **24**(7) (1917), 313–317, https://doi.org/10.2307/2973552

[4] JOHNSON, R.A., *Advanced Euclidean Geometry*, New York, NY: Dover, 2nd ed. Editor John W. Young, 1960.

[5] KIMBERLING, C., *Encyclopedia of Triangle Centers*, 2019, https://faculty.evansville.edu/ck6/encyclopedia/ETC.html

[6] KIMBERLING, C., Central lines of triangle centers, 2020, https://faculty.evansville.edu/ck6/encyclopedia/CentralLines.html

[7] OSTERMANN, A., WANNER, G., *Geometry by Its History*, Springer Verlag, Basel, 2012, https://doi.org/0.1007/978-3-642-29163-0

[8] REZNIK, D., GARCIA, R., A matryoshka of Brocard porisms, *Eur. J. Math.* **8** (2022), 308–329, https://doi.org/10.1007/s40879-022-00529-5

[9] SHAIL, R., Some properties of Brocard points, *Math. Gaz.* **80**(489) (1996), 485–491, https://doi.org/10.2307/3618511

[10] WANNER, G., The Cramer–Castillon problem and Urquhart's 'most elementary' theorem, *Elem. Math.* **61**(2) (2006), 68–64, https://doi.org/10.4171/EM/33

[11] WEISSTEIN, E., *Wolfram Mathworld*, 2019, https://mathworld.wolfram.com/

Dominique Laurain
orcid.org/0009-0007-4986-6592
e-mail: dominique.laurain31@orange.fr

Enseeiht, Toulouse, France

Peter Moses
orcid.org/0000-0003-3610-3725
e-mail: moparmatic@gmail.com

Moparmatic Inc., Worcestershire, England

Dan Reznik
orcid.org/0000-0002-0542-6014
e-mail: dreznik@gmail.com

Data Science Consulting, Rio De Janeiro, Brazil

https://doi.org/10.31896/k.28.5
Review
Accepted 4. 12. 2024.

VLADIMIR VOLENEC
EMA JURKIN
MARIJA ŠIMIĆ HORVATH

A Complete Quadrilateral in Rectangular Coordinates II

A Complete Quadrilateral in Rectangular Coordinates II

ABSTRACT

This paper is a continuation of research on a geometry of a complete quadrilateral in the Euclidean plane. We present the well-known facts on the complete quadrilateral but all proved in the same way by using rectangular coordinates, symmetrically on all four sides of the quadrilateral with four parameters a,b,c,d. The properties related to the central circle, orthopolar circle, Hervey's circle, Kantor's point and Plücker's points are observed. During this study, some new results come up.

Key words: complete quadrilateral, central circle, orthopolar circle, Hervey's circle, Kantor's point, Plücker's points

MSC2020: 51N20

Potpuni četverostran u pravokutnim koordinatama II

SAŽETAK

Ovaj rad je nastavak proučavanja geometrije potpunog četverostrana u euklidskoj ravnini. Iznosimo neke poznate činjenice o potpunom četverostranu, ali ih ovdje dokazujemo jedinstvenom metodom koristeći pravokutne koordinate, simetrično s obzirom na četiri stranice četverostrana, odnosno četiri parametra a,b,c,d. Promatramo svojstva vezana za centralnu kružnicu, ortopolarnu kružnicu, Herveyevu kružnicu, Kantorovu točku i Plückerove točke. Tijekom ovog istraživanja dobili smo i neke nove rezultate.

Ključne riječi: potpuni četverostran, centralna kružnica, ortopolarna kružnica, Herveyeva kružnica, Kantorova točka, Plückerove točke

1 Introduction

In this paper we present a continuation of research on a geometry of a complete quadrilateral in the Euclidean plane. The first part is given in [34] where we explained that we presented the well known facts on the complete quadrilateral but all proved in the same way by using rectangular coordinates, symmetrically on all four sides of the quadrilateral with four parameters a,b,c,d. The same method we apply in this paper as well. Hence, the title of the paper is fully justified. During this investigation, some of new results come up and in the text they are written in the form of theorem. We will not give an exhaustive introduction on the points, lines, circles of the quadrilateral but we will refer to the first paper [34]. Nevertheless, some elements of the complete quadrilateral and valid equalities are still mentioned.

Our complete quadrilateral has the lines $\mathcal{A},\mathcal{B},\mathcal{C},\mathcal{D}$ and the vertices $T_{AB}=\mathcal{A}\cap\mathcal{B}$, $T_{CD}=\mathcal{C}\cap\mathcal{D}$, $T_{AC}=\mathcal{A}\cap\mathcal{C}$, $T_{BD}=\mathcal{B}\cap\mathcal{D}$, $T_{AD}=\mathcal{A}\cap\mathcal{D}$, $T_{BC}=\mathcal{B}\cap\mathcal{C}$. Parabola $\mathcal{P}$ inscribed to the complete quadrilateral is of the form

$$\mathcal{P}\ldots y^2=4x, \tag{1}$$

with the focus

$$S=(1,0), \tag{2}$$

and the directrix $\mathcal{H}$ is $x=-1$. By A,B,C,D we denote the contact points of the lines $\mathcal{A},\mathcal{B},\mathcal{C},\mathcal{D}$ and its inscribed parabola $\mathcal{P}$

$$A=(a^2,2a),\ \ B=(b^2,2b),\ \ C=(c^2,2c),\ \ D=(d^2,2d). \tag{3}$$

The lines are of the forms

$$\begin{aligned}&\mathcal{A}\ \ldots\ ay=x+a^2,\quad \mathcal{B}\ \ldots\ by=x+b^2,\\ &\mathcal{C}\ \ldots\ cy=x+c^2,\quad \mathcal{D}\ \ldots\ dy=x+d^2,\end{aligned} \tag{4}$$

and vertices

$$T_{AB}=(ab,a+b),\ \ T_{AC}=(ac,a+c),\ \ T_{AD}=(ad,a+d),$$
$$T_{CD}=(cd,c+d),\ \ T_{BD}=(bd,b+d),\ \ T_{BC}=(bc,b+c). \tag{5}$$

Fig. 1 presents the complete quadrangle with its elements. There are denoted the diagonal points and lines as well.

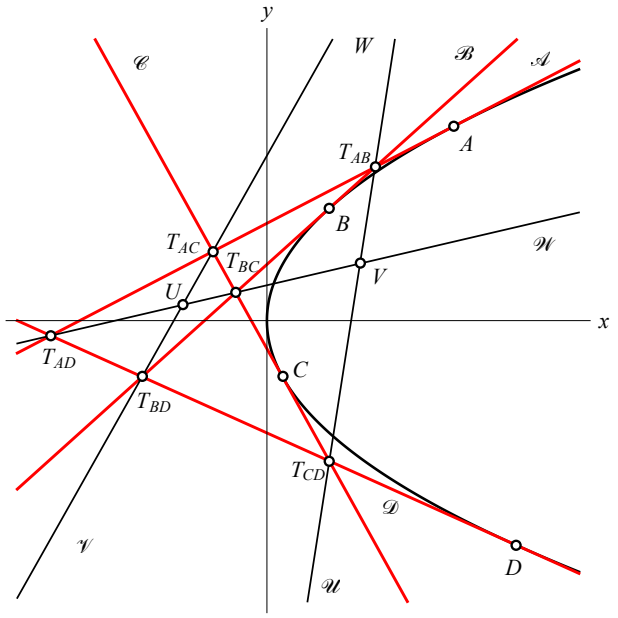

Figure 1: *The complete quadrangle $\mathcal{ABCD}$.*

Further on, the midpoints of pairs of points T_{AB},T_{CD}; T_{AC},T_{BD}; T_{AD},T_{BC} are lying on the median

$$\mathcal{N}\ \ldots\ y=\frac{1}{2}s. \tag{6}$$

Basic symmetric functions will be useful hereby as well:

$$s=a+b+c+d,\quad q=ab+ac+ad+bc+bd+cd,$$
$$r=abc+abd+acd+bcd,\quad p=abcd.$$

We also use abbreviations $\alpha=1+a^2$, $\beta=1+b^2$, $\gamma=1+c^2$ and $\delta=1+d^2$.
Let $\mathcal{S}_a,\mathcal{S}_b,\mathcal{S}_c$, $\mathcal{S}_d$ be circumcircles of trilaterals $\mathcal{BCD}$, $\mathcal{ACD}$, $\mathcal{ABD}$, $\mathcal{ABC}$, respectively. The circle $\mathcal{S}_d$ has the equation

$$\mathcal{S}_d\ \ldots x^2+y^2-(ab+ac+bc+1)x-(a+b+c-abc)y$$
$$+ab+ac+bc=0, \tag{7}$$

and the center

$$S_d=\left(\frac{1}{2}(ab+ac+bc+1),\frac{1}{2}(a+b+c-abc)\right). \tag{8}$$

Circles $\mathcal{S}_a,\mathcal{S}_b,\mathcal{S}_c$ and their centers S_a,S_b,S_c are obtained analogously because of the symmetry on a,b,c,d.
The central circle $\mathcal{M}$ of the quadrilateral $\mathcal{ABCD}$, the circle passing through the centers of $\mathcal{S}_a,\mathcal{S}_b,\mathcal{S}_c$ $\mathcal{S}_d$, has the equation

$$\mathcal{M}\ldots x^2+y^2-\frac{1}{2}(3+q-p)x+\frac{1}{2}(r-s)y-\frac{1}{2}(1+q-p)=0, \tag{9}$$

and center

$$M=\left(\frac{1}{4}(3+q-p),\frac{1}{4}(s-r)\right) \tag{10}$$

that we call a central point of the $\mathcal{ABCD}$, see Fig. 2.

2 Results

The lines $\mathcal{A}$ and ST_{AD} have the slopes $\frac{1}{a}$ and $\frac{a+d}{ad-1}$, so for the tangent of the angle $\angle(\mathcal{A},ST_{AD})$ due to formula (22) from [34] we obtain $\frac{1}{d}$, meaning that this angle is equal to the angle $\angle(\mathcal{N},\mathcal{D})$. Hence, *for the complete quadrilateral $\mathcal{ABCD}$ with the focus S and vertices $T_{AB},T_{AC},T_{AD},T_{BC},T_{BD},T_{CD}$ the equalities $\angle(\mathcal{A},ST_{AD})=\angle(\mathcal{B},ST_{BD})=\angle(\mathcal{C},ST_{CD})=\angle(\mathcal{N},\mathcal{D})$ are valid as well as three more sets of such equalities*. The statement appears in [9].
The tangent to the circle $\mathcal{S}_d$ with the equation (7) in the point T_{BC} has the equation

$$2bcx+2(b+c)y-(ab+ac+bc+1)(x+bc)$$
$$-(a+b+c-abc)(y+b+c)+2(ab+ac+bc)=0,$$

that after some computing obtains the form

$$(bc-ab-ac-1)x+(b+c-a+abc)y=$$
$$=b^2c^2+b^2+c^2+bc-ab-ac$$

and it passes through the point

$$S'_A=\left(\frac{1}{\alpha}(a^2+bc+bd+cd-ab-ac-ad+abcd),\right.$$
$$\left.\frac{1}{\alpha}(b+c+d-a+abc+abd+acd-bcd)\right) \tag{11}$$

and because of symmetry on b,c,d the tangents to $\mathcal{S}_b$ and $\mathcal{S}_c$ at the points T_{CD} and T_{BD} are incident to S'_A as well (see Fig. 2). It was proved in [34] that lines $T_{BC}S_d,T_{BD}S_c,T_{CD}S_b$ are intersected in one point $S_A=(\frac{1}{\alpha}[a(abc+abd+acd-bcd+b+c+d)+1],\frac{a}{\alpha}(-abcd+ab+ac+ad-bc-bd-cd+1))$, an intersection of circles $\mathcal{M}$ and $\mathcal{A}$. The points S'_A and S_A have for the midpoint the point S_a analogous to S_d from (8). It means that the point S'_A is diametrically opposite to S_A on the circle $\mathcal{S}_a$. Moreover, *for the complete quadrilateral $\mathcal{ABCD}$, the points S'_A,S'_B,S'_C,S'_D are diametrically opposite to S_A,S_B,S_C,S_D on circles $\mathcal{S}_a,\mathcal{S}_b,\mathcal{S}_c,\mathcal{S}_d$, respectively.* [6] and [26] have this statement.

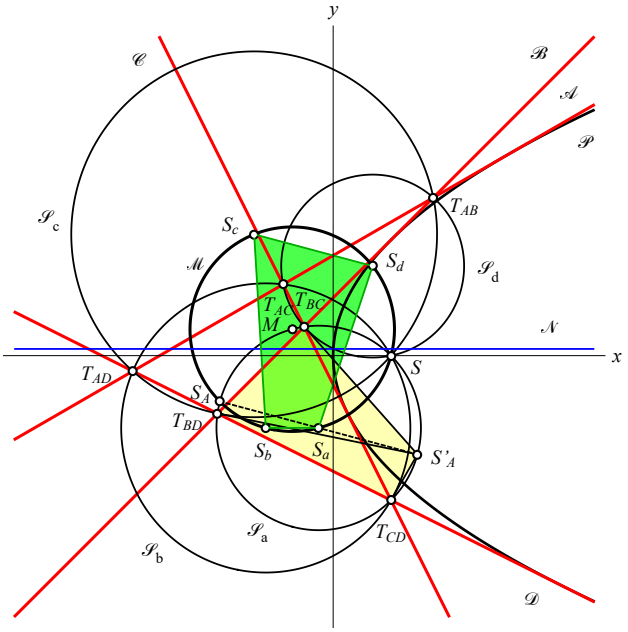

Figure 2: *Circumcenters S_a, S_b, S_c, S_d of trilaterals $\mathcal{BCD}$, $\mathcal{ACD}$, $\mathcal{ABD}$, $\mathcal{ABC}$ lie on the central circle $\mathcal{M}$ with center M.*

As for the point S'_A from (11) we have $x-1=\frac{1}{\alpha}(bc+bd+cd-ab-ac-ad+abcd-1)$ and

$$(bc+bd+cd-ab-ac-ad+abcd-1)^2+$$
$$+(b+c+d-a+abc+abd+acd-bcd)^2=$$
$$=(a^2+1)(b^2+1)(c^2+1)(d^2+1)=\alpha\beta\gamma\delta$$

the equality $SS'^{\,2}_A=\frac{\beta\gamma\delta}{\alpha}$, and similarly $SS'^{\,2}_B=\frac{\alpha\gamma\delta}{\beta}$, $SS'^{\,2}_C=\frac{\alpha\beta\delta}{\gamma}$, $SS'^{\,2}_D=\frac{\alpha\beta\gamma}{\delta}$ are valid. Obviously, the equalities $T_{AB}S^2=\alpha\beta$, $T_{AC}S^2=\alpha\gamma$, $T_{AD}S^2=\alpha\delta$, $T_{BC}S^2=\beta\gamma$, $T_{BD}S^2=\beta\delta$, $T_{CD}S^2=\gamma\delta$ are valid. For points S and S_d from (2) and (8) we get $SS_d^2=\frac{1}{4}\alpha\beta\gamma$, and analogously $SS_a^2=\frac{1}{4}\beta\gamma\delta$, $SS_b^2=\frac{1}{4}\alpha\gamma\delta$, $SS_c^2=\frac{1}{4}\alpha\beta\delta$ follow. Out of these equalities we obtain

$$SS_a:SS_b:SS_c:SS_d=\frac{1}{\sqrt{\alpha}}:\frac{1}{\sqrt{\beta}}:\frac{1}{\sqrt{\gamma}}:\frac{1}{\sqrt{\delta}}. \qquad (12)$$

The lines SS_a and ST_{BC} have the slopes $\frac{b+c+d-bcd}{bc+bd+cd-1}$, $\frac{b+c}{bc-1}$ so for tangent of the angle $\angle(ST_{BC},SS_a)$ due to formula (22) in [34] and after some computing we get the value $-d$. Because of symmetry on a,b,c the angles $\angle(ST_{AC},SS_b)$ and $\angle(ST_{AB},SS_c)$ have the same value for the tangents. Lines SS'_D and SS_d have the slopes

$$\frac{a+b+c-d+abd+acd+bcd-abc}{ab+ac+bc-ad-bd-cd+abcd-1}$$

and

$$\frac{a+b+c-abc}{ab+ac+bc-1},$$

so for the tangent of the angle $\angle(SS'_D,SS_d)$ we get the value $-d$ again. Because of that, there are the equalities among angles

$$\angle(ST_{BC},SS_a)=\angle(ST_{AC},SS_b)=\angle(ST_{AB},SS_c)=\angle(SS'_D,SS_d).$$

Besides that, the equalities

$$SS_a:ST_{BC}=SS_b:ST_{AC}=SS_c:ST_{AB}=SS_d:SS'_D=\frac{1}{2}\sqrt{\delta}$$

are valid. This means that cyclic quadrangles $T_{BC}T_{AC}T_{AB}S'_D$ and $S_aS_bS_cS_d$ are directly similarly and that the factor of similarity is equal to $\frac{1}{2}\sqrt{\delta}$, and the center of similarity is the focus S. These statements can be found in [26]. Similarly as this, the cyclic quadrangles $S'_AT_{CD}T_{BD}T_{BC}$, $T_{CD}S'_BT_{AD}T_{AC}$ and $T_{BD}T_{AD}S'_CT_{AB}$ are similar to quadrangle $S_aS_bS_cS_d$ where the center of similarity is the focus S, and factors of similarity are $\frac{1}{2}\sqrt{\alpha}$, $\frac{1}{2}\sqrt{\beta}$, $\frac{1}{2}\sqrt{\gamma}$, see Fig. 3. The angles of these studied similarities have the tangents $-d,-a,-b,-c$, respectively. However, these are slopes of lines perpendicular to lines $\mathcal{D},\mathcal{A},\mathcal{B},\mathcal{C}$ so the mentioned angles of similarity are the same as the ones formed by median $\mathcal{N}$ and normals to the lines $\mathcal{D},\mathcal{A},\mathcal{B},\mathcal{C}$, respectively. We have just proved our original theorem.

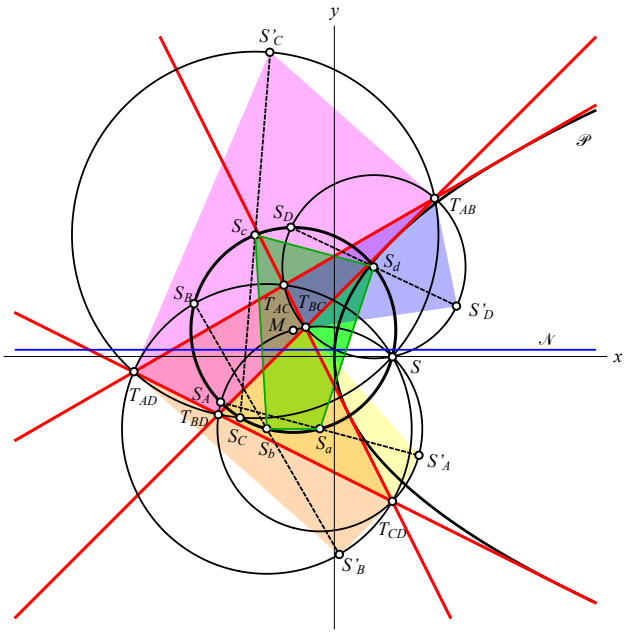

Figure 3: *Visualisation of Theorem 1*

Theorem 1 *Let $\mathcal{ABCD}$ be a complete quadrilateral. The cyclic quadrangles $S'_AT_{CD}T_{BD}T_{BC}$, $T_{CD}S'_BT_{AD}T_{AC}$, $T_{BD}T_{AD}S'_CT_{AB}$ and $T_{BC}T_{AC}T_{AB}S'_D$ are similar to quadrangle $S_aS_bS_cS_d$. Angles of similarity are the same as the ones formed by median $\mathcal{N}$ and normals to the lines $\mathcal{A},\mathcal{B},\mathcal{C},\mathcal{D}$, respectively.*

From the latest results the next follows: *triangles $S_aS_bS_c$, $S_aS_bS_d$, $S_aS_cS_d$, $S_bS_cS_d$ are directly similar to trilaterals $\mathcal{ABC}$, $\mathcal{ABD}$, $\mathcal{ACD}$, $\mathcal{BCD}$ where the center of each similarity is the focus S*, and that is the statement in [31].
The circle with the equation

$$x^2+y^2-(ab+cd)x-sy+p+(a+b)(c+d)=0 \qquad (13)$$

is incident to T_{AB} and T_{CD} and the center of the circle is the point $\left(\frac{1}{2}(ab+cd),\frac{1}{2}s\right)$, the midpoint of these two points. Hence, (13) is the circle with diameter $T_{AB}T_{CD}$. Similar, the circle with the diameter $T_{AC}T_{BD}$ has the equation

$$x^2+y^2-(ac+bd)x-sy+p+(a+c)(b+d)=0. \qquad (14)$$

Subtracting these two equations, the radical axis of these circles with the equation $(a-d)(c-b)x+(a-d)(c-b)=0$ is obtained. It is the line with equation $x=-1$, being the directrix $\mathcal{H}$. Because of symmetry, it is the radical axis of the third circle with diameter $T_{AD}T_{BC}$ as well. The statement that *circles with diameters $T_{AB}T_{CD}$, $T_{AC}T_{BD}$ and $T_{AD}T_{BC}$ have the directrix $\mathcal{H}$ for the radical axis,* can be found in [13] and it is attributed to Bodenmiller, and some of authors call it the Plücker's theorem. The elementary proofs can be found in [5], [19] and [23]. The intersection point of the line $\mathcal{H}$ with each of these three circles are the points with ordinates that fulfill the equation

$$y^2-sy+p+q+1=0, \qquad (15)$$

i.e.

$$P_{1,2}=\left(-1,\frac{1}{2}(s\pm\sqrt{s^2-4p-4q-4})\right), \qquad (16)$$

that are so called *Plücker's points* of the quadrilateral $\mathcal{ABCD}$, real ones and imaginary. The pencil of circles incident to these two points is Plücker's pencil of circles.
Let the points A'',B'',C'',D'' be orthogonal projections of any Plücker's point $P_i, i\in 1,2$, to the lines $\mathcal{A},\mathcal{B},\mathcal{C},\mathcal{D}$, respectively. Then, *$A'',B''$ are incident to the circle with the diameter P_iT_{AB}, and points C'',D'' are on the circle with the diameter P_iT_{CD}*. However, these two diameters are perpendicular because the points $P_i, i\in 1,2$, are incident to the circle with diameter $T_{AB}T_{CD}$, so then *the circles $P_iA''B''$ and $P_iC''D''$ are orthogonal circles.* This statement appears in [33].
The circle $\mathcal{P}'$ with equation

$$\mathcal{P}'\ldots x^2+y^2-\frac{1}{2}(p+q+1)x-sy+\frac{1}{2}(p+q-1)=0 \qquad (17)$$

is incident to the focus $S=(1,0)$ and Plücker's points (16). Namely, out of $x=-1$ and (17) we obtain the equation (15). It is so called the *orthopolar circle* of the quadrilateral $\mathcal{ABCD}$. The center of this circle is the point

$$P=\left(\frac{1}{4}(p+q+1),\frac{1}{2}s\right), \qquad (18)$$

orthopolar center of the quadrilateral $\mathcal{ABCD}$, incident to the median $\mathcal{N}$, see Fig. 4. For the radius ρ' of the circle $\mathcal{P}'$ we get $16\rho'^2=(p+q-3)^2+4s^2$.

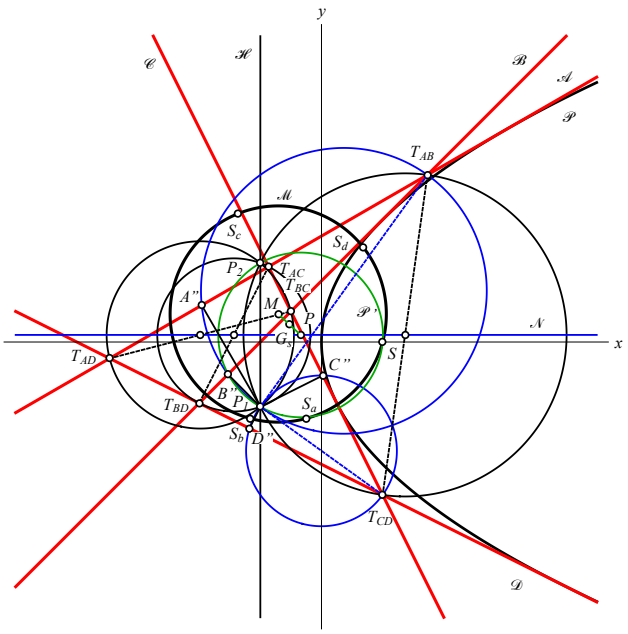

Figure 4: *Plücker's points P_1,P_2, orthopolar circle $\mathcal{P}'$, and orthopolar center P of the quadrilateral $\mathcal{ABCD}$.*

For the point P from (18) and the point S_d from (8) we obtain the equality

$$16PS_d^2=(ad+bd+cd-ab-ac-bc-1+abcd)^2 +4(abc+d)^2,$$

and adding up this equality and three more analogous ones we get

$$16\left(PS_a^2+PS_b^2+PS_c^2+PS_d^2\right)=4(a^2+1)(b^2+1)(c^2+1)(d^2+1)$$

i.e. because of (21) in [34] we show that *for the orthopolar center P and the centers S_a,S_b,S_c,S_d the equality $PS_a^2+PS_b^2+PS_c^2+PS_d^2=4\rho'^2$ is valid.* This appears in [26].
The points S_a,S_b,S_c,S_d from (8) have the centroid $G_s=\left(\frac{1}{4}(q+2),\frac{1}{8}(3s-r)\right)$, the midpoint of P from (18) and M from (10). This proves the statement in [27] that *the point symmetric to the point M with respect to the centroid G_s is incident to the median of $\mathcal{ABCD}$.* The point G_s is called *a dimidium point* of the quadrilateral $\mathcal{ABCD}$. Adding the equations (9) and (17) of the circles $\mathcal{M}$ and $\mathcal{P}'$ we obtain the equation of the so called *dimidium circle* of that quadrilateral with the form

$$x^2+y^2-\frac{1}{2}(2+q)x-\frac{1}{4}(3s-r)y+\frac{1}{2}q=0. \qquad (19)$$

Its center is the dimidium point G_s and it passes through the focus $S=(1,0)$.
We observe the triangle HMP where $H=\left(-1,\frac{1}{4}(3s+r)\right)$ is the centroid of the orthocenters of four trilaterals of the quadrilateral $\mathcal{ABCD}$, M is its central point from (10), and P is its orthopolar center from (18). The triangle HMP has the centroid in the point $T=\left(\frac{1}{6}q,\frac{1}{2}s\right)$ from (10) in [34], and that is the centroid of all six vertices of the quadrilateral $\mathcal{ABCD}$. *The midpoint of the points H and M is the point $\left(\frac{1}{8}(q-p-1),\frac{1}{2}s\right)$ and it is incident to the median $\mathcal{N}$. The orthopolar center P is incident to the median as well.* These statements are coming from [2].
The circle $\mathcal{P}_d$ with equation

$$x^2+y^2+2x-2(a+b+c+abc)y \qquad (20)$$
$$+a^2+b^2+c^2+ab+ac+bc+abc(a+b+c)=0$$

has the center in the orthocenter $H_d=(-1,a+b+c+abc)$ of the trilateral $\mathcal{ABC}$ and the radius given by

$$\rho_d^2=1+ab+ac+bc+abc(a+b+c+abc).$$

The point T_{AB} has the polar line $abx+(a+b)y+x+ab-(a+b+c+abc)(y+a+b)+a^2+b^2+c^2+ab+ac+bc+abc(a+b+c)=0$ with respect to the circle $\mathcal{P}_d$, i.e. the line $x-cy+c^2=0$ that is the line $\mathcal{C}$. Similarly, we obtain lines $\mathcal{B}$ and $\mathcal{A}$ for polar lines of points T_{AC} and T_{BC}, respectively. Hence, the circle $\mathcal{P}_d$ is the polar circle of the trilateral $\mathcal{ABC}$. Analogously, the polar circle $\mathcal{P}_c$ of the trilateral $\mathcal{ABD}$ is of the form

$$x^2+y^2+2x-2(a+b+d+abd)y \qquad (21)$$
$$+a^2+b^2+d^2+ab+ad+bd+abd(a+b+d)=0.$$

The radical axis of (20) and (21) is of the final form $2y+s=0$ that makes the equation of the median. The same applies to the polar circles of the other two trilaterals. Hence, from [8] and [24] we have the statement: *The polar circles of $\mathcal{ABC}$, $\mathcal{ABD}$, $\mathcal{ACD}$ and $\mathcal{BCD}$ belong to one pencil of circles whose radical axis is the median of the quadrilateral $\mathcal{ABCD}$.* As it appears in [3] we will show that *this pencil of circles is conjugate to Plücker's pencil of circles, i.e. each circle of one pencil is orthogonal to each circle of another pencil*, see Fig. 5. It is enough to prove that the Plücker's points $P_{1,2}$ are conjugated with respect to the circle (20). Two points (x_i,y_i), $i=1,2$, are conjugated with respect to the circle (20) under the condition that

$$x_1x_2+y_1y_2+x_1+x_2-(a+b+c+abc)(y_1+y_2)$$
$$+a^2+b^2+c^2+ab+ac+bc+abc(a+b+c)=0$$

holds. For Plücker's points from (16) the equalities $x_1x_2=1$, $y_1y_2=p+q+1$, $x_1+x_2=-2$, $y_1+y_2=s$ are valid, and the next equality

$$p+q-(a+b+c+abc)s+a^2+b^2+c^2$$
$$+ab+ac+bc+abc(a+b+c)=0$$

is valid as well.
Putting $y=\frac{1}{2}s$ into (20) we obtain $4x^2+8x+s^2-4p-4q=0$ with solutions $x_{1,2}=-1\pm\frac{1}{2}\sqrt{4(p+q+1)-s^2}$. Hence, the polar circles of four trilaterals of quadrilateral $\mathcal{ABCD}$ have the common points (real or imaginary)

$$P'_{1,2}=\left(1\pm\frac{1}{2}\sqrt{4(p+q+1)-s^2},\frac{1}{2}s\right).$$

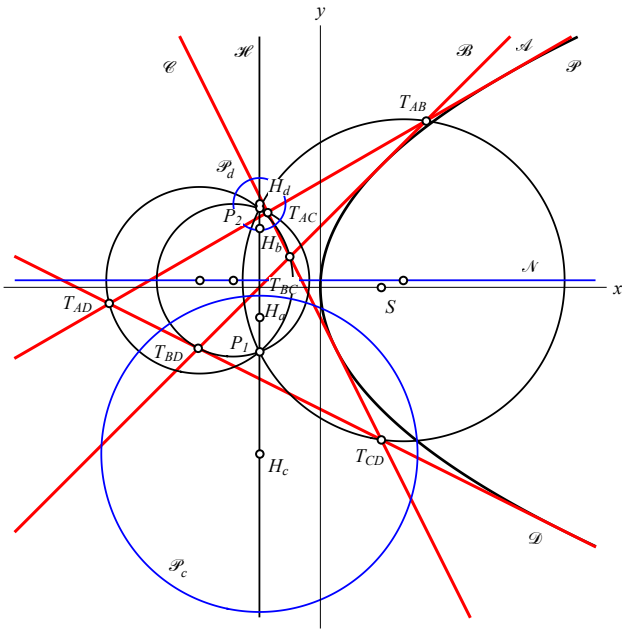

Figure 5: *Two conjugated pencils of circles.*

Let us remind that Plücker's pencil of circle has the common points $P_{1,2}$ from (16). Out of two conjugated pencil of circles, one is always elliptic, and another is hyperbolic, or both of them are parabolic. It depends on the sign of $4(p+q+1)-s^2$. The case, when both of pencils are parabolic, we get $4(p+q+1)=s^2$ i.e. $P_1=P_2=P'_1=P'_2=\left(-1,\frac{1}{2}s\right)$.
The points T_{AB},T_{CD} from (5) are conjugated with respect to the circle with the equation $x^2+y^2+2hx+2jy+k=0$ if and only if the equality $abcd+(a+b)(c+d)+h(ab+cd)+j(a+b+c+d)+k=0$ is valid, i.e.

$$(h-1)(ab+cd)+js+k+p+q=0.$$

The analogous equalities for pairs of points T_{AC},T_{BD} and T_{AD},T_{BC} are

$$(h-1)(ac+bd)+js+k+p+q=0$$
$$(h-1)(ad+bc)+js+k+p+q=0.$$

If two out of these three equalities are valid, than $h=1$ follows, and the third equality is valid as well. Besides,

$k = -js - p - q$ is valid and the observed circle has the equation $x^2 + y^2 + 2x + 2jy - js - p - q = 0$ and the center incident to the directrix of the quadrilateral $\mathcal{ABCD}$. Any two circles of this form have the radical axis with the equation $2y - s = 0$, and it is the median of the quadrilateral $\mathcal{ABCD}$. Hence, *if two pairs of opposite vertices of the quadrilateral are conjugated with respect to some circle, then it is valid for the third pair as well, and the circle belongs to one pencil of circles whose the radical axis is the median and its centers are incident to the directrix of the quadrilateral*, as it is in [22]. This statement is in accordance with the Hesse's theorem: if two pairs of the opposite vertices of the quadrilateral are conjugated with respect to some conic, then this holds for the third pair of its opposite vertices as well.

The previous statement can be refined a little more. Each circle with the center lying on the directrix of the quadrilateral $\mathcal{ABCD}$ has the equation of the form $x^2 + y^2 + 2hx + 2jy + k = 0$, where $h = 1$. Because of that the points T_{AB}, T_{CD} are conjugated with respect to this circle under the condition $js + k + p + q = 0$, so such a circle has the equation $x^2 + y^2 + 2x + 2jy - sj - q - p = 0$ where j is a parameter. The symmetry on a, b, c, d of the previous condition proves our original statement:

Theorem 2 *Let $\mathcal{ABCD}$ is a complete quadrilateral. If one pair of opposite vertices of the quadrilateral is conjugated with respect to the circle with the center on the directrix of the quadrilateral, then it is also valid for other two pairs of opposite vertices.*

We give below the well known statement: If two points are conjugated with respect to the circle then this circle is orthogonal to the circles for which these two points are diametrically opposite. For the sake of completeness in proving all the statements using rectangular coordinates, we will prove this statement. Without loss of generality, we can take that our circle has the center $(0,0)$, the radius equal to 1 and the equation $x^2 + y^2 = 1$, so two points are conjugated with respect to it under the condition that for their coordinates the equality $x_1x_2 + y_1y_2 = 1$. We can take one of these points of the forms $(u,0)$, and then from previous condition follows that another point is of the form $\left(\frac{1}{u}, v\right)$. The center of another circle is the point $\left(\frac{1}{2}(u + \frac{1}{u}), \frac{1}{2}v\right)$, and the square of its radius is $\frac{1}{4}\left((u - \frac{1}{u})^2 + v^2\right)$, while for the square of distance of these two circles we get the form $\frac{1}{4}\left((u + \frac{1}{u})^2 + v^2\right)$. Our statement follows from the fact that

$$\frac{1}{4}\left(\left(u - \frac{1}{u}\right)^2 + v^2\right) + 1 = \frac{1}{4}\left(\left(u + \frac{1}{u}\right)^2 + v^2\right).$$

From the previous consideration, due to this proven statement, it follows that circles with centers on the directrix, to which the opposite vertices of the quadrilateral $\mathcal{ABCD}$ are conjugate points, form one pencil of circles, which are orthogonal to the circles, of which the diagonals of that quadrilateral are diameters, and the last three circles belong to another pencil of circles (with centers on the median of the quadrilateral).

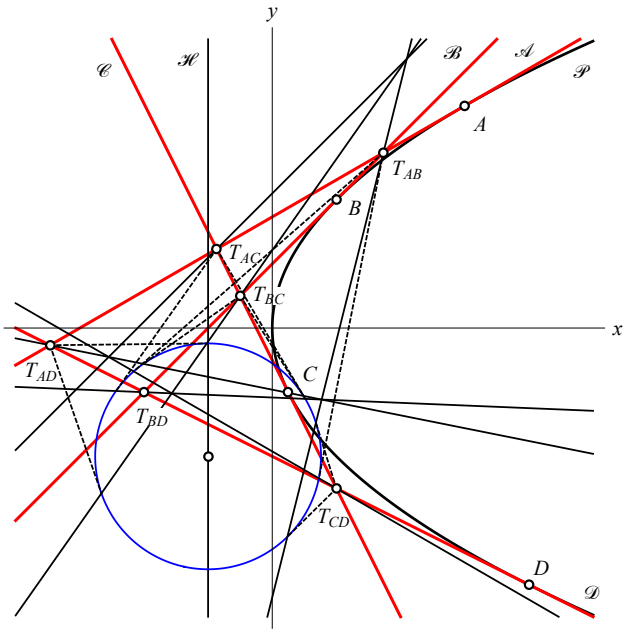

Figure 6: *The complete quadrilateral $\mathcal{ABCD}$ whose opposite vertices are conjugated with respect to the circle with the center on the directrix of the quadrilateral.*

The trilaterals $\mathcal{ABC}$ has the orthocenter $H_d = (-1, a+b+c+abc)$ and circumcenter S_d given by (8), and their midpoint is the Euler's center N_d of that trilateral and it is given by

$$N_d = \left(\frac{1}{4}(ab + ac + bc - 1), \frac{1}{4}(3a + 3b + 3c + abc)\right) \tag{22}$$

Normals to the side $\mathcal{D}$ have the slope $-d$, hence the normal from the point N_d to this line is $4dx + 4y = 3s + r - 4d$. This line is incident to the point

$$H = \left(-1, \frac{1}{4}(3s + r)\right), \tag{23}$$

the same is valid and for the perpendiculars of the Euler's centers of trilaterals $\mathcal{ABD}$, $\mathcal{ACD}$, $\mathcal{BCD}$ to the lines $\mathcal{C}, \mathcal{B}, \mathcal{A}$, respectively. The point H is the *Morley's point* of the quadrilateral $\mathcal{ABCD}$. It is incident to the directrix of this quadrilateral and it is the centroid of points $H_a, H_b.H_c, H_d$, see Fig. 7. The fact that *normals from Euler's centers of four trilaterals $\mathcal{BCD}$, $\mathcal{ACD}$, $\mathcal{ABD}$, $\mathcal{ABC}$ to lines $\mathcal{A}, \mathcal{B}, \mathcal{C}, \mathcal{D}$ are incident to one point on directrix* we find in [20] and [21].

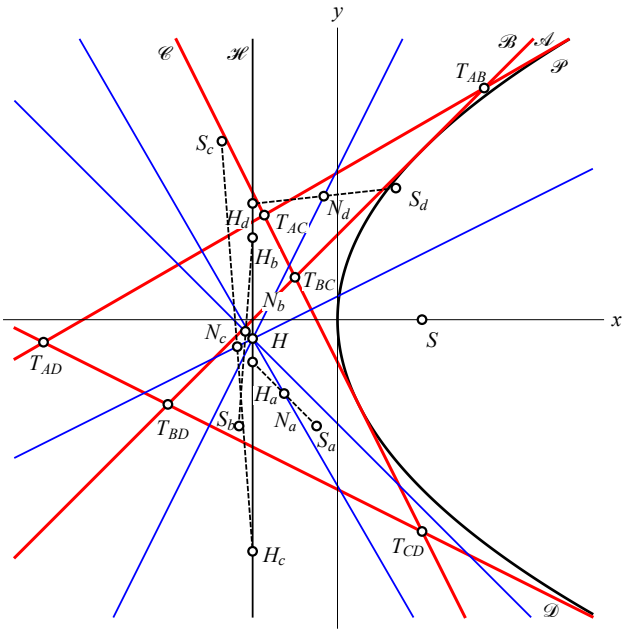

Figure 7: *Morley's point H of $\mathcal{ABCD}$*

The parallel line to $\mathcal{D}$ through the point N_d from (22) has the equation $x-dy=\frac{1}{4}(ab+ac+bc-1-3ad-3bd-3cd-abcd)$ and it passes through the point $\left(\frac{1}{4}(ab+ac+bc+ad+bd-3cd-1-abcd),a+b\right)$. The parallel line to $\mathcal{C}$ and through the point N_d is incident to this point as well. The midpoint of it and $T_{CD}=(cd,c+d)$ is the point $\left(\frac{1}{8}(q-p-1),\frac{1}{2}s\right)$. Hence, *the quadrilateral $\mathcal{ABCD}$ is symmetric to the quadrilateral formed by parallels to $\mathcal{A},\mathcal{B},\mathcal{C},\mathcal{D}$ through the Euler's centers of $\mathcal{BCD}$, $\mathcal{ACD}$, $\mathcal{ABD}$, $\mathcal{ABC}$ with the center of the symmetry $\left(\frac{1}{8}(q-p-1),\frac{1}{2}s\right)$ that is incident to the median $\mathcal{N}$ of the quadrilateral $\mathcal{ABCD}$*. This point is in [32] called nine-point center homothetic center $QL-P22$.

Points S_c,S_b,S_a are analogous to the point S_d from (8). These three points have the centroid

$$G_D=\Big(\frac{1}{6}(ab+ac+2ad+bc+2bd+2cd+3),\\ \frac{1}{6}(2a+2b+2c+3d-abd-acd-bcd)\Big),\qquad(24)$$

i.e. it is the centroid of the triangle $S_aS_bS_c$, and circumcenter of the triangle is the point M from (10). As in any triangle the following is valid: for the circumcenter S, orthocenter H and the centroid G the equality $H+2S=3G$ holds. So, for the orthocenter H_D of the triangle $S_aS_bS_c$ the equality $H_D=3G_D-2M$ holds and from (10) and (24) we get

$$H_D=\left(\frac{1}{2}(ad+bd+cd+p),\frac{1}{2}(d+abc+s)\right).\qquad(25)$$

The midpoint of the points S_d and H_D is the orthopolar center P from (18). The coordinates of the point H_D given in (25) obviously satisfy the equation (4) of the side $\mathcal{D}$. Therefore, we can conclude that the points H_A, H_B, H_C, H_D lie on the sides $\mathcal{A}$, $\mathcal{B}$, $\mathcal{C}$, $\mathcal{D}$, respectively. So, the fact found in [7] and [25] is valid: *The orthopolar center P is the midpoint of pairs of points S_a,H_A; S_b,H_B; S_c,H_C; S_d,H_D where H_A,H_B,H_C,H_D are orthocenters of triangles $S_bS_cS_d$, $S_aS_cS_d$, $S_aS_bS_d$, $S_aS_bS_c$, incident to $\mathcal{A}$, $\mathcal{B}$, $\mathcal{C}$, $\mathcal{D}$, respectively*, see Fig. 10.

The circle $\mathcal{S}_d$ with the equation (7) has the tangent line at $T_{AB}=(ab,a+b)$ of the form

$$2abx+2(a+b)y-(ab+ac+bc+1)(x+ab)\\ -(a+b+c-abc)(y+a+b)+2(ab+ac+bc)=0.$$

This tangent intersects the line $\mathcal{D}$ with $dy=x+d^2$ in the point

$$x=\frac{acd+bcd-abd-a^2d-b^2d+ad^2+bd^2-cd^2-a^2b^2d+abcd^2}{c+d-a-b-abc-abd+acd+bcd}\\ y=\frac{ac+bc-a^2-ab-b^2+d^2-a^2b^2-abd^2+acd^2+bcd^2}{c+d-a-b-abc-abd+acd+bcd}.\qquad(26)$$

The equation

$$[c+d-a-b-ab(c+d)+cd(a+b)]\\ \cdot[x^2+y^2-(ab+cd)x-sy+p+(a+b)(c+d)]\\ +[1-ab-cd+(a+b)(c+d)+abcd]\\ \cdot[(a+b-c-d)x+(cd-ab)y+ab(c+d)-cd(a+b)]=0$$

is the linear combination of the equation (13) of the circle with diameter $T_{AB}T_{CD}$ and the equation $(cd-ab)y=(c+d-a-b)x+(a+b)cd-ab(c+d)$ of the line $T_{AB}T_{CD}$, so it is the equation of the circle $ST_{AB}T_{CD}$. The point from (26) is incident to this circle as well. Hence, the following statement from [1] and [3] is proved: *the intersection points of the tangents at the point T_{AB} to the circles S_c and S_d with the sides $\mathcal{C}$ and $\mathcal{D}$, respectively, and the intersections of the tangents at the point T_{CD} to the circles S_a and S_b with the sides $\mathcal{A}$ and $\mathcal{B}$, respectively, lie on the circle $ST_{AB}T_{CD}$. Similarly, two quadruples of analogous intersection points lie on the circles $ST_{AC}T_{BD}$ and $ST_{AD}T_{BC}$.*

It can be checked that the circle with equation

$$(a-b)(x^2+y^2)\\ +(ab^2-a^2b+b^2c-a^2d-a+b+c-d)x-\\ (ab^2c-a^2bd+a^2-b^2+ac-bd)y\\ +a^2b^2c-a^2b^2d+a^2b-ab^2+a^2c-b^2d=0$$

passes through the points T_{AB},T_{AD},T_{BC} and the circle with

$$2(x^2+y^2)-[(a+b)(c+d)+2ab+2]x\\ +[(ab+1)(c+d)-2(a+b+c+d)]y+\\ +(a+b)(c+d)+2ab=0$$

passes through the points S and T_{AB}, and through the midpoints of the line segment $T_{AC}T_{AD}$ and $T_{BC}T_{BD}$. Their radical axis is

$$(a^2+b^2+2)x-(a^2b+ab^2+a+b)y+2a^2b^2+a^2+b^2=0,$$

and due to symmetry on c and d, the circle that is incident to T_{AB},T_{AC},T_{BD} also belongs to the same pencil of circles. All three of circles have the common point T_{AB} and an additional point S_{ab}. However, the circles $T_{AB}T_{AD}T_{BC}$ and $T_{AB}T_{AC}T_{BD}$ are circumcircles of the trilaterals $\mathcal{ABW}$ and $\mathcal{ABV}$ of the quadrilateral $\mathcal{ABVW}$, so the point S_{ab} is the focus of that quadrilateral. We have just proved the statement from [3]: *If S_{ab} is the focus of the quadrilateral $\mathcal{ABVW}$, then the circle $\mathcal{S}_{ab}=ST_{AB}S_{ab}$ passes through the midpoints of line segments $T_{AC}T_{AD}$ and $T_{BC}T_{BD}$. There are five more such circles $\mathcal{S}_{cd}$, $\mathcal{S}_{ac}$, $\mathcal{S}_{bd}$, $\mathcal{S}_{ad}$, $\mathcal{S}_{bc}$ incident to triples of points S,T_{CD},S_{cd}; S,T_{AC},S_{ac}; S,T_{BD},S_{bd}; S,T_{AD},S_{ad}; S,T_{BC},S_{bc} and passing through the two of midpoints of corresponding line segments, where S_{cd}, S_{ac}, S_{bd}, S_{ad}, S_{bc} are foci of quadrilaterals $\mathcal{CDVW}$, $\mathcal{ACUW}$, $\mathcal{BDUV}$, $\mathcal{ADUV}$, $\mathcal{BCUV}$.*

Euler's line of the trilateral $\mathcal{ABC}$, i.e. the line connecting $S_d=\left(\frac{1}{2}(ab+ac+bc+1),\frac{1}{2}(a+b+c-abc)\right)$ and $H_d=(-1,a+b+c+abc)$ has the slope $-\frac{a+b+c+3abc}{ab+ac+bc+3}$, so the perpendicular line from N_d from (22) has the equation

$$\begin{aligned}&4(ab+ac+bc+3)x-4(a+b+c+3abc)y=\\&-3a^2b^2c^2-8abc(a+b+c)+a^2b^2+a^2c^2+b^2c^2\\&-3(a^2+b^2+c^2)d-4(ab+ac+bc)-3.\end{aligned}$$

The point

$$K=\left(\frac{1}{4}(q+3p-1),\frac{1}{4}(3s+r)\right) \tag{27}$$

fulfill this equation. With analogous statements for other three trilaterals of the quadrilateral $\mathcal{ABCD}$ we have proved statement from [15] and [18]: *The perpendicular lines to Euler's lines of four trilaterals of the quadrilateral at its Euler's centers are incident to one point K.* We will call the point K *Kantor's point* of the quadrilateral $\mathcal{ABCD}$, see Fig. 8. *The points M and K from* (10) *and* (27) *have the point P from* (18) *as their midpoint*, as stated in [2].

The point H and the point K from (23) and (27) have the same ordinate, so *the line HK is parallel to median, i.e. perpendicular to the directrix* that is the result given in [2], [7] and [10].

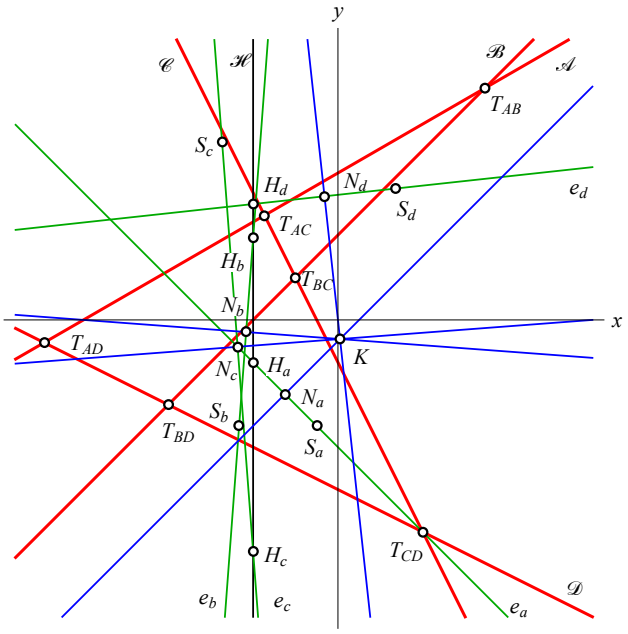

Figure 8: *Euler's lines e_a, e_b, e_c, e_d and Kantor's point K of $\mathcal{ABCD}$*

The center M from (10) and Kantor's point K from (27) have the midpoint P, the orthopolar center from (18), and points M and P have the dimidium center G_s for the midpoint. Thus, for the oriented lengths we have ratios $KP:PG_s:G_sM=2:1:1$. The point $P22=\left(\frac{1}{8}(q-p-1),\frac{1}{2}s\right)$ is the midpoint of the Morley's point H from (23) and central point M from (10), as well as the midpoint of the orthopolar center P from (18) and the point $P20=\left(-\frac{1}{2}(p+1),\frac{1}{2}s\right)$. For the centroid $T=\left(\frac{1}{6}q,\frac{1}{2}s\right)$, dimidium point $G_s=\left(\frac{1}{4}(q+2),\frac{1}{8}(3s-r)\right)$ and Morley's point $H=\left(-1,\frac{1}{4}(3s+r)\right)$, the equality $3T=2G_s+H$ is valid meaning that these points are collinear and that for oriented lengths the equality $TH=-2TG_s$ holds. Out of (23) and (27) the equality $K-H=\left(\frac{1}{4}(q+3p+3),0\right)$ follows, and for the point T and P from $P-T=\left(\frac{1}{12}(q+3p+3),0\right)$ is valid, so the lines HK and TP are parallel, and for the oriented lengths the equality $HK=3TP$ holds. The points $T,P,P20$ and $P22$ are incident to the median $\mathcal{N}$ and we derived the equality $\overrightarrow{TP}=\left(\frac{1}{12}(q+3p+3),0\right)$. Out of the equalities $P20=\left(-\frac{1}{2}(1+p),\frac{1}{2}s\right)$ and $P22=\left(\frac{1}{8}(q-p-1),\frac{1}{2}s\right)$, the forms $\overrightarrow{P20P22}=\left(\frac{1}{8}(q+3p+3),0\right)$, $\overrightarrow{P22T}=\left(\frac{1}{24}(q+3p+3),0\right)$ follow, and because of that $P20P22:P22T:TP=3:1:2$. From the previous consideration points $T,M,P,G_s,H,K,P20$ and $P22$ in each quadrilateral have mutual relationships as it is presented on the Fig. 9. Then the fact from [32] that *lines $MP20,PH$ and G_sP22 are parallel* follows.

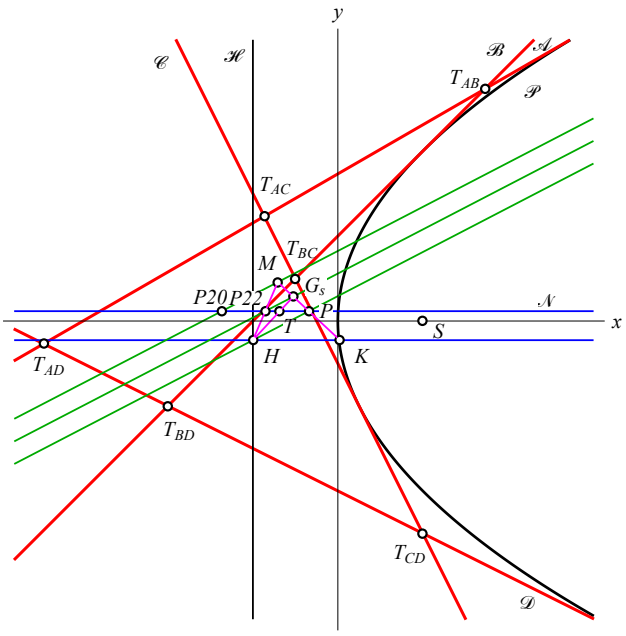

Figure 9: *Centroid T, orthopolar center P, dimidium point G_s, Morley's point H and Kantor's point K of $\mathcal{ABCD}$*

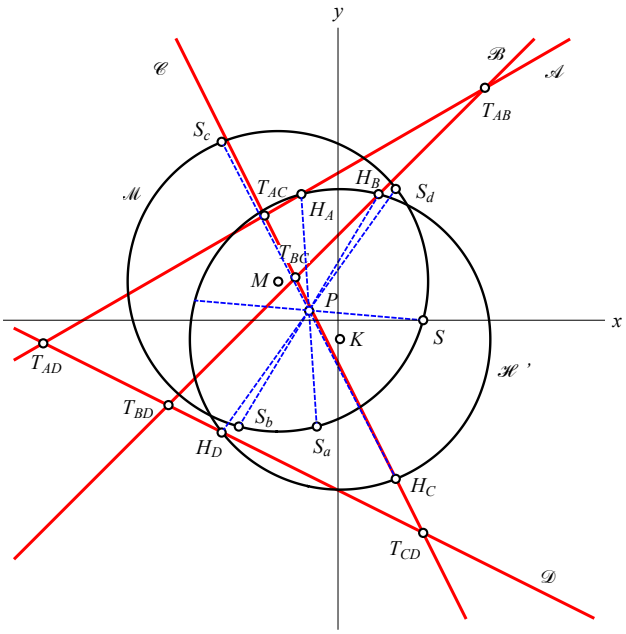

Figure 10: *Hervey's circle $\mathcal{H}'$ of $\mathcal{ABCD}$*

Symmetry with respect to the point P from (18) is done by replacement

$$x \to \frac{1}{2}(1+q+p)-x, \quad y \to s-y. \tag{28}$$

By this symmetry the points S_a, S_b, S_c, S_d are mapped into H_A, H_B, H_C, H_D and because of that the last mentioned points are incident to one circle $\mathcal{H}'$ whose equation is derived from the equation (9) of the central circle $\mathcal{M}$. We obtain the circle $\mathcal{H}'$

$$x^2+y^2-\frac{1}{2}(q+3p-1)x-\frac{1}{2}(3s+r)y + \frac{1}{2}(s^2+sr-p+p^2+pq)=0, \tag{29}$$

so called *Hervey's circle* of the quadrilateral $\mathcal{ABCD}$. Its center is Kantor's point K of the quadrilateral $\mathcal{ABCD}$, see Fig. 10. The fact that *$H_AH_BH_CH_D$ lie on one circle with the center K* appears in [17]. The point symmetric to the focus S with respect to the point P obviously is incident to the circle $\mathcal{H}'$.

From (17) and (21) given in [34] the next equations are obtained

$$16(\rho_a^2+\rho_b^2+\rho_c^2+\rho_d^2) = 12s^2+8q^2+4r^2-4sr - 2qp-6q+4p+4,$$
$$16\rho^2 = s^2+q^2+r^2+p^2-2sr-2qp-2q+2p+1,$$

and out of (2), (10) and (27) the following equalities can be derived

$$16SK^2 = 9s^2+q^2+r^2+9p^2+6sr+6pq-10q-30p+25,$$
$$16MK^2 = 4s^2+4r^2+16p^2+8sr-32p+16.$$

And now, we easily get the equality $\rho_a^2+\rho_b^2+\rho_c^2+\rho_d^2-7\rho^2 = SK^2-MK^2$ that is statement from [11]. The solution of Guillotin reaches $\overrightarrow{MS_a}+\overrightarrow{MS_b}+\overrightarrow{MS_c}+\overrightarrow{MS_d}=\overrightarrow{MK}$ that then can be found in [14], while [32] attributes it to Morley. This means that equality $S_a+S_b+S_c+S_d = 3M+K$ holds for the points themselves. However, it is easy to see by (8) and analogous formulas, and (10) and (27) that the left and the right sides are equal to $\left(q+2, \frac{1}{2}(3s-r)\right)$.

We can prove famous Zeeman's theorem from [12] saying: *if one side of the quadrilateral is parallel to Euler's line of the trilateral formed by the remaining three sides, then this holds for the rest three analogous combinations*. Indeed, slopes $-\frac{a+b+c+3abc}{ab+ac+bc+3}$ and $\frac{1}{d}$ of the Euler's line of the trilateral $\mathcal{ABC}$ and the line $\mathcal{D}$ are the same under the condition $q+3p+3=0$ that is symmetric on a,b,c,d. The quadrilateral with such properties is called *Zeeman's quadrilateral*. The midpoint of Kantor's point K from (27) and central point M from (10) is $(\frac{1}{4}(1+q+p), \frac{1}{4}(s-r))$. *In the case of Zeeman's quadrilateral $1+q+p=\frac{2}{3}q$ holds, hence this midpoint is the centroid T*. The statement comes from [12]. *In the same case Kantor's point K from* (27) *and Morley's point H from* (23) *coincide*, that is the result in [17].

As explained in [16], if perpendiculars are dropped on any line from the vertices of a triangle, the perpendiculars to the opposite sides from their feet are concurrent at a point called the orthopole of the line. The construction of the

orthopol O_d of the line $\mathcal{D}$ with respect to the trilateral $\mathcal{ABC}$ is shown in Fig. 12.

The perpendicular line from the point S to the line $\mathcal{A}$ has the equation $y+ax=a$ and intersects the line $\mathcal{A}$ in the point $A''=(0,a)$. Similarly, ortoghonal projections of the focus S to lines $\mathcal{B},\mathcal{C},\mathcal{D}$ are points $B''=(0,b)$, $C''=(0,c)$, $D''=(0,d)$, respectively. All of four points lie on $y-$axis that is vertex tangent to parabola $\mathcal{P}$. Let $\mathcal{A}'',\mathcal{B}'',\mathcal{C}'',\mathcal{D}''$ be parallel lines to the lines $\mathcal{A},\mathcal{B},\mathcal{C},\mathcal{D}$ through the points H_a,H_b,H_c,H_d. The lines $\mathcal{A}''$ and $\mathcal{B}''$ have the equations

$$ay=x+1+ab+ac+ad+abcd,$$
$$by=x+1+ab+bc+bd+abcd,$$

and their intersection point is $(-1-ab-abcd,c+d)$. The midpoint of this point and the point $T_{AB}=(ab,a+b)$ is the point $N=(-\frac{1}{2}(p+1),\frac{1}{2}s)$ from (28) in [34]. Similarly, the same is valid for the quadrilaterals $\mathcal{ABCD}$ and $\mathcal{A}''\mathcal{B}''\mathcal{C}''\mathcal{D}''$, hence these two quadrilaterals are symmetric with respect to the point N. The perpendicular from $\mathcal{A}''\cap\mathcal{B}''$ to the line $\mathcal{H}$ has the equation $y=c+d$ and intersects it in the point $(-1,c+d)$, and the perpendicular line from that point to the line $\mathcal{C}''$ has the equation $y+cx=d$ so it passes through the point $D''=(0,d)$. Because of symmetry on a,b,c we conclude that D'' is the orthopole of $\mathcal{H}$ with respect to the trilateral $\mathcal{A}''\mathcal{B}''\mathcal{C}''$. In the same way we obtain three more orthopoles. The statement that *orthogonal projections of the point S to lines $\mathcal{A},\mathcal{B},\mathcal{C},\mathcal{D}$ are orthopoles of the line $\mathcal{H}$ with respect to trilaterals $\mathcal{B}''\mathcal{C}''\mathcal{D}''$, $\mathcal{A}''\mathcal{C}''\mathcal{D}''$, $\mathcal{A}''\mathcal{B}''\mathcal{D}''$, $\mathcal{A}''\mathcal{B}''\mathcal{C}''$* appears in [28] and [29].

Parallel lines to $\mathcal{A},\mathcal{B},\mathcal{C},\mathcal{D}$ through the points S_a,S_b,S_c,S_d form a quadrilateral symmetric to the quadrilateral $\mathcal{ABCD}$ with respect to the point P, and parallel to lines $\mathcal{A},\mathcal{B},\mathcal{C},\mathcal{D}$ through points H_a,H_b,H_c,H_d form a quadrilateral symmetric to $\mathcal{ABCD}$ with respect to point N. The second quadrilateral is obtained by using translation for a vector $\mathbf{v}$ from the first quadrilateral. If τ is any real number and if T_a,T_b,T_c,T_d are points such that $S_aT_a=\tau S_aH_a$, $S_bT_b=\tau S_bH_b$, $S_cT_c=\tau S_cH_c$, $S_dT_d=\tau S_dH_d$ hold, then lines through the points T_a,T_b,T_c,T_d parallel to $\mathcal{A},\mathcal{B},\mathcal{C},\mathcal{D}$ form the quadrilateral that is obtained by using the translation for vector $\tau\mathbf{v}$ from the first new before mentioned quadrilateral. It is symmetric to $\mathcal{A},\mathcal{B},\mathcal{C},\mathcal{D}$ with respect to the point T_τ that is obtained from P by the translation for the vector $\tau\overrightarrow{PN}$. All of these centers of symmetry T_τ are incident to the common median of all of mentioned quadrilaterals. Particularly, *the quadrilateral made by lines parallel to $\mathcal{A},\mathcal{B},\mathcal{C},\mathcal{D}$ through centroids G_a,G_b,G_c,G_d of trilaterals $\mathcal{BCD}$, $\mathcal{ACD}$, $\mathcal{ABD}$, $\mathcal{ABC}$, is symmetric to the quadrilateral $\mathcal{ABCD}$ with respect to* a point T_τ such that $\overrightarrow{PT_\tau}=\frac{1}{3}\overrightarrow{PN}$. It is easy to see that $T_\tau=(\frac{1}{6}q,\frac{1}{2}s)$, and that is *the centroid T of the vertices of $\mathcal{ABCD}$*. This statement appears in [4].

The points S_a,S_b,S_c,S_d are in accordance with (8). The midpoint of e.g. S_c and S_d have coordinates of the form

$$x=\frac{1}{4}(2ab+ac+ad+bc+bd+2),$$
$$y=\frac{1}{4}(2a+2b+c+d-abc-abd),$$

and the line S_aS_b has the slope $\frac{1-cd}{c+d}$ so the perpendicular line to this line through the point P from (18) has the equation

$$(c+d)x+(1-cd)y=\frac{1}{4}(c+d)(p+q+1)+\frac{1}{2}(1-cd)s,$$

that is fulfilled by before mentioned coordinates. Analogously, the perpendicular lines from the point P to any side of the cyclic quadrangle $S_aS_bS_cS_d$ pass through the midpoints of corresponding opposite sides. A well known properties of the cyclic quadrangle is following: the perpendicular lines from the midpoint of the side to the opposite side pass through one point such that Wallace's lines of the vertices of this quadrangle with respect to the triangles formed by remaining three vertices are incident to this point as well as Euler's circles of all four triangles. This point is so called *anticenter* of this cyclic quadrangle. Hence, the orthopolar center P of the quadrilateral $\mathcal{ABCD}$ is the anticenter of the cyclic quadrangle $S_aS_bS_cS_d$. Because of symmetry with respect to the point P it follows that *P is the anticenter for the cyclic quadrangle $H_AH_BH_CH_D$* as well. We find this statement in [21].

The line $\mathcal{D}_0$ through the point S_d from (8) and parallel to $\mathcal{D}$ has the equation

$$dy-x=\frac{1}{2}(ad+bd+cd-bc-bd-cd-abcd-1).$$

This equation is possible to obtain by substitutions (28), so lines $\mathcal{D}$ and $\mathcal{D}_0$ are symmetric with respect to the orthopolar center P. Similarly, this is valid for the remaining sides of $\mathcal{ABCD}$. Hence, we shown our original theorem:

Theorem 3 *Let $\mathcal{ABCD}$ be a complete quadrilateral. Quadrilaterals $\mathcal{ABCD}$ and $\mathcal{A}_0\mathcal{B}_0\mathcal{C}_0\mathcal{D}_0$ are symmetric with respect their join orthopolar center P, where $\mathcal{A}_0$, $\mathcal{B}_0$, $\mathcal{C}_0$, $\mathcal{D}_0$ are lines through the circumcenters S_a, S_b, S_c, S_d of trilaterals $\mathcal{BCD}$, $\mathcal{ACD}$, $\mathcal{ABD}$, $\mathcal{ABC}$, and parallel to $\mathcal{A},\mathcal{B},\mathcal{C},\mathcal{D}$ respectively. The circumcenters of trilaterals of one quadrilateral are incident to corresponding sides of the other quadrilateral. The central circle of one quadrilateral is Hervey's circle of the other. The central point of one quadrilateral is Kantor's point of the other.*

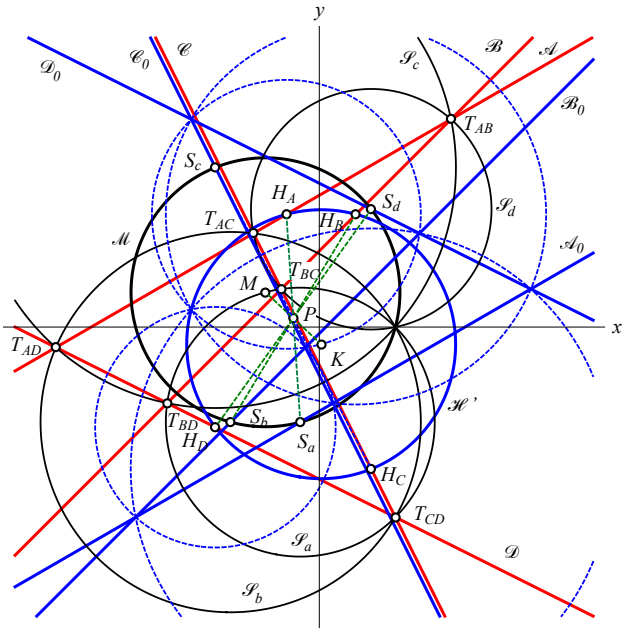

Figure 11: *Hervey's circle $\mathscr{H}'$ of $\mathcal{ABCD}$ is central circle of $\mathcal{A}_0\mathcal{B}_0\mathcal{C}_0\mathcal{D}_0$, and vice versa.*

The line $\mathcal{D}_0$ through the point S_d from (8) parallel to $\mathcal{D}$ is $x-dy=\frac{1}{2}(1+ab+ac+bc-ad-bd-cd+abcd)$, and the normal from the point T_{AB} to the line $\mathcal{D}_0$ has the equation $dx+y=a+b+abd$ and intersects it in the point having coordinates

$$x=\frac{1}{2\delta}(1+ab+ac+ad+bc+bd-cd+abcd+2abd^2),$$
$$y=\frac{1}{2\delta}(2a+2b-d+ad^2+bd^2+cd^2+abd-acd-bcd-abcd^2).$$

The normal from this point to the line $\mathcal{C}$ has the equation

$$2\delta(cx+y)=2a+2b+c-d+abc+abd+ac^2+ad^2 +bc^2+bd^2+cd^2-c^2d+abc^2d+abcd^2$$

and passes through the point O_{d0} with coordinates

$$x=\frac{1}{2\delta}(ab+ac+bc-ad-bd-cd+abcd-1),$$
$$y=\frac{1}{2\delta}(2a+2b+2c-d+abd+acd+bcd +ad^2+bd^2+cd^2+abcd^2).$$

As these coordinates are symmetric on a,b,c this point is incident to two more analogous normals, i.e. the point O_{d0} is the orthopole of the line $\mathcal{D}_0$ with respect to the trilateral $\mathcal{ABC}$. It is easy to prove that the point O_{d0} is incident to orthopolar circle $\mathcal{P}'$ of the quadrilateral $\mathcal{ABCD}$ with equation (17). The same is valid for orthopoles O_{a0},O_{b0},O_{c0} of lines $\mathcal{A}_0,\mathcal{B}_0,\mathcal{C}_0$ with respect to trilaterals $\mathcal{BCD}$, $\mathcal{ACD}$, $\mathcal{ABD}$ that justify the name of this circle. The fact that *four orthopoles $O_{a0},O_{b0},O_{c0},O_{d0}$ lie on one circle incident to focus*, we find in [30]. Leemans uses in his proof inscribed parabola with the equation $y^2=4x$ as well, and as the result he obtains the equation (17) using notations different from ours. The point O_{d0} can be written in the form

$$O_{d0}=\left(\frac{1}{2\delta}(q+p-1-2ds+2d^2),\frac{1}{2\delta}(2s-3d+dq+dp)\right). \tag{30}$$

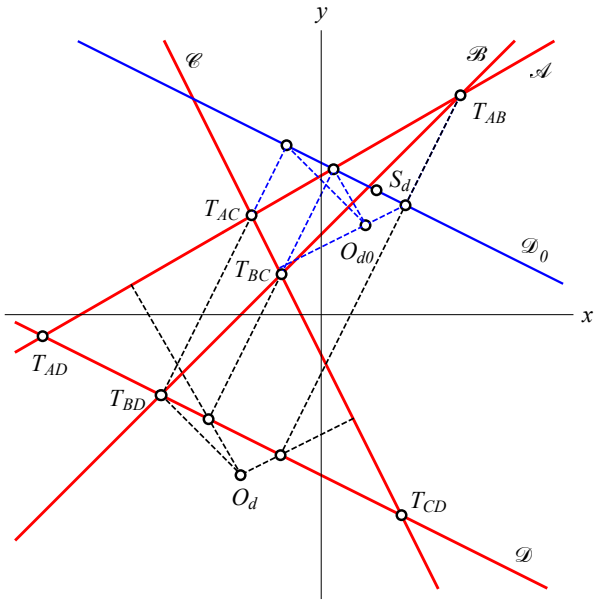

Figure 12: *The orthopoles O_d and O_{d0} of the lines $\mathcal{D}$ and $\mathcal{D}_0$ with respect to the trilateral $\mathcal{ABC}$, respectively.*

The line $\mathcal{D}'''$ symmetric to the line $\mathcal{D}$ with respect to the axis $\mathcal{X}$ of the parabola $\mathcal{P}$ has the slope $-\frac{1}{d}$, so the line through O_{d0} parallel to this line has the equation $x+dy=\frac{1}{2\delta}(q+p-1-d^2+qd^2+pd^2)$ i.e. the equation $x+dy=\frac{1}{2}(q+p-1)$. This line intersects the axis $\mathcal{X}$ in the point $\left(\frac{1}{2}(q+p-1),0\right)$. It is easy to check that this point is incident to orthopolar circle with the equation (17). The line through the point S_d from (8) parallel to the line $\mathcal{D}'''$ has the equation $x+dy=\frac{1}{2}(1+q-p)$ and intersects the axis $\mathcal{X}$ in the point $(\frac{1}{2}(1+q-p),0)$ which lies on the central circle with the equation (9). These results are in [31] attributed to R. Bouvaist-u: *the lines through the circumcenters of four trilaterals $\mathcal{BCD}$, $\mathcal{ACD}$, $\mathcal{ABD}$, $\mathcal{ABC}$, and parallel to the lines symmetric to $\mathcal{A}$, $\mathcal{B}$, $\mathcal{C}$, $\mathcal{D}$ with respect to the axis of the inscribed parabola $\mathcal{P}$ intersect in the intersection point of the axis and the central circle different from the focus S.* For the point O_{d0} from (30) we have $x-1=\frac{1}{2\delta}(q+p-3-2ds)$, so together with second coordinate from (30) the equality $4\delta^2{SO_{d0}}^2=(d^2+1)(p^2+2pq+q^2-6p-6q+4s^2+9)$ is obtained, i.e.

$${SO_{d0}}^2=\frac{1}{4\delta}(p^2+2pq+q^2-6p-6q+4s^2+9),$$

and formulas for distances of focus S to the points ${O_{a0}}^2, {O_{b0}}^2, {O_{c0}}^2$ look similarly and from them the equality

$$SO_{a0} : SO_{b0} : SO_{c0} : SO_{d0} = \frac{1}{\sqrt{\alpha}} : \frac{1}{\sqrt{\beta}} : \frac{1}{\sqrt{\gamma}} : \frac{1}{\sqrt{\delta}} \qquad (31)$$

follows. From (31) for $x-1$ and the second coordinate in (30) follows that SO_{d0} has the slope $\frac{2s-3d+dq+dp}{q+p-3-2ds}$ and, analogously, the line SO_{c0} has $\frac{2s-3c+cq+cp}{q+p-3-2cs}$. After applying formula (22) in [34] and leaving out the common factor $p^2+2pq+q^2-6p-6q+4s^2+9$ we obtain $\tan\angle(SO_{d0},SO_{c0}) = \frac{c-d}{cd+1}$. Lines ST_{AC} and ST_{AD} have the slopes $\frac{a+c}{ac-1}$ and $\frac{a+d}{ad-1}$ and for them we obtain $\tan\angle(ST_{AC},ST_{AD}) = \frac{c-d}{cd+1}$. Hence, $\angle(SO_{d0},SO_{c0}) = \angle(ST_{AC},ST_{AD})$. Earlier we have proved that focus S is the center of similarity of quadrangles $T_{CD}S'_BT_{AD}T_{AC}$ and $S_aS_bS_cS_d$. Because of that $\angle(ST_{AC}ST_{AD}) = \angle(SS_d,SS_c)$. We obtain the equality $\angle(SO_{d0}SO_{c0}) = \angle(SS_d,SS_c)$. With such other equalities with other index pairs, for example, $\angle(SO_{a0}SO_{b0}) = \angle(SS_a,SS_b)$ etc. and from equalities (12) and (31) we conclude that *cyclic quadrangles $S_aS_bS_cS_d$ and $O_{a0}O_{b0}O_{c0}O_{d0}$ are directly similar with the center of similarity S*. This result appears in [26].

According to [34] the orthopole O_d of the line $\mathcal{D}$ with respect to $\mathcal{ABC}$ is given by $O_d = \left(-1, \frac{1}{\delta}\left(a+b+c+(ab+ac+bc)d+abcd^2+d^2\right)\right)$. Its coordinates can be rewritten as $O_d = \left(-1, \frac{1}{\delta}\left(s-d+qd-sd^2+pd+2d^3\right)\right)$. The difference between the ordinates of the points O_d and O_{d0} is equal to $\frac{1}{2\delta}\left(-d-qd-pd+2sd^2-4d^3\right)$, and difference between their abscissas is equal to $\frac{1}{2\delta}\left(1+q+p-2sd+4d^2\right)$. Thus, the slope of the line O_dO_{d0} is $-d$. Therefore, O_dO_{d0} is perpendicular to $\mathcal{D}$. Similarlly, the lines O_aO_{a0}, O_bO_{b0}, O_cO_{c0} are perpendicular to the sides $\mathcal{A}$, $\mathcal{B}$, $\mathcal{C}$ (see Fig. 13). So, the following theorem, which is our original result, is proved:

Theorem 4 *Let $\mathcal{ABCD}$ be a complete quadrilateral. The lines O_aO_{a0}, O_bO_{b0}, O_cO_{c0}, O_dO_{d0} are perpendicular to the sides $\mathcal{A}$, $\mathcal{B}$, $\mathcal{C}$, $\mathcal{D}$, where O_a, O_b, O_c, O_d are orthopoles of $\mathcal{A}$, $\mathcal{B}$, $\mathcal{C}$, $\mathcal{D}$ with respect to $\mathcal{BCD}$, $\mathcal{ACD}$, $\mathcal{ABD}$, $\mathcal{ABC}$, and O_{a0}, O_{b0}, O_{c0}, O_{d0} are orthopoles of $\mathcal{A}_0$, $\mathcal{B}_0$, $\mathcal{C}_0$, $\mathcal{D}_0$ with respect to $\mathcal{BCD}$, $\mathcal{ACD}$, $\mathcal{ABD}$, $\mathcal{ABC}$, respectively.*

Some long, but elementary calculations show that the midpoint of the point S_d given by (8), and the point O_{d0} given by (30) has the coordinates

$$\begin{aligned} x &= \frac{1}{4\delta}\left(2ab+2ac+2bc-ad-bd-cd+dr+d^2\right)\\ y &= \frac{1}{4\delta}(3a+3b+3c-d+abd+acd+bcd-abc\\ &\quad +2(a+b+c)d^2). \end{aligned} \qquad (32)$$

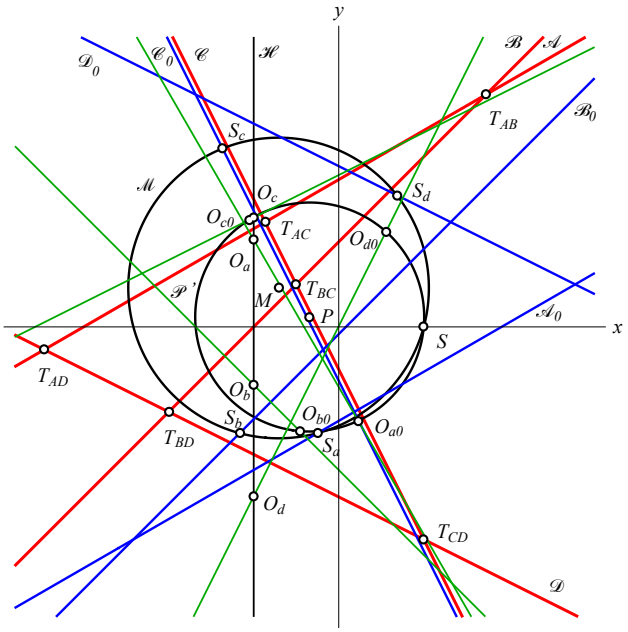

Figure 13: *Lines O_aO_{a0}, O_bO_{b0}, O_cO_{c0}, O_dO_{d0} are perpendicular to $\mathcal{A}$, $\mathcal{B}$, $\mathcal{C}$, $\mathcal{D}$, where O_a, O_b, O_c, O_d are orthopoles of $\mathcal{A}$, $\mathcal{B}$, $\mathcal{C}$, $\mathcal{D}$ with respect to $\mathcal{BCD}$, $\mathcal{ACD}$, $\mathcal{ABD}$, $\mathcal{ABC}$, and O_{a0}, O_{b0}, O_{c0}, O_{d0} are orthopoles of $\mathcal{A}_0$, $\mathcal{B}_0$, $\mathcal{C}_0$, $\mathcal{D}_0$ with respect to $\mathcal{BCD}$, $\mathcal{ACD}$, $\mathcal{ABD}$, $\mathcal{ABC}$, respectively.*

It follows from (11) that the point S'_D has the coordinates

$$S'_D = \Big(\frac{1}{\delta}(d^2+ab+bc+ac-ad-bd-cd+abcd),\\ \frac{1}{\delta}(a+b+c-d+abd+acd+bcd-abc)\Big),$$

and therefore the point given by (32) is at the same time the centroid of the quadrangle $T_{AB}T_{BC}T_{AC}S'_D$. The fact that *the midpoints of the line segments S_aO_{a0}, S_bO_{b0}, S_cO_{c0}, S_dO_{d0} are the centroids of the quadrangles $T_{BC}T_{CD}T_{BD}S'_A$, $T_{AC}T_{CD}T_{AD}S'_B$, $T_{AB}T_{BD}T_{AA}S'_C$, $T_{AB}T_{BC}T_{AC}S'_D$, respectively*, can be found in [26].

If we write the coordinates of the point S_d in the following form

$$\left(\frac{1}{2}(q+1-sd+d^2), \frac{1}{2}(s-d+d^3-sd^2+qd-r)\right),$$

then we can check that they fulfill the equation

$$\begin{aligned} &2(s+r-2d+2pd)x+2(sd+rd+2-2p)y\\ &\quad +3sp-rp+r-3s-sq-qr+4d-4pd=0. \end{aligned} \qquad (33)$$

The coordinates of the point O_{d0} given by (30) also fulfill (33). So, that equation represents the line S_dO_{d0}. Similarly, the line S_cO_{c0} has the equation

$$\begin{aligned} &2(s+r-2c+2pc)x+2(sc+rc+2-2p)y\\ &\quad +3sp-rp+r-3s-sq-qr+4c-4pc=0. \end{aligned} \qquad (34)$$

By subtracting those two equations and dividing the result by the factor $2(d-c)$, we get the equation

$$2(p-1)x+(s+r)y-2(p-1)=0, \tag{35}$$

the equation of the radical axis of the circles $\mathcal{M}$ and $\mathcal{P}'$ given by (9) and (17). Therefore, lines S_dO_{d0} and S_cO_{c0} intersect each other in a point lying on the radical axis of the central and the orthopolar circle. The lines S_aO_{a0} and S_bO_{b0} pass through the same point as well. From (33) and (34) we obtain its coordinates as

$$\begin{aligned} x=\frac{1}{2k}\big(&pr^2-2qrs-3ps^2+qr^2+2prs+qs^2+8p^2\\ &-r^2+2rs+3s^2-16p+8\big), \end{aligned} \tag{36}$$

$$y=\frac{1}{k}\big(-p^2r+3p^2s-pqr-pqs+4pr-4ps+qr+qs-3r+s\big),$$

where $k=4(p-1)^2+(s+r)^2$. The connection line MP of the centers of the central and the orthopolar circles has the equation

$$4(s+r)x-8(p-1)y+3sp-rp-qr-sq-r-5s=0.$$

Its intersection with the radical axis (35) of $\mathcal{M}$ and $\mathcal{P}'$ has the coordinates

$$\begin{aligned} x=\frac{1}{4k}\big(&pr^2-2prs-3ps^2+qr^2+2qrs+qs^2\\ &+16p^2+r^2+6rs+5s^2-32p+16\big)\\ y=\frac{1}{2k}\big(&-p^2r+3p^2s-pqr-pqs+4pr-4ps\\ &+qr+qs-3r+s\big), \end{aligned} \tag{37}$$

being, therefore, the midpoint of the point (36) and the focus S whose coordinates can be written in the form $S=\big(\frac{1}{2k}(8p^2-16p+8+2s^2+4sr+2r^2),0\big)$. The fact that *the intersection of the lines S_aO_{a0}, S_bO_{b0}, S_cO_{c0}, S_dO_{d0} is the intersection point of the central circle $\mathcal{M}$ and the orthopolar circle $\mathcal{P}'$ (different from S)*, can be found in [26]. It is depicted in Fig. 14.

By using the equalities $d^4-sd^3+qd^2-rd+p=0$ and $abc=r-qd+sd^2-d^3$ the coordinates of the midpoint od S_d and O_{s0} given by (32) get the form

$$\left(\frac{1}{4\delta}(2q-3sd+rd+4d^2),\frac{1}{4\delta}(3s-4d-r+2qd)\right).$$

They satisfy equation (19), so we have proved one more result given in [26]: *the midpoints of the segments S_aO_{a0}, S_bO_{b0}, S_cO_{c0}, S_dO_{d0} lie on the dimidium circle of the quadrilateral $\mathcal{ABCD}$.*

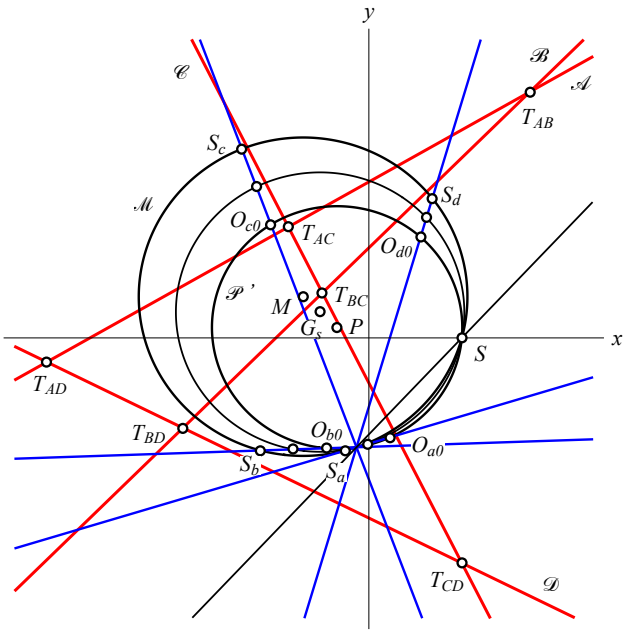

Figure 14: *Lines S_aO_{a0}, S_bO_{b0}, S_cO_{c0}, S_dO_{d0} pass through the intersection point of the orthopolar circle $\mathcal{P}'$ and central circle $\mathcal{M}$ of the quadrilateral $\mathcal{ABCD}$.*

References

[1] CLAWSON, J.W., The complete quadrilateral, *Ann. of Math.* **20**(4) (1919), 232–261, https://doi.org/10.2307/1967118

[2] CLAWSON, J.W., More theorems on the complete quadrilateral, *Ann. of Math.* **23**(1) (1921), 40–44, https://doi.org/10.2307/1967780

[3] CLAWSON, J.W., Points, lines and circles connected with the complete quadrilateral, Note 509, *Math. Gaz.* **9**(129) (1917), 85–88, https://doi.org/10.2307/3603503

[4] CLAWSON, J.W., Problem 4007, *Amer. Math. Monthly* **49**(10) (1942), 692–694, https://doi.org/10.2307/2302595

[5] DAVIES, T.S., Question 1878, *Lady's Gentl. Diary* (1855), 58–60.

[6] DEAUX, R., Involution de Möbius et point de Miquel, *Mathesis* **55** (1945), 223–230.

[7] FETTIS, H.E., The complete quadrilateral, *Math. Mag.* **22**(1) (1948), 19–22, https://doi.org/10.2307/3029708

[8] FONTENÉ, G., Sur un quadrangle mobile, *Nouv. Ann. Math.* Serie 3 **17** (1898), 101–106.

[9] GOORMAGHITIGH, R., Sur le point de Miquel, *Mathesis* **64** (1955), 9–13.

[10] GOORMAGHITIGH, R., Sur le point de Hervey d'un quadrilatère et sur les quadrilatéres de Zeeman, *Mathesis* **56** (1947), 175–178.

[11] GOORMAGHITIGH, R., Question 3557, *Mathesis* **61** (1952), 159. solution par R. Gullotin, **62** (1953), 379.

[12] GOORMAGHITIGH, R., Génèralisation d'un théorème de Zeeman, *Mathesis* **68** (1959), 356–361.

[13] GUDERMANN, C., Grundriss der analytischen Sphärik, DüMont-Schauberg, Köln 1830, S. 138.

[14] GULLOTIN, R., Sur le point de Kantor-Hervey, *Mathesis* **62** (1953), 334–336.

[15] HERVEY, F.R.J., Problem 10088 and solution, *Educ. Times* **54** (1891), 37.

[16] JOHNSON, R.A., *Advanced Euclidean Geometry*, Dover Publications, Mineola, NY (1960).

[17] LEVELUT, A., A note on the Hervey point of a complete quadrilateral, *Forum Geom.* **11** (2011), 1–7.

[18] KANTOR, S., Quelques théorèmes nouveaux sur l'hypocycloide à trois rebroussements, *Bull. Sci. Math. Astr.* **3**(1) (1879), 136–144.

[19] MÖBIUS, A.F., Zwei rein geometrische Beweise des Bodenmiller'schen Satzes, *Ber. Verh. Kön. Sächs. Ges. Wiss. Leipzig* **6** (1854), 87–91.

[20] MORLEY, F., Orthocentric properties of the plane *n*-line, *Trans. Amer. Math. Soc.* **4**(1) (1903), 1–12, https://doi.org/10.2307/1986445

[21] MUSSELMAN, J.R., On four lines and their associated parabola, *Amer. Math. Monthly* **44**(8) (1937), 513–521, https://doi.org/10.2307/2301227

[22] RADFORD E.M., Solutions, *Math. Gaz.* **4**(75) (1908), 345–376, https://doi.org/10.2307/3603970

[23] SCHLÖMILCH, O., Über das vollständige Viereck, *Ber. Verh. Kön. Sächs. Ges. Wiss. Leipzig*, **6** (1854), 4–13.

[24] SEYDEWITZ, F., Neue Untersuchungen über die Bestimmung einer gleichseitigen Hyperbel vermittelst vier gegebener Bedingungen, *Arch. Math. Phys.* **3** (1843), 225–235.

[25] TERRIER, P., Quadrilatéres et sections coniques, *Nouv. Ann. Math.* (2) **14** (1875), 514–523.; (2) **15** (1876), 108–114.

[26] THÉBAULT, V., Sur le cercle des orthopôles, *Bull. Soc. Roy. Sci. Liége* **14** (1945), 299–307.; *Mathesis* **55** (1945), suppl.9p.

[27] THÉBAULT, V., Question 3223, *Mathesis* **54** (1940), 401; solutions par R. Bouvaist et r. Blanchard, *Mathesis* **55** (1945), 113–119.

[28] THÉBAULT, V., Problem 3890, *Amer. Math. Monthly* **50**(4) (1943), 264–267, https://doi.org/10.2307/2303944

[29] THÉBAULT, V., CLAWSON, J. W., Problem 3991, *Amer. Math. Monthly* **49**(8) (1942), 550–551, https://doi.org/10.2307/2302878

[30] THÉBAULT, V., BOUVAIST, R., Question 2944, *Mathesis* **50** (1936), 60; solutions par J. Leemans, **50** (1936), 352-354.

[31] THÉBAULT, V., Sur le quadrilatère complet, *Mathesis* **51** (1937), 187–191, 242-243.

[32] TIENHOVEN, C., *Encyclopedia of Quadri-Figures*, https://chrisvantienhoven.nl/mathematics/encyclopedia

[33] TUMMERS, J.H., Question 3169, *Mathesis* **54** (1940), 48.

[34] VOLENEC, V., JURKIN, E., ŠIMIĆ HORVATH, M., A Complete Quadrilateral in Rectangular Coordinates, *KoG* **26** (2022), 62–78, https://doi.org/10.31896/k.26.6

Vladimir Volenec
orcid.org/0000-0001-7418-8972
e-mail: volenec@math.hr

University of Zagreb Faculty of Science
Bijenička cesta 30, HR-10000 Zagreb, Croatia

Ema Jurkin
orcid.org/0000-0002-8658-5446
e-mail: ema.jurkin@rgn.unizg.hr

University of Zagreb
Faculty of Mining, Geology and Petroleum Engineering
Pierottijeva 6, HR-10000 Zagreb, Croatia

Marija Šimić Horvath
orcid.org/0000-0001-9190-5371
e-mail: marija.simic@arhitekt.hr

University of Zagreb Faculty of Architecture
Kačićeva 26, HR-10000 Zagreb, Croatia

https://doi.org/10.31896/k.28.6
Stručni rad
Prihvaćeno 3. 5. 2024.

ANDREJ NOVAK
MARTINA ARMANDA

Primjena Cahn-Hilliardove jednadžbe za uslikavanje binarnih slika

The application of the Cahn-Hilliard equation for digital image inpainting

ABSTRACT

We investigate the application of the Cahn-Hilliard (CH) equation for digital image inpainting, focusing on various choices of nonlinear potential, including the double well potential and classifiers based on shock filters. These potentials are crucial in shaping the inpainting results, and their selection depends on the characteristics of specific images and the desired properties of reconstruction. Additionally, we present a numerical scheme based on the principle of convexity splitting, and we demonstrate the results of inpainting simple binary shapes. Throughout the text, we emphasize the fundamental features of the Cahn-Hilliard equation to enable a better understanding of the role of partial differential equations in image processing.

Key words: Cahn-Hilliard equation, digital image inpainting, numerical methods, image processing

MSC2010: 68U10, 65M06, 94A08, 35K55

Primjena Cahn-Hilliardove jednadžbe za uslikavanje binarnih slika

SAŽETAK

Istražujemo primjenu Cahn-Hilliardove (CH) jednadžbe za potrebe uslikavanja digitalnih slika, fokusirajući se na različite izbore nelinearnog potencijala, uključujući potencijal dvostruke jame i klasifikatore temeljene na šok filteru. Ovi potencijali su ključni u oblikovanju rezultata uslikavanja, a njihov odabir ovisi o karakteristikama specifičnih slika i željenim svojstvima rekonstrukcije. Također, predstavljamo numeričku shemu zasnovanu na principu cijepanja po konveksnosti, te prikazujemo rezultate uslikavanja jednostavnih binarnih oblika. Kroz tekst stavljamo naglasak na osnovne karakteristike Cahn-Hilliardove jednadžbe kako bismo omogućili bolje razumijevanje uloge parcijalnih diferencijalnih jednadžbi u obradi slika.

Ključne riječi: Cahn-Hilliardova jednadžba, uslikavanje digitalnih slika, numeričke metode, obrada slike

1 Uvod

Problem uslikavanja potječe iz potrebe za restauracijom umjetničkih slika, gdje su muzejski restauratori ručno obnavljali slike koje su pretrpjele oštećenja. Potreba za obradom slika prirodno se proširila od umjetničkih slika, preko fotografije i filma, do digitalnih slika s pojavom računala. Nepoznate ili oštećene regije slike nazivamo domenom uslikavanja.

Za sliku f, definiranu na domeni slike $\Omega \subset \mathbb{R}^2$, cilj je rekonstruirati sliku na domeni uslikavanja (dio koji je oštećen) $\omega \subset \Omega$ tako da se dobivena rekonstrukcija prirodno uklapa u ostatak slike (tj. da se prirodno prošire karakteristike slike unutar domene uslikavanja).

Inspirirani tehnikama ručnog uslikavanja, Bertalmio i suradnici [2] bili su među prvima koji su uveli neizotropnu parcijalnu diferencijalnu jednadžbu (PDJ) koja iz okoline domene uslikavanja $\Omega \setminus \omega$ glatko prenosi informacije u smjeru izofota (krivulja konstantnog intenziteta sive) unutar domene uslikavanja ω. Napomenimo da je neizotropna difuzija u ovom slučaju poželjan izbor zato što osigurava oštrinu rekonstruirane slike. Preciznije, razmatrali su sljedeću jednadžbu:

$$u_t = \nabla^\perp u \cdot \nabla \Delta u \text{ na } \omega, \tag{1}$$

$$u = f(\mathbf{x}) \text{ na } \Omega \setminus \omega, \tag{2}$$

gdje je okomiti gradijent $\nabla^\perp u = (-u_y, u_x)$ smjer najmanje promjene intenziteta slike, a Laplacian Δu je mjera glatkoće slike. Budući da izofote ovise o geometriji domene uslikavnja i ne smiju se presjeći u konačnom vremenu, nužno je ovaj proces ispreplesti s jednadžbom u kojoj postoje difuzijski efekti [33].

Općenito, uslikavanje digitalnih slika može se podijeliti u dvije skupine: strukturno orijentirane metode i metode

temeljene na teksturi. Obje skupine imaju bogatu teorijsku i praktičnu pozadinu [22, 36, 37]. U ovom radu bavit ćemo se strukturno orijentiranim uslikavanjem binarnih slika, što podrazumijeva obnovu rubova i jednoliko obojenih dijelova slike (bez teksture), za koje su posebno prikladni pristupi temeljeni na PDJ.

Prije skoro dva desetljeća Bertozzi i suradnici [4, 5] su predložili modificiranu Cahn–Hilliardovu jednadžbu kao model za uslikavanje visokokontrastnih ili binarnih slika koji značajno pojednostavljuje prethodno korištene metode (primjerice Esedoglu–Shenov model [23]).

2 Cahn-Hilliardova jednadžba

Cahn-Hilliardova (također CH u nastavku) jednadžba je makroskopski model polja koji opisuje razdvajanje faza [34] binarne legure pri fiksnoj temperaturi. Štoviše, CH jednadžba se koristi u biologiji [25], modeliranju tokova fluida [30, 29], a posebno u obradi slika [7, 8, 10, 11, 12, 31]. Neka je $f : \Omega \subset \mathbb{R}^2 \to \{-1,1\}$ dana binarna slika. Interpolacija $u : (0,T) \times \Omega \to \{-1,1\}$ originalne slike f dobiva se kao rješenje modificirane CH jednadžbe:

$$u_t = \Delta\left(\nu H'(u) - \mu\Delta u\right) + \lambda(\mathbf{x})(f-u), \text{ na } (0,T)\times\Omega, \quad (3)$$

$$u\big|_{t=0} = f(\mathbf{x}), \quad (4)$$

zajedno s odgovarajućim rubnim uvjetima koje ćemo kasnije precizirati. Konstante $\mu, \nu > 0$ ovise o konkretnoj situaciji, a za neki veliki $\lambda_0 > 0$, izraz vjernosti $\lambda : \Omega \to \mathbb{R}$ definiran je na sljedeći način:

$$\lambda(\mathbf{x}) = \begin{cases} \lambda_0, & \text{ako } \mathbf{x} \in \Omega \setminus \omega, \\ 0, & \text{ako } \mathbf{x} \in \omega. \end{cases} \quad (5)$$

U posebnom slučaju kada $H(u) = \frac{1}{2}(1-u^2)^2$ (naziva se potencijal dvostruke jame) i $\lambda = 0$, jednadžba (3) svodi se na dobro poznatu CH jednadžbu [13]. Izraz vjernosti osigurava da rezultirajuća slika u ne odstupa značajno od originalne slike f izvan domene uslikavanja. Opisno govoreći, za velike λ_0 izraz $\lambda(\mathbf{x})(u-f)$ ne smije biti velik zato što se u protivnom ne može kontrolirati ostatkom jednadžbe. Stoga, za velike λ_0, slika u mora ostati bliska originalnoj slici na $\Omega\setminus\omega$ (budući da je tada umnožak $\lambda_0(u-f)$ umjeren i, grubo govoreći, može se kontrolirati s $u_t - \Delta(\nu H'(u) - \mu\Delta u)$). Usput napominjemo da je to također razlog zašto rubni uvjeti za (3) nisu od presudne važnosti i utjecat će samo u vrlo maloj okolini ruba domene slike (pretpostavljajući da je domena uslikavanja daleko od ruba domene slike).

3 Izbor nelinearnog potencijala H

U ranim istraživanjima, promatrao se funkcional $H(u)$ koji predstavlja nelinearni potencijal s dvije jame koje odgovaraju vrijednostima $u = -1$ i $u = 1$. U kontekstu uslikavanja binarnih slika, vrijednosti $u = 1$ i $u = -1$ mogu označavati bijele i crne piksele, respektivno. Ukratko, budući da H usmjerava intenzitete piksela prema jednoj od ovih jama, moglo bi se, posuđujući terminologiju iz strojnog učenja, smatrati da H djeluje kao klasifikator. Tijekom posljednjih deset godina, potraga za fizički smislenim potencijalom H bila je opsežna. Početna motivacija za to nastala je zbog činjenice da rješenja CH jednadžbe s potencijalom dvostruke jame ne ostaju unutar intervala $[-1,1]$. U mnogim primjenama to narušava zakone fizike koji upravljaju sustavom; međutim, s računalnog stajališta, ovaj problem se može riješiti tehnikom uvođenja praga. Pri tome redefiniramo bilo koje vrijednosti $u > 1$ kao $u = 1$ i bilo koje vrijednosti $u < -1$ kao $u = -1$. Na primjer, ovaj pristup može se naći u istraživanjima Cherfils et al. [16, 17], gdje se u završnim koracima numerička shema isprepleće s pragom.

Druga mogućnost je korištenje logaritamskog potencijala [18, 19]:

$$H_{log}(u) = \frac{\theta}{2}\left((1+u)\log(1+u) + (1-u)\log(1-u)\right) + \\ + \frac{\theta_c}{2}(1-u^2), \quad (6)$$

gdje su $0 < \theta < \theta_c$ konstante. Singularnost $H'_{log}(u)$ dodatno nameće uvjet omeđenosti rješenja $u \in (-1,1)$. U usporedbi s polinomijalnim potencijalima, primjenom logaritamskog potencijala na digitalnim slikama mogu se ostvariti bolji rezultati uslikavanja te konstruirati numeričke sheme koje brže konvergiraju [16].

Nedavno je razmatrana verzija CH jednadžbe koja koristi kvadratni potencijal [7, 26]. Preciznije, ovaj pristup uključuje korištenje potencijala definiranog na sljedeći način:

$$H_{quad}(u) = \psi(u) + \frac{1}{2}(1-u)^2,$$

$$\psi(u) = I_{[-1,1]}(u) = \begin{cases} 0, & \text{ako } u \in [-1,1], \\ +\infty, & \text{inače}, \end{cases} \quad (7)$$

gdje s $I_{[-1,1]}$ označavamo indikatorsku funkciju koja uzima vrijednost 0 ako je u unutar intervala $[-1,1]$, a $+\infty$ ako nije. U [7], autori su koristili metodu konačnih elemenata za probleme uslikavanja digitalnih slika i pokazali da se s ovakvim (jednostavnijim) potencijalom mogu dobiti zadovoljavajući rezultati uslikavanja.

4 Numerička rješenja temeljena na pristupu cijepanja po konveksnosti

S obzirom na široku primjenjivost, ali i numeričke izazove koje predstavlja CH jednadžba, do sada je razvijen čitav arsenal numeričkih metoda [6, 7, 15]. Ovdje ćemo se posvetiti pristupu cijepanja po konveksnosti čije je temelje postavio Eyre [24], a kasnije i drugi istraživači [15, 27, 28]. Naime, neka je $\mathcal{H}$ Hilbertov prostor i $E = E_1 - E_2$ energija takva da se može pisati kao razlika dviju konveksnih energija E_1 i E_2. Tada diskretizacija

$$\frac{u^{n+1}-u^n}{dt} = -\nabla_{\mathcal{H}} E_1(u^{n+1}) - \nabla_{\mathcal{H}} E_2(u^n), \tag{8}$$

gradijentnog toka

$$u_t = -\nabla_{\mathcal{H}} E(u), \tag{9}$$

zadovoljava svojstvo energetske stabilnosti $E(u^{n+1}) \leq E(u^n)$ (vidi [1] za detalje oko izvoda bezuvjetno stabilnih shema prvog i drugog reda). CH jednadžba se izvodi kao H^{-1} gradijentni tok Ginzburg-Landauove energije definirane na sljedeći način:

$$E_1[u] = \int_\Omega \left[\nu H(u(\mathbf{x})) + \frac{1}{2}\mu |\nabla u(\mathbf{x})|^2 \right] d\mathbf{x}, \tag{10}$$

gdje u tipično označava koncentraciju, $H(u)$ je gustoća slobodne energije Helmholtza, ν i μ su konstante koje utječu na debljinu tranzicijskog područja između dviju faza. Napominjemo da se Soboljev prostor $H^{-1}(U)$ definira kao dualni prostor prostora $H_0^1(U)$. Ovaj prostor uključuje sve neprekidne linearne funkcionalne na $H_0^1(U)$, gdje U predstavlja odgovarajući otvoreni podskup od $\mathbb{R}^n$. Prostor $H_0^1(U)$ sadrži funkcije iz $L^2(U)$ čije slabe deriacije također pripadaju $L^2(U)$, s dodatnim uvjetom da funkcije iščezavaju na rubu skupa U u smislu tragova (za više detalja iz funkcionalne analize čitatelja upućujemo na [9]). Nadalje, član s izrazom vjernosti može se izvesti kao L^2 gradijentni tok energije definirane s

$$E_2[u] = \frac{\lambda}{2} \int_{\Omega\setminus\omega} (f-u)^2 \, d\mathbf{x}. \tag{11}$$

Uočimo da se modificirana CH jednadžba (3) ne može formalno definirati kao gradijentni tok.

Kako bismo numerički riješili ovu jednadžbu, koristimo metodu cijepanja po konveksnosti. Postupak je sljedeći: želimo podijeliti svaku od energija na konveksni i konkavni dio kako bismo konstruirali poluimplicitnu numeričku shemu u kojoj se konveksni dio diskretizira implicitno, dok se konkavni dio diskretizira eksplicitno. Stoga, ako zapišemo energije na sljedeći način

$$E_1(u) = E_{11}(u) - E_{12}(u), \tag{12}$$
$$E_2(u) = E_{21}(u) - E_{22}(u), \tag{13}$$

rezultirajuća shema cijepanja po konveksnosti je uvjetno stabilna ako su sve energije E_{ij}, $i, j = 1, 2$ konveksne.

Da bismo postigli konveksnost energija, dodajemo i oduzimamo isti izraz od E_1 i E_2, te dobivamo:

$$E_{11}(u) = \int_\Omega \left(\frac{\varepsilon}{2} |\nabla u|^2 \frac{C_1}{2} |u|^2 \right) d\mathbf{x}, \tag{14}$$

$$E_{12}(u) = \int_\Omega \left(-\frac{1}{\varepsilon} H(u) + \frac{C_1}{2} |u|^2 \right) d\mathbf{x}, \tag{15}$$

$$E_{21}(u) = \int_{\Omega\setminus\omega} \frac{C_2}{2} |u|^2 d\mathbf{x}, \tag{16}$$

$$E_{22}(u) = \int_{\Omega\setminus\omega} \left(-\lambda_0 (f-u)^2 + \frac{C_2}{2} |u|^2 \right) d\mathbf{x}. \tag{17}$$

Konstante $C_1, C_2 > 0$ trebaju biti dovoljno velike kako bi se osiguralo da su energije E_{12} i E_{22} konveksne. Očito, E_{11}, E_{21} su konveksne neovisno o C_1 i C_2, a ako je $2C_2 > \lambda_0$ tada je E_{22} konveksna. Primijetimo da u svrhu simulacija uvijek možemo pronaći dovoljno velik C_1 tako da je E_{12} konveksna. Konstantu $\varepsilon > 0$ uvodimo tako da je $\mu = \varepsilon$ i $\nu = \varepsilon^{-1}$, zato što je pokazano da $\mu\nu \approx 1$ daje najprirodnije rezultate uslikavanja.

Podjela definirana s (14),(15),(16),(17), daje sljedeću shemu za vremenski korak:

$$\begin{aligned} \frac{u^{n+1}-u^n}{dt} = &- \nabla_{H^{-1}} (E_{11}(u^{n+1}) - E_{12}(u^n)) - \\ &- \nabla_{L^2} (E_{21}(u^{n+1}) - E_{22}(u^n)), \end{aligned} \tag{18}$$

gdje n označava vremenski korak, a dt veličinu koraka. Umetanjem E_{ij} u (18), dobivamo:

$$\begin{aligned} &(1 + C_2 dt) u^{n+1} + \varepsilon \, dt \, \Delta^2 u^{n+1} - C_1 \, dt \, \Delta u^{n+1} \\ &= \frac{dt}{\varepsilon} \Delta h_\delta(u^n) - C_1 \, dt \, \Delta u^n + \lambda \, dt \, (f - u^n) + (1 + C_2 dt) u^n. \end{aligned} \tag{19}$$

U daljnim računima pretpostavljamo da je Ω digitalna slika veličine $P \times Q$ s Neumannovim rubnim uvjetom

$$\nabla u \cdot \mathbf{n} = \nabla(\Delta u) \cdot \mathbf{n} = 0. \tag{20}$$

Zbog značajnog pojednostavljenja operatora Δ i Δ^2 u Fourierovom prostoru, opisanog u nastavku, koristit ćemo Fourierovu pretvorbu za prostornu diskretizaciju (više detalja o Fourierovoj pretvorbi se može pronaći u 6. poglavlju

[21]).
Inverzna diskretna Fourierova pretvorbu svakog elementa u_{pq} definirana je kao

$$u_{pq} = \sum_{k=0}^{P-1} \sum_{l=0}^{Q-1} \widehat{u}_{kl}\, e^{2\pi i k p/P} e^{2\pi i l q/Q}, \tag{21}$$

s k, l koji predstavljaju indekse u Fourierovom prostoru, a $\widehat{u}_{kl}$ element matrice $\widehat{u}$.
Diskretni Laplaceov operator koji djeluje na u_{pq} dobiven metodom konačnih razlika može se zapisati kao

$$\Delta u_{pq} = \frac{u_{p+1,q} + u_{p-1,q} - 2u_{pq}}{dx^2} + \frac{u_{p,q+1} + u_{p,q-1} - 2u_{pq}}{dy^2}. \tag{22}$$

Biramo prostorne korake $dx = dy = 1$ i, umetanjem u_{pq} iz (21) u (22) i uspoređujući izraze pod zbrojevima, dobivamo

$$\begin{aligned}\Delta\widehat{u}_{kl} &= \left(e^{2\pi i k/P} + e^{-2\pi i k/P} - 2 + e^{2\pi i l/Q} + e^{-2\pi i l/Q} - 2\right)\widehat{u}_{kl} \\ &= 2\left(\cos(2\pi k/P) + \cos(2\pi l/Q) - 2\right)\widehat{u}_{kl} \\ &:= K_{kl} \cdot \widehat{u}_{kl}. \end{aligned} \tag{23}$$

Pri čemu uvažavanjem $K_{kl} = 2\left(\cos(2\pi k/P) + \cos(2\pi l/Q) - 2\right)$, istim postupkom za Δ^2 dobivamo

$$\Delta^2\widehat{u}_{kl} = K_{kl}^2 \cdot \widehat{u}_{kl}. \tag{24}$$

Sada, s ovim definicijama operatora Δ i Δ^2, dobivamo jednadžbu za vremensku evoluciju elemenata u_{kl} zapisujući cijelu jednadžbu (19) u Fourierovom prostoru

$$\begin{aligned}&(1 + C_2 dt)\widehat{u^{n+1}}_{kl} + \varepsilon dt\, K_{kl}^2 \widehat{u^{n+1}}_{kl} - C_1\, dt\, K_{kl} \widehat{u^{n+1}}_{kl} \\ &= \frac{dt}{\varepsilon} K_{kl} \widehat{(h_\delta(u^n))}_{kl} - C_1\, dt\, K_{kl} \widehat{u^n}_{kl} + \widehat{(\lambda\, dt (f - u^n))}_{kl} \\ &\quad + C_2\, dt\, \widehat{u^n}_{kl} + \widehat{u^n}_{kl}. \end{aligned} \tag{25}$$

Konačno, preuređivanjem (25) rezultira sljedećom shemom:

$$\widehat{u^{n+1}}_{kl} = \frac{\widehat{u^n}_{kl} + dt\left(\frac{1}{\varepsilon} K_{kl} \cdot \widehat{(h_\delta(u^n))}_{kl} - C_1 K_{kl} \cdot \widehat{u^n}_{kl} + \widehat{(\lambda(f - u^n))}_{kl} + C_2 \widehat{u^n}_{kl}\right)}{1 + C_2 + \varepsilon K_{kl}^2 - C_1 K_{kl}}. \tag{26}$$

Da bismo dobili u^{n+1}, primijenimo inverznu diskretnu Fourierovu transformaciju na $\widehat{u^{n+1}}$. Na kraju spomenimo da za uslikavanje većih regija često moramo implementirati metodu u dva koraka. Prvo, započinjemo proces uslikavanja s većim vrijednostima ε, što rezultira povezivanjem oblika s difuzno razmazanim rubovima. Drugi korak zatim koristi rezultate prvog koraka i nastavlja s mnogo manjim vrijednostima ε kako bi se izoštrio rub nakon ponovnog spajanja.

5 Rezultati

U ovom odjeljku predstavljamo rezultate uslikavanja binarnih slika korištenjem CH jednadžbe. Istražujemo uslikavanje standardnih oblika kao što su pruge ili križ. Također pokazujemo mehanizam uslikavanja prikazujući rezultate uslikavanja nakon 100, 1000, 2000 vremenskih koraka. Na kraju, dajemo primjere kako pojednostaviti i proširiti predloženu metodu s ciljem smanjenja računalne složenosti i poboljšanja kvalitete uslikavanja. Sve su simulacije dobivene korištenjem programskog paketa Matlab, a izvedene na standardnom stolnom računalu. Radi jednostavnosti, skalirali smo slike (u tonovima sive) tako da su intenziteti u rasponu $[-1, 1]$. Napominjemo da je indeks strukturne sličnosti (SSIM) metoda za mjerenje sličnosti između dviju slika. SSIM je uveden kao poboljšanje tradicionalnih metoda poput PSNR (*engl.* peak signal-to-noise ratio) i MSE (*engl.* mean squared error), koje ponekad ne odražavaju percipiranu vizualnu sličnost. SSIM indeks poprima vrijednost između -1 i 1, gdje 1 označava maksimalnu sličnost između dvije slike.

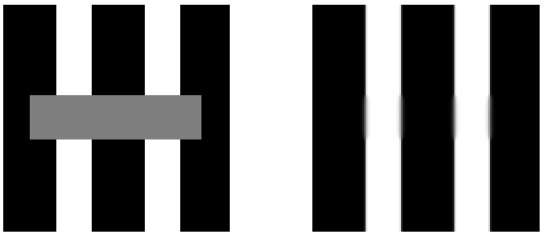

(a) Početna slika f (b) Rezultat uslikavanja s CH jednadžbom

Slika 1: *Rezultati uslikavanja slike paralelnih pruga.*

Na Slici 1 vidimo rezultate djelovanja CH jednadžbe s potencijalom dvostruke jame na standardnoj binarnoj slici pruga. Sivo područje na slici 1(a) označava domenu uslikavanja. Odabir parametara izvršen je metodom iscrpnog pretraživanja. Kao što možemo vidjeti, ovaj pristup uslikavanju prirodno nastavlja karakteristike slike unutar područja uslikavanja s visokim SSIM-om 0.9701. Slika 1(b) je dobivena nakon 3000 vremenskih koraka. Koristili smo dvoskalni pristup, pri čemu smo ukupni broja iteracija i podijelili u $i = i_1 + i_2$, gdje se iteracije i_2 izvode s promijenjenim parametrom ε. Kao što je prije spomenuto, ovo je standardan pristup u uslikavanja većih domena (vidi na primjer [3]). Počinjemo s $\varepsilon = 100$, a nakon 1500 iteracija se približavamo ravnotežnom stanju. Zatim prelazimo na manju vrijednost $\varepsilon = 1$ te činimo dodatnih 1500 vremenskih koraka.

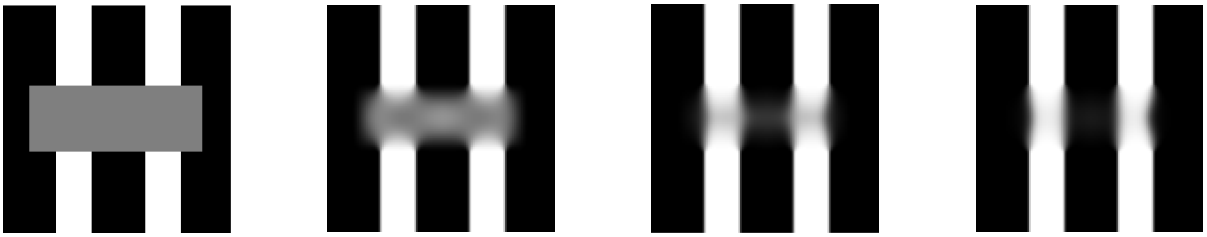

(a) Početna slika f (b) Rezultat dobiven sa 100 iteracija (c) Rezultat dobiven s 1000 iteracija (d) Rezultat dobiven s 2000 iteracija

Slika 2: *Mehanizam uslikavanja prikazan na slici paralelnih pruga.*

Na Slici 2 možemo vidjeti evoluciju procesa uslikavanja dobivenu s ukupno 100, 1000 i 2000 vremenskih koraka. U početku koristimo $\varepsilon = 100$, a nakon što smo učinili polovicu od ukupnih vremenskih koraka, prelazimo na manju vrijednost $\varepsilon = 2$ te činimo ostale vremenske koraka. Uočite da je domena uslikavanja u ovom slučaju veća nego na Slici 1.

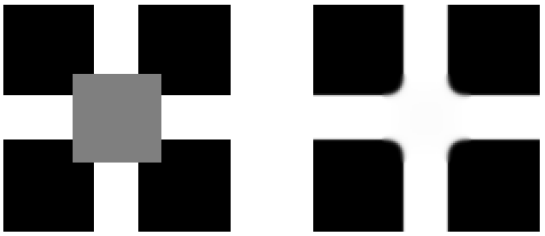

(a) Početna slika f (b) Rezultat uslikavanja CH

Slika 3: *Rezultati uslikavanja slike koja sadrži bijeli križ.*

Sljedeća testna slika sastoji se od bijelog križa s oštećenim područjem koje se nalazi u sredini slike. Odgovarajući rezultati uslikavanja prikazani su na Slici 3 i u skladu su s rezultatima iz literature (vidi na primjer Sliku 3.1 u [6] ili Slike 1 i 2 u [4]). Korišteni parametri je ista dvoskalna tehnika kao i prije s $\varepsilon = 100$ pa $\varepsilon = 1$, a pripadni SSIM je 0.9608.

Iako su rezultati dobiveni CH jednadžbom impresivni, pažljivim promatranjem područja koja sadrže crno-bijelo ili bijelo-crno prijelaze na Slici 1(b) mogu se uočiti difuzijski efekti koji se ne pojavljuju na Slici 4(a) koja je rekonstruirana jednadžbom sa sljedećim klasifikatorom [32]

$$H'_\delta(u) = h_\delta(u) = \nu \frac{\Delta u}{|\Delta u| + \delta} |\nabla u|, \tag{27}$$

pri čemu je $\delta > 0$ konstanta. Ovaj klasifikator je baziran na regulariziranoj verziji šok filtera $h_0 = -\operatorname{sgn}(\Delta u)|\nabla u|$ kojeg su uveli Rudin i Osher [35, 38].

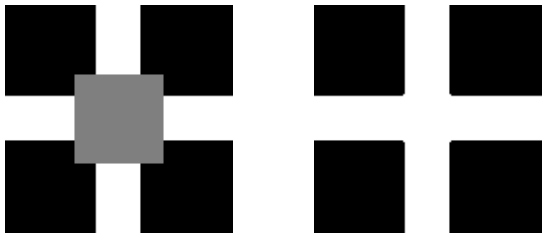

(a) Početna slika f (b) Rezultat uslikavanja

Slika 4: *Rezultati uslikavanja dobiveni korištenjem* (27)*. Završne slike su isprepletene s pragom.*

Slično, na slici 3(b) također možemo uočiti nedostatak oštrih rubova crnih kvadrata koje bismo očekivali u domeni uslikavanja. Na slici 4(c) vidimo da predložena jednadžba oblikuje rubove i prirodno proširuje značajke slike. Kao i prije, korišten je dvoskalni pristup s $\varepsilon = 25$, te $\varepsilon = 2.7$ kroz sveukupno 800 vremenskih koraka.

Motivirani konstrukcijom dokaza postojanja rješenja koji počiva na tehnikama fiksne točke [32], možemo razmotriti varijantu potencijala (27) koji daje linearnu jednadžbu tako da fiksiramo nelinearni dio (klasifikator) tako da ovisi samo o početnoj slici. Preciznije, kada kažemo linearna varijanta predložene jednadžbe, mislimo na sljedeće:

$$u_t = \Delta \left(\frac{1}{\varepsilon} \frac{\Delta f}{|\Delta f| + \delta} |\nabla f| - \varepsilon \Delta u \right) + \lambda (f - u). \tag{28}$$

Prednost ovog pristupa je da se nelinearni dio (27) sada prikazuje kao $h(f)$. Stoga se može unaprijed izračunati i održavati konstantnim tijekom evolucije u vremenu.

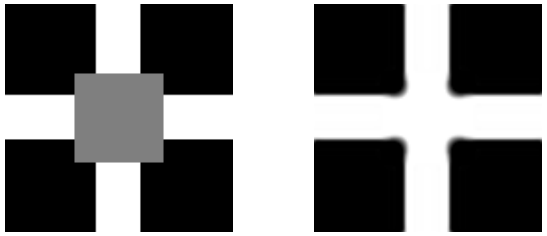

(a) Početna slika f (b) Rezultati uslikavanja

Slika 5: *Rezultati uslikavanja dobiveni korištenjem linearne varijante modificirane CH* (28)*.*

Početna vrijednost bila je $\varepsilon = 25$, a nakon 2500 vremenskih koraka mijenjamo je na $\varepsilon = 2.7$. Ukupno je izvršeno 8000 vremenskih koraka. Rezultirajuća slika, slika 5(b), usporediva je s onom dobivenom nelinearnom verzijom potencijala i stoga bi se moglo tvrditi da ova metoda predstavlja kompromis između jednostavnosti računanja i kvalitete uslikavanja. Očigledni nedostatak korištenja linearnog potencijala su difuzijski učinci oko uglova križa, ali to se može eliminirati uvođenjem praga. Ovaj pristup u dva koraka standardan je u slikanju s Cahn-Hilliardovom jednadžbom (vidi na primjer [7, 14]). Za dobivanje vrijednosti praga prikladna je Matlab funkcija `graythresh`.

6 Zaključak

U ovom kratkom izlaganju željeli smo prikazati osnovne značajke CH jednadžbe s primjenom na uslikavanju binarnih oblika. Kroz eksperimentalne rezultate demonstrirali smo potencijal CH jednadžbe u obnovi rubova i jednoliko obojene dijelove slike, čime se prirodno nastavljaju karakteristike slike unutar domene uslikavanja. Štoviše, pokazali smo da modificirana CH jednadžba, primijenjena kroz dvoskalni pristup, omogućava efikasno uslikavanje područja s minimalnim difuzijskim artefaktima. Ovaj rad otvara put prema razumijevanju složenih mehanizama uslikavanja i potiče na razvoj naprednih algoritama za obradu digitalnih slika.

6.1 Zahvale

Ovo istraživanje je podržano od strane Hrvatske zaklade za znanost pod brojem projekta HRZZ-MOBODL-2023-08-7617 i IP-2022-10-7261 Analysis of Partial Differential Equations and Shape Optimization (ADESO). Stalna adresa A. N. je Sveučilište u Zagrebu.

Literatura

[1] BACKOFEN, R., WISE, S.M., SALVALAGLIO, M., VOIGT, M., Convexity splitting in a phase field model for surface diffusion, *Int. J. Num. Anal. Model.* **16** (2020), 192–209.

[2] BERTALMIO, M., SAPIRO, G., CASELLES, V., BALLESTER, C., Image inpainting, *Proceedings of the 27th annual conference on Computer graphics and interactive techniques,* 417–424, ACM Press/Addison-Wesley Publishing Co., 2000, https://doi.org/10.1145/344779.344972

[3] BERTALMIO, M., BERTOZZI, A., SAPIRO, G., Navier-Stokes, fluid dynamics, and image and video inpainting, *Computer Vision and Pattern Recognition*, 2001. CVPR 2001. *Proceedings of the 2001 IEEE Computer Society Conference on Computer Vision and Pattern Recognition, Vol. 1. IEEE*, 2001, https://doi.org/10.1109/CVPR.2001.990497

[4] BERTOZZI, A., ESEDOGLU, S., GILLETTE, A., Inpainting of binary images using the Cahn–Hilliard equation, *IEEE Trans Image Process.* **16** (2006), 285–291, https://doi.org/10.1109/tip.2006.887728

[5] BERTOZZI, A., ESEDOGLU, S., GILLETTE, A., Analysis of a two-scale Cahn–Hilliard model for binary image inpainting, *Multiscale Modeling & Simulation* **6**(3) (2007), 913–936, https://doi.org/10.1137/060660631

[6] BERTOZZI, A., SCHÖNLIEB, C. B., Unconditionally stable schemes for higher order inpainting, *Comm. Math. Sci.* **9**(2) (2011), 413–457, https://dx.doi.org/10.4310/CMS.2011.v9.n2.a4

[7] BOSCH, J., KAY, D., STOLL, M., WATHEN, J. A., Fast solvers for Cahn–Hilliard inpainting, *SIAM J. Imaging Sci.* **7**(1) (2014), 67–97, https://doi.org/10.1137/130921842

[8] BOSCH, J., STOLL, M., A fractional inpainting model based on the vector-valued Cahn–Hilliard equation, *SIAM J. Imaging Sci.* **8** (2015), 2352–2382, https://doi.org/10.1137/15M101405X

[9] BREZIS, H., *Functional analysis, Sobolev spaces and partial differential equations*, Springer, 2011, https://doi.org/10.1007/978-0-387-70914-7

[10] BRKIĆ, L. A., MITROVIĆ, D., NOVAK, A., On the image inpainting problem from the viewpoint of a nonlocal Cahn-Hilliard type equation, *J. Adv. Res.* **25** (2020), 67–76, https://doi.org/10.1016/j.jare.2020.04.015

[11] BRKIĆ, L. A., NOVAK, A., A nonlocal image inpainting problem using the linear Allen–Cahn equation, *Advances in Non-Integer Order Calculus and Its Applications*, Malinowska, Agnieszka B., Mozyrska, D., Sajewski, Ł. (ur.), 2020, 229–239, https://doi.org/10.1007/978-3-030-17344-9_17

[12] BURGER, M., HE, L., SCHÖNLIEB, C. B., Cahn–Hilliard inpainting and a generalization for grayvalue images, *SIAM J. Imaging Sci.* **2**(4) (2009), 1129–1167, https://doi.org/10.1137/080728548

[13] CAHN, J. W., HILLIARD, J. E., Free energy of a nonuniform system. I. Interfacial free energy, *J. Chem. Phys.* **28**(2) (1958), 258–267, https://doi.org/10.1063/1.1744102

[14] CARRILLO, J. A., KALLIADASIS, S., LIANG, F., PEREZ, S. P., Enhancement of damagedimage prediction through Cahn–Hilliard image inpainting, *R. Soc. Open Sci.* **8** (2021), 201294. https://doi.org/10.1098/rsos.201294

[15] CHENG, M., WARREN, J. A., An efficient algorithm for solving the phase field crystal model, *J. of Computational Physics* **227**(12) (2008), 6241–6248, https://doi.org/10.1016/j.jcp.2008.03.012

[16] CHERFILS, L., HUSSEIN, F., MIRANVILLE, A., On the Bertozzi–Esedoglu–Gillette–Cahn–Hilliard equation with logarithmic nonlinear terms, *SIAM J. Imaging Sci.* **8**(2) (2015), 1123–1140, https://doi.org/10.1137/140985627

[17] CHERFILS, L, HUSSEIN, F., MIRANVILLE, A., Finite-dimensional attractors for the Bertozzi–Esedoglu–Gillette–Cahn–Hilliard equation in image inpainting, *Inverse Problems & Imaging* **9**(1) (2015), 105–125, https://doi.org/10.3934/ipi.2015.9.105

[18] CHERFILS, L., MIRANVILLE, A., ZELIK, S., The Cahn-Hilliard equation with logarithmic potentials, *Milan J. Math.* **79** (2011), 561–596, https://doi.org/10.1007/s00032-011-0165-4

[19] COPETTI, M. I. M, ELLIOTT, C. M., Numerical analysis of the Cahn–Hilliard equation with a logarithmic free energy, *Numer. Math.* **63** (1992), 39–65, https://doi.org/10.1007/BF01385847

[20] DAI, S., DU, Q., Weak Solutions for the Cahn–Hilliard Equation with Degenerate Mobility, *Arch. Rational Mech. Anal.* **219** (2016), 1161–1184, https://doi.org/10.1007/s00205-015-0918-2

[21] DEMMEL, J., *Applied numerical linear algebra*, SIAM, Philadelphia, PA, 1997.

[22] ESEDOGLU, S., OSHER, S. J., Decomposition of images by the anisotropic Rudin–Osher–Fatemi model, *Comm. Pure App. Math.* **57**(12) (2004), 1609–1626, https://doi.org/10.1002/cpa.20045

[23] ESEDOGLU, S., JIANHONG, S., Digital inpainting based on the Mumford–Shah–Euler image model, *Eur. J. App. Math.* **13** (2002), 353–370, https://doi.org/10.1017/S0956792501004904

[24] EYRE, D. J., Unconditionally gradient stable time marching the Cahn-Hilliard equation, *MRS Online Proceedings Library (OPL)* **529** (1998), 39–46, https://doi.org/10.1557/PROC-529-39

[25] FISCHER, P., MERGHEIM, J., STEINMANN, P., On the C1 continuous discretization of nonlinear gradient elasticity: A comparison of NEM and FEM based on Bernstein–Bézier patches, *International journal for numerical methods in engineering* **82**(10) (2010), 1282–1307, https://doi.org/10.1002/nme.2802

[26] GARCKE, H., FONG LAM, K., STYLES, V., Cahn–Hilliard inpainting with the double obstacle potential, *SIAM Journal on Imaging Sciences* **11**(3) (2018), 2064–2089, https://doi.org/10.1137/18M1165633

[27] GLASNER, K., ORIZAGA, S., Improving the accuracy of convexity splitting methods for gradient flow equations, *J. Comp. Phys.* **315** (2016), 52–64, https://doi.org/10.1016/j.jcp.2016.03.042

[28] GOMEZ, H., HUGHES, T. J.R., Provably unconditionally stable, second-order time-accurate, mixed variational methods for phase-field models, *J. Comp. Phys.* **230** (2011), 5310–5327, https://doi.org/10.1016/j.jcp.2011.03.033

[29] HAN, D., WANG, X., A second order in time, uniquely solvable, unconditionally stable numerical scheme for Cahn–Hilliard–Navier–Stokes equation, *J. Comp. Phys.* **290** (2015), 139–156, https://doi.org/10.1016/j.jcp.2015.02.046

[30] LIU, C., SHEN, J., A phase field model for the mixture of two incompressible fluids and its approximation by a Fourier-spectral method, *Physica D: Nonlinear Phenomena* **179**(3-4) (2003), 211–228, https://doi.org/10.1016/S0167-2789(03)00030-7

[31] MIRANVILLE, A., *The Cahn–Hilliard equation: recent advances and applications*, Society for Industrial and Applied Mathematics, 2019.

[32] NOVAK, A., REINIĆ, N., Shock filter as the classifier for image inpainting problem using the Cahn-Hilliard equation, *Comp. & Math. App.* **123** (2022), 105–114, https://doi.org/10.1016/j.camwa.2022.07.021

[33] NOVAK, A., ŠTAJDUHAR, A., Application of Linear and Nonlinear Heat Equation in Digital Image Processing, *KoG* **18** (2014), 45–52.

[34] NOVICK-COHEN, A., The Cahn–Hilliard equation, *Handbook of differential equations: evolutionary equations 4* (2008), 201–228, https://doi.org/10.1016/S1874-5717(08)00004-2

[35] OSHER, S., RUDIN, L. I., Feature-oriented image enhancement using shock filters, *SIAM J. Num. Anal.* **27**(4) (1990), 919–940, https://doi.org/10.1137/0727053

[36] RUDIN, L. I., OSHER, S., FATEMI, E., Nonlinear total variation based noise removal algorithms, *Physica D: Nonlinear Phenomena* **60** (1992), 259–268, http://doi.org/10.1016/0167-2789(92)90242-F

[37] SHEN, J., CHAN, T. F., Mathematical models for local nontexture inpaintings, *SIAM J. App. Math.* **62**(3) (2002), 1019–1043, https://doi.org/10.1137/S0036139900368844

[38] WEICKERT, J., Coherence-enhancing shock filters, Michaelis, B., Krell, G. (ur.) *Pattern Recognition, DAGM 2003. Lecture Notes in Computer Science*, **2781**, Springer, Berlin, Heidelberg, https://doi.org/10.1007/978-3-540-45243-0_1

Andrej Novak
orcid.org/0000-0002-7828-4870
e-mail: andrej.novak@phy.hr

Sveučilište u Zagrebu
Prirodoslovno-matematički fakultet
Bijenička cesta 32, 10000 Zagreb, Hrvatska

Sveučilište u Beču
Fakultet za matematiku
1090 Beč, Austrija

Martina Armanda
e-mail: marty4arm@gmail.com

Sveučilište u Zagrebu
Prirodoslovno-matematički fakultet
Bijenička cesta 32, 10000 Zagreb, Hrvatska

Studentica u vrijeme pisanja ovog rukopisa.

INSTRUCTIONS FOR AUTHORS

SCOPE. "KoG" publishes scientific and professional papers from the fields of geometry, applied geometry and computer graphics.

SUBMISSION. Scientific papers submitted to this journal should be written in English, professional papers should be written in Croatian or English. The papers have not been published or submitted for publication elsewhere.
The manuscript should be sent in PDF format via e-mail to the editor:

Ema Jurkin
ema.jurkin@rgn.unizg.hr

The first page should contain the article title, author and coauthor names, affiliation, a short abstract in English, a list of keywords and the Mathematical subject classification.

UPON ACCEPTANCE. After the manuscript has been accepted for publication authors are requested to send its LaTex file via e-mail to the address:

ema.jurkin@rgn.unizg.hr

Figures should be titled by the figure number that match to the figure number in the text of the paper.

The corresponding author and coauthors will receive hard copies of the issue free of charge.

How to get KoG?

The easiest way to get your copy of KoG is by contacting the editor's office:

Marija Šimić Horvath
marija.simic@arhitekt.unizg.hr
Faculty of Architecture
Kačićeva 26, 10 000 Zagreb, Croatia
Tel: (+385 1) 4639 176

The price of the issue is €15 + mailing expenses €5 for European countries and €10 for other parts of the world.

The amount is payable to:

ACCOUNT NAME:	Hrvatsko društvo za geometriju i grafiku Kačićeva 26, 10000 Zagreb, Croatia
IBAN:	HR8623600001101517436